Politecnico di Milano

Facoltà di Ingegneria Industriale

Corso di Laurea di Ingegneria Spaziale

A Co-Simulation Approach for Mixed Smooth and Nonsmooth Dynamics in Multibody Problems

RELATORE
Prof. Pierangelo Masarati

TESI DI LAUREA DI
Matteo Fancello
Matr. N. 675769

Anno Accademico 2011/2012

Contents

List of Figures

List of Tables

Abstract

The problem of unilateral constraints, such as frictionless and frictional contact phenomena, in multi-rigid-body problems, is characterized by a nonsmooth dynamics. By and large there are two ways to approach this nonsmoothness: continuous contact approaches and hard constraint (complementarity) approaches. The first ones use a regularization of the nonsmooth aspects of the problem, e. g. by substituting the impenetrability constraint with stiff reaction laws at contact. The complementarity approach is built on the basis of a mathematical framework able to consistently describe solutions that include nonsmoothness, and leads to the description of the phenomena in terms of Complementarity Problems.

This work originates from the interest to integrate some form of modeling unilateral constraints in the MBDyn multibody dynamics software. First, the continuous contact approach has been considered, and constitutive laws based on this regularization approach have been implemented and tested. Then the state of the art for the complementarity approach has been reviewed, and the classic Moreau-Jean timestepping has been considered in order to add a tool for implementing frictionless and frictional contacts in the MBDyn software. The focus of the exploration has been on retaining the robustness and accuracy of the DAE integration implemented in MBDyn, along with its powerful modeling capabilities, and the robustness and rigorous approach in dealing with nonsmooth events of the NonSmooth Contact Dynamics framework.

A co-simulation approach of the smooth dynamics through MBDyn alongside the application of timestepping methods to the nonsmooth part of the problem has been developed and tested. A validation of the approach has been made through comparison with models simulated entirely with state-of-the-art nonsmooth dynamics software Siconos and with a recently developed method that combines the HHT integration method with the time-stepping schemes to obtain a higher order event-capturing integration. Following that same approach an adaptation of the multistep integration scheme used by MBDyn to nonsmooth dynamics has been made. A more complex application of aerospace interest and an application with frictional contact have been developed with the co-simulation approach, in order to gain insight to the strenghts and weaknesses of the method.

Sommario

I problemi che comprendono vincoli unilaterali, come contatti con e senza attrito, in sistemi multicorpo rigidi, sono caratterizzati da una dinamica *nonsmooth*, ovvero con forti proprietà di irregolarità.

Possono essere affrontati in due modi principali: con una regolarizzazione del problema, metodi *continuous contact,* o con metodi nonsmooth *event-capturing* o *event-driven* che si basano su un quadro matematico consistente con le caratteristiche *nonsmooth,* tramite il quale la soluzione della dinamica diviene un problema di complementarietà.

Questo lavoro nasce dall'interesse ad integrare la possibilità di modellare vincoli unilateri nel software per la dinamica multicorpo MBDyn. Si è inizialmente considerato lo stato dell'arte per l'approccio *continuous contact,* e sono state implementate e testate leggi costitutive che ne consentono l'applicazione. Successivamente l'approccio nonsmooth, ed in particolare il metodo *event-capturing* introdotto da Moreau e Jean, è stato studiato con lo scopo di aggiungere uno strumento per gestire contatti con attrito in MBDyn. L'obiettivo dell'approccio esplorato è stato quello di mantenere l'integrazione di problemi differenziali algebrici (DAE) implementata in MBDyn, per trarre vantaggio dalle sue caratteristiche di accuratezza e versatilità nei problemi multidisciplinari, e trattare parte del problema con un approccio consistente con le sue caratteristiche nonsmooth.

Si è sviluppato quindi un metodo di co-simulazione che prevede una parte della dinamica del problema integrata da MBDyn assieme ad una parte della dinamica che risente direttamente di caratteristiche nonsmooth integrata tramite un metodo nonsmooth *event-capturing*. Una validazione empirica dell'implementazione è stata effettuata tramite la comparazione con risultati dal software stato dell'arte per la dinamica nonsmooth Siconos. Traendo spunto da un recente lavoro si è inoltre sviluppato un adattamento dello schema di integrazione multistep usato in MBDyn a problemi di dinamica nonsmooth, ed i risultati di questo metodo su semplici esempi hanno ulteriormente validato l'approccio di co-simulazione. Una più complessa applicazione del campo aerospaziale comprendente contatti senza attrito è stata testata con successo. Una estensione del metodo alla modellazione di contatti con attrito è stata applicata ad un modello di meccanismo deambulante.

Chapter 1

Introduction

Many engineering problems involve the simulation of multibody dynamical systems composed of several rigid bodies as well as joints, contacts (non-interpenetration), and friction constraints.

Although finite element analysis is a powerful and accurate method to simulate contact problems, for many applications the method of multi-rigid-body systems is the most efficient for the dynamic analysis of the overall motion of mechanical systems. Therefore the numerical dynamics of collections of bodies treated as perfectly indeformable, subject to the constraints of non-interpenetrability, with friction taken into account in the event of contact, is currently an active domain of research.

The problem of unilateral constraints, such as frictionless and frictional contact phenomena, in multi-rigid-body problems, is characterized by a *nonsmooth* dynamics. To quote J.J.Moreau [35]:

> In fact 'Nonsmoothness' is the salient feature of the problems in view. After the set of possible positions of the investigated system has been parametrized through an element $q \in R^n$, the geometric restriction that the non-interpenetrability constraints impose on q are formulated as a set of inequalities. Hence, instead of running in a smooth manifold, as in traditional analytical dynamics, the point q is confined in a region of R^n whose boundary is made of a lot of hyper-surfaces: this is nonsmoothness in space. Furthermore, collisions are expected to induce velocity jumps: this is nonsmoothness in time. To end, the contact forces or 'reactions' associated with the non-interpenetrability constraints are governed by highly irregular laws. These forces vanish as soon as the corresponding contacts break while, if contact holds, the commonly stipulated mechanical conditions do not express them as functions of q. If in addition, dry friction is taken into account (usually in the form of Coulomb's law), it introduces some irregular relationships between contact forces and the

sliding velocities. All this may be called nonsmoothness in law.

By and large there are two ways to approach this nonsmoothness: continuous contact approaches and hard constraint (complementarity) approaches.

In the first ones, which are regularization approaches, also called penalty methods, it is assumed that every time two rigid bodies come in frictional contact, the interaction can be represented by a collection of stiff springs along with damping elements that act at the interface of the two bodies. By allowing a small interpenetration between bodies and including in the model the stiff contact forces originated, this "continuous contact" approach allows the adoption of normal ODE or DAE integrators, requiring little effort on the programming side, which is an important advantage. The immediate disadvantage is that the resulting DAE can be quite stiff, and this in turn leads to a heavy computational burden. Moreover, the need to tune many physical parameters on a case-by-case basis to describe the contact interactions is not always welcome by end users.

The complementarity approach is built on the basis of a mathematical framework able to consistently describe solutions that include nonsmoothness, avoiding the need to formulate stiff regularized problems.

There exist two types of numerical schemes for the integration of these nonsmooth systems: the *event-driven* schemes and the event-capturing, or *time-stepping,* schemes.

The *event-driven* type, is based on a decomposition of the dynamics in the time intervals in which the dynamics is smooth and the discrete events, i.e. times of non-differentiability of the solution. Between events the solutions are differentiable enough, so that any high-order scheme for the solution of ODE or DAE may be used until an event is detected. Detection and localization of the nonsmooth events must be accurate enough so that the order is preserved, and followed by a reinitialization of state, implementing an integrate-detect-restart procedure at each change of status of the contacts. The main drawbacks of this approach are the need of an accurate detection of the time instant at which there is an event, and the fact that they may fail when handling multiple unilateral constraints, because there is no way to guarantee an upper bound on the number of subproblems to solve in finite time intervals, e.g. in presence of Zeno like accumulation phenomena . Also in this framework it is not possible to establish a general convergence proof.

The principle of the *time-stepping* schemes, also described as event-capturing, is to write down a time discretization of the whole dynamical system (the smooth dynamics, the complementarity conditions) and to form a nonsmooth one-step problem which, once solved, allows the scheme to advance from step k to step k + 1, through the solution of a complementarity problem, or a quadratic problem, or a projection algorithm. Convergence results have been proved. The advantages are the ability to

accommodate a large number of events (e.g. accumulations) and the ability to work without accurate detection of the events. A drawback is their low order (higher order methods may be applied in some cases, however, the nonsmoothness brings back the order to one).

This work originates from the interest to add tools for modeling unilateral contacts in the MBDyn Multibody Dynamics software (http://www.mbdyn.org/). MBDyn is a free general purpose Multibody Dynamics analysis software, released under GNU's GPL, developed at the Dipartimento di Ingegneria Aerospaziale of the University "Politecnico di Milano". The aim of this work has been on retaining the robustness and accuracy of the DAE integration implemented in MBDyn software, while adding the capability to deal with frictionless and frictional contacts.

First (2), the continuous contact approach has been considered, and constitutive laws based on this regularization approach have been implemented and tested.

Then an event-capturing method, the nonsmooth contact dynamics, has been considered (3), in order to add a tool for implementing frictionless and frictional contacts in the MBDyn software. A solution that avoided rewriting the general architecture of the MBdyn software, with its accurate and efficient integration method and its versatile library of elements for heterogeneous problems, has been explored (4). This approach, a form of co-simulation, consists in a coupled integration with a part of the model integrated with classic DAE schemes and at the same time a part integrated with time-stepping schemes. It is expected that for suited applications this approach allows for a satisfying solution of the frictional contact problem and retains some of the properties of MBDyn integration in the smooth phases of motion.

A dynamically loaded module for the software MBDyn has been developed and a validation of that approach has been made through a comparison with simple models simulated entirely with state-of-the-art nonsmooth dynamics software Siconos. Then a recently developed method adapting the Newmark-type HHT integration scheme to the nonsmooth framework to obtain a higher order event-capturing integration has been considered (5). The same approach has been applied to the multistep integrator used by MBDyn. A comparison with the two methods and the developed co-simulation has been made on simple examples, and the results have been used to empirically validate this last approach.

A more complex application of aerospace interest has been tested, in order to gain insight to the strenghts and weaknesses of the co-simulation approach, while demonstrating its robustness and versatility (6). An extension of the module developed to include frictional contact ha been developed, and applied to a model of a simple walking mechanism (7).

Chapter 2

A Continuous Contact Approach

A common approach in dealing with the nonsmooth nature of contact phenomena is to apply a smoothing approximation, to replace the nonsmooth governing relationships by a regularization in the description of non-interpenetration and frictional constraints. The non-interpenetrability constraints are replaced by some stiff repulsion laws which take effect as soon as two members of the system come close to each other. A local deformability is assumed and continuous non-impulsive contact forces are integrated in the time-steps during which the contact take place. Models of the constitutive force-displacement law are necessary in order to evaluate this forces.

This automatically handles the possible collisions as long as one considers them elastic, while the dissipation of energy in collisions may be accounted for by adding some damping actions or by using different repulsion laws in the episodes of approach and of separation. It is a popular approach because of the simplicity of implementation in already existing codes for multibody analysis, since it consists in adding stiff contact forces to the DAE equations integrated by standard solvers.

A review of some formulations of the contact force law is presented here. It is followed by the description of an implementation of this approach in MBDyn (http://www.mbdyn.org), a free software for multibody analysis developed at Politecnico di Milano, and by the results of some simple tests, to serve as benchmarks for subsequent comparisons with different approaches.

2.1 Dissipative contact force models

The simplest model to represent the variation of force induced at the surfaces of two bodies in contact is equivalent to that of a parallel spring-damper element. The model is referred to as the Kelvin-Voigt model.

$$F_N = K\delta + D\dot{\delta}$$

where F_N denotes the normal contact force, K is the spring stiffness and δ represents the relative penetration or deformation of the colliding bodies, D is the damping coefficient of the damper and $\dot{\delta}$ represents the relative normal contact velocity.

This model has the advantage of simplicity, but presents weaknesses. The contact force at the moment of impact is not null, due to the damping component which is at its maximum at the beginning of contact. This discontinuous behavior is not realistic because when the contact begins, both elastic and damping force components must be null. Moreover, at the end of the restitution phase, the penetration is null, the relative contact velocity is negative and, thus, the resulting contact force is also negative. This indicates that the bodies in impact must exert tension on each other right before separation, which does not make sense from a physical point of view.

Other popular force models to represent the collision between two bodies are based on the work by Hertz [17], founded on the elasticity theory [15, 45] .

The Hertz theory is restricted to frictionless surfaces and linearly elastic solids, and it is subject to the hypothesis that the zone of contact is of small dimensions in comparison with the radii of curvature of the impacting bodies in its vicinity and that it has a very large radii of curvature in comparison with its linear dimensions.

The force-approach law relates the contact force with a nonlinear power function of penetration or deformation of the colliding bodies δ and is expressed as

$$F_N = K\delta^n$$

The parameters in the model are determined based on the geometric and material properties of the contact surfaces.

For a contact between a sphere i and a plane surface body j, the generalized stiffness parameter depends on the radius of the sphere R_i and the material properties of the contacting surfaces, and can be expressed as

$$K = \frac{4}{3\left(\sigma_i + \sigma_j\right)}\sqrt{R_i} \tag{2.1}$$

in which the material parameters σ_i and σ_j are given by

$$\sigma = \frac{1-\nu^2}{E}$$

The exponent n is set to $\frac{3}{2}$ in cases where there is a parabolic distribution of contact stresses, and can be set either higher or lower for different materials and geometric configurations, using experimental results.

To this strictly elastic reaction a damping term must be added to represent the energy loss during the contact process.

Hunt and Crossley [20] developed a model based on the observation that for

most materials with a linear elastic range and for velocities not exceeding $0.5\,m/s$ the value of the restitution coefficient appears to be related to the initial impact velocity as:

$$e = 1 - \alpha\dot{\delta}^{(-)} \tag{2.2}$$

where e is the restitution coefficient, while $\dot{\delta}^{(-)}$ is the velocity at the moment of impact.

With the assumption that the energy dissipated during the contact is relatively small when compared to the maximum absorbed elastic energy the following expression has been developed:

$$F_N = K\delta^n + K\delta^n \cdot \frac{3}{2}(1-e)\frac{1}{\dot{\delta}^{(-)}} \cdot \dot{\delta} \tag{2.3}$$

The Hunt and Crossley force model expresses the damping as a function of penetration, which sounds physically reasonable. Furthermore, this model does not present discontinuities at the initial instant of contact and at the end of contact, i.e., it starts and ends with zero value.

A similar continuous contact model, using the Hertz contact law together with a hysteresis damping law has been proposed by Lankarani e Nikravesh [28, 27].

It shares with the former law the hypothesis that the energy dissipated during the contact is relatively small compared to the maximum absorbed elastic energy. This assumption results in laws that perform poorly for contacts with a low value of the coefficient of restitution, so the optimal range is for values of the coefficient of restitution close to 1.

Unlike the Hunt and Crossley law the analytical formulation here is not based on the assumption in equation (2.2).

$$F_N = K\delta^n + K\delta^n \cdot \frac{3}{4}\left(1-e^2\right)\frac{1}{\dot{\delta}^{(-)}} \cdot \dot{\delta} \tag{2.4}$$

By analyzing equation (2.3) and equation (2.4), it can be observed that for a perfectly elastic contact, i.e. $e = 1$, the hysteresis damping factor assumes a zero value, while for a perfectly plastic contact, i.e. $e = 0$, the hysteresis damping factor does not assume an infinite value as it would be expected.

More recently, Flores et al. [10] described a contact force model that has a realistic characteristic also for plastic and soft materials. This contact force model was developed with the foundation of the Hertz law together with a hysteresis damping parameter that accounts for the energy dissipation during the contact process.

$$F_N = K\delta^n + K\delta^n \cdot \frac{8}{5}\frac{(1-e)}{e}\frac{1}{\dot{\delta}^{(-)}} \cdot \dot{\delta} \tag{2.5}$$

equation (2.5) shows that for a perfectly elastic contact, i.e. $e = 1$, the value of the hysteresis damping factor is zero, and when the contact is purely plastic, i.e. $e = 0$, the hysteresis damping factor tends to infinity, which is reasonable from a physical point of view and gives a more accurate correspondence between the coefficient of restitution given as input and the effective restitution, particularly for low values of the former.

All these methods require the choice of parameters like K, D, n and e which depend on the geometry and the material of the bodies in contact and which can be the object of experimental study or obtained with a more accurate finite element analysis.

2.2 Implementation of continuous contact in MBDyn

MBDyn is an free general-purpose multibody dynamics analysis software, released under GNU's GPL 2.1 (http://www.mbdyn.org). It features a library of elements that allows to simulate the behavior of heterogeneous mechanical, aeroservoelastic systems. It has been developed at the Dipartimento di Ingegneria Aerospaziale of the University "Politecnico di Milano", Italy.

A penalty method to account for contacts and impacts has been added to MBDyn, following an approach analogous to the one that has been implemented in commercial softwares like MSC ADAMS to deal with contacts through a "penalty" or regularized approach.

In order to be able to examine this approach in subsequent comparisons with other solutions, a module has been developed to implement the Hunt Crossley, Lankarani Nikravesh and Flores et al. formulations in form of constitutive laws to be used in conjunction with 1-dimensional and 3-dimensional deformable elements between the nodes involved in the contact.

Constitutive laws, as implemented in MBDyn, are generic implementations of constitutive relations in the form $f = f(\varepsilon, \dot{\varepsilon})$ to be used by different deformable joint elements, for example a viscoelastic law. The joint elements define how ε and $\dot{\varepsilon}$ are computed from the kinematic of the model, and how the resulting force $f = f(\varepsilon, \dot{\varepsilon})$, given by the constitutive laws, is applied. Constitutive laws are also used in non-structural components, to allow some degree of generality in defining input/output relationships. Therefore it is possible to call different constitutive laws in elements without having to hardcode the same into the element, and so reusing the same implementation for different types of elements. Moreover, the constitutive law has been implemented leveraging the ability of MBDyn of loading dynamic runtime

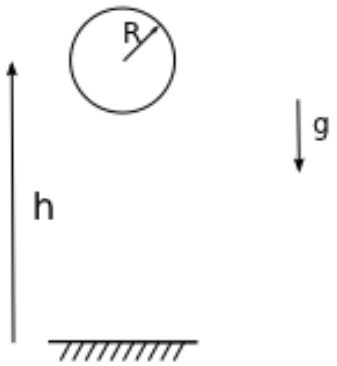

Figure 2.1: Bouncing ball problem

Table 2.1: Bouncing ball problem: parameters

radius R [m]	0.1
height h [m]	1.0
mass m [kg]	1.0
gravity acc. g [m/s]	-9.81
timestep [s]	$1.e-5$
Newton coef. of restitution	0.8

modules through GNU's *libltdl*, so the implementation could be added as a loadable module without altering the base code.

To test the implementation presented it has been applied to some simple examples, often used as benchmark in testing contact problems approaches. It consists of a spherical mass accelerating towards a horizontal plane along its normal due to gravity force. Geometrical and inertial properties of the problem are showed in table 2.1.

A generalized stiffness parameter has been determined using equation (2.1) with the hypothesis that both the ball and the plane material is steel, resulting in $K = 2.4 \cdot 10^{10} N/m^{\frac{3}{2}}$, and the exponent of the Hertz formulation is set to $n = \frac{3}{2}$.

The influence in the use of different dissipative contact force models is illustrated in figure 2.2, 2.3, showing the dynamics computed for two values of the coefficient of restitution: $e = 0.2$ and $e = 0.8$. The results show the vertical position of the ball vs time and the hysteresis plot relative to the first bounce. The correlation between the input and the resulting coefficients of restitution is summarized in 2.4.

The Flores et al. model of equation (2.5) dissipates more energy for low restitution coefficients as shown by the larger hysteresis loop, and as a result the rebounding velocity is lower than with the other contact force models. Hunt and Crossley and Lankarani an Nikravesh model tend to underestimate the energy loss in impacts involving lower values of the restitution coefficient.

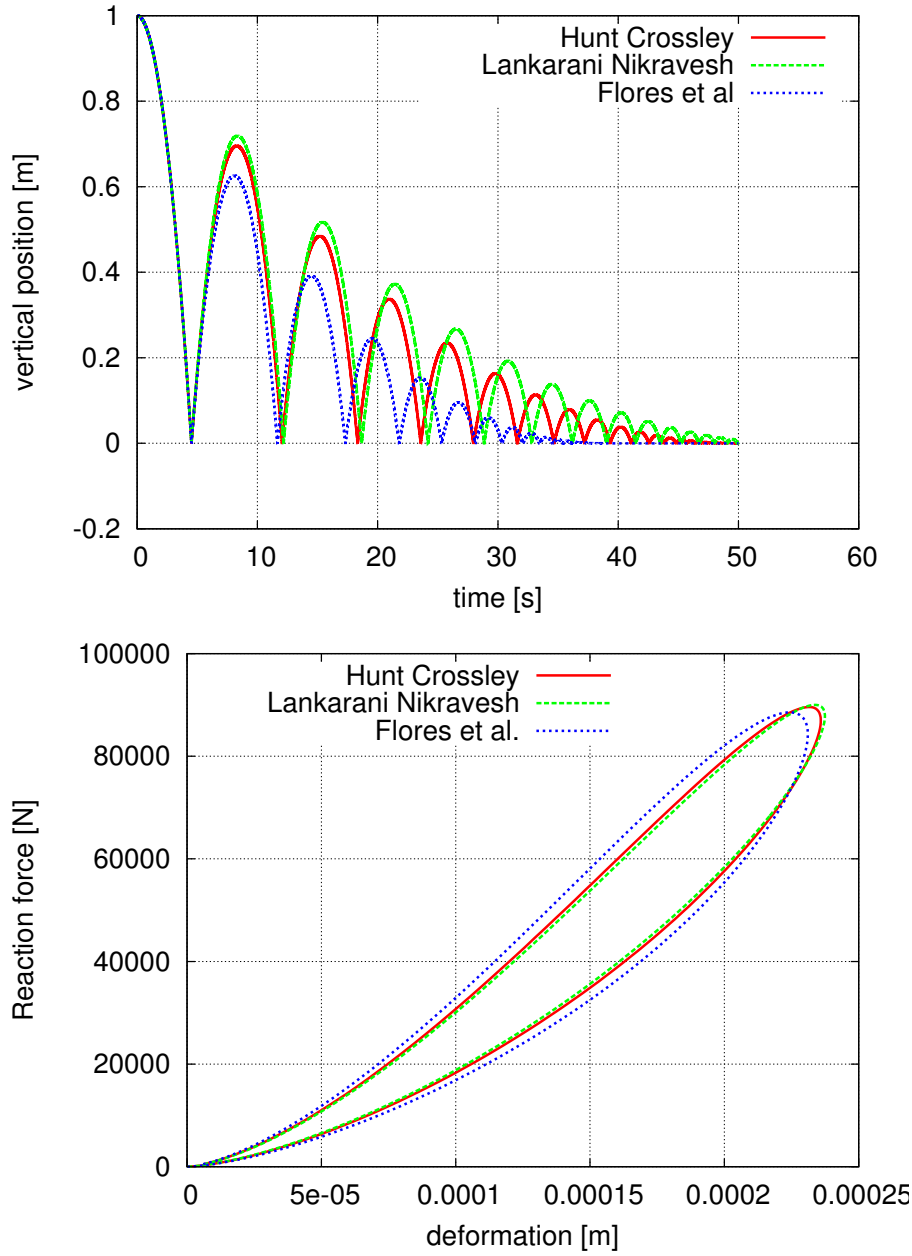

Figure 2.2: Bouncing ball model, coefficient of restitution $e = 0.8$. Vertical position vs time. Force-penetration relation.

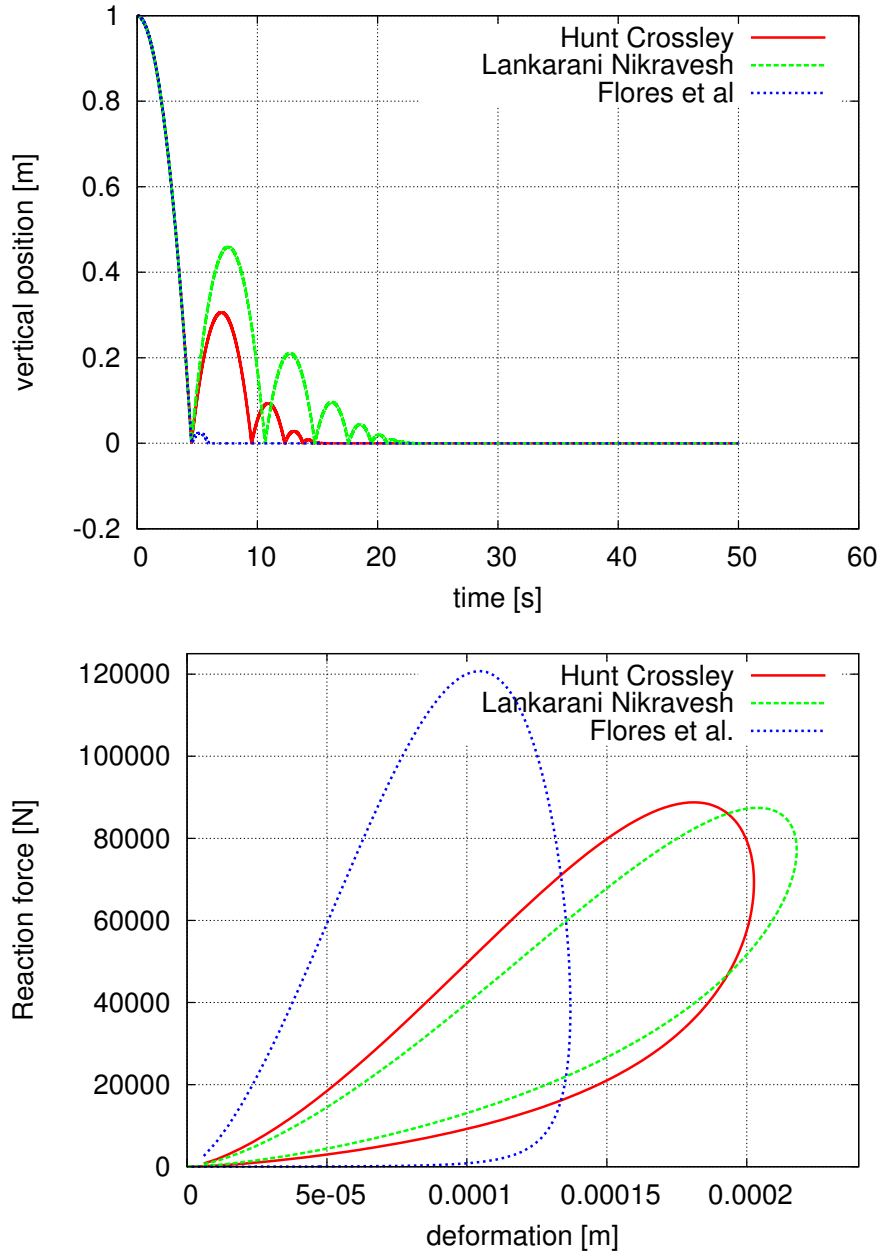

Figure 2.3: Bouncing ball model, coefficient of restitution $e = 0.2$. Vertical position vs time. Force-penetration relation.

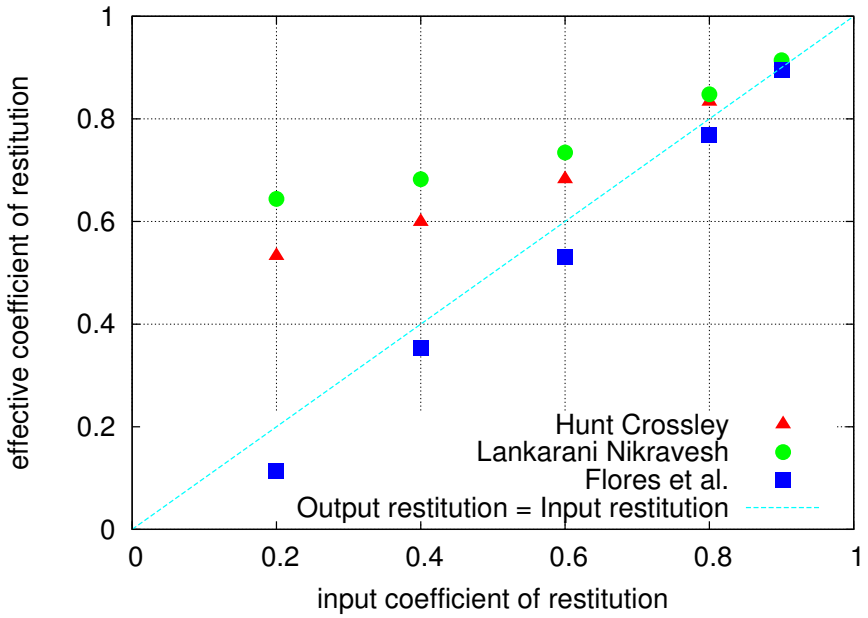

Figure 2.4: Effective dissipation with the three models, function of the input coefficient of restitution

The comparative behavior in terms of the input restitution coefficient and the resulting output responses is illustrated in figure 2.4. The closer the data-points to the 45-degrees dashed line, the more closely the contact force model used represent the contact-impact process.

As indicated in table 2.1 the timestep used for the simulation is very small. It cannot be increased further, since the solution with larger timesteps does not converge, due to the stiffness introduced in the problem. This highlights the immediate disadvantage of the regularization approach, which is that the resulting DAE can be quite stiff. The presented laws are based on a physical interpretation, but may be possible to tune the parameters in order to achieve the desired compromise between accuracy and computational efficiency, but the tradeoff remains. The more accurate the approximation, the stiffer the problem. Also it may not be easy, or convenient for certain applications, to tune the parameters of the smoothing approach.

Chapter 3

Non Smooth Contact Dynamics

3.1 Non Smooth Contact Dynamics framework

In the following it is presented the Non Smooth Contact Dynamics (NSCD) framework. This chapter only describes the framework and the NSCD algorithm, and the steps taken in order to familiarize with the method, while the innovative contribution is the way it will be applied in chapter chapter 4. The approach followed is originated from Moreau and Jean seminal papers [34, 35, 21], and the notation used here to formulate the problem follows a version of the NSCD introduced in [2]. In this section the theory later applied is briefly presented. A frictionless impact law is first illustrated, and the formulation of the dynamics problem in terms of measure differential inclusions and its discretization is shown. The solution of the time discretized problem as an LCP problem is briefly treated. The subsequent section in this chapter illustrates the steps taken to first familiarize with the Non Smooth Contact Dynamics algorithm. An implementation of the NSCD has been first tested on simple examples and compared with state-of-the-art nonsmooth software Siconos's results. A DAE problem reduced to ODE with a direct elimination of Lagrangian multipliers has been solved using standard components of the SiconosKernel library.

Mechanisms involving contacts and impacts between parts can be modeled in terms of multibody systems with unilateral constraints. The simulation of rigid contacts requires the solution of nonsmooth equations of motion: the dynamics is nonsmooth because of the discontinuous nature of non-interpenetration, collision, and adhesion constraints.

An approach that allows for robust and efficient simulation of this problems is the *time-stepping*, or event-capturing, method, originated from the work of J.J.Moreau and M.Jean [34, 35, 21]. In this seminal works the unilateral contact between rigid bodies received a formulation in terms of elementary convex analysis which proves

suitable for computation.

Mathematically, the nonsmooth evolution problems are governed by measure differential inclusions. The directing idea of this contact dynamics approach is that the main object of computation is the velocity function $t \to u \in \mathbb{R}^n$, that has to be a function of locally bounded variation. Time-stepping algorithms essentially have to determine the evolution of this function, by applying the principles of dynamics and the specified force laws. The position function $t \to q$ is only to be updated at each step through adequate integration.

This method has the advantage of not requiring an explicit event handling and accurate collision detection, and accumulations of events or a large number of events in finite time are handled without difficulties. Furthermore, the convergence analysis of this family of schemes leads to existence of solutions for rather complicate systems [31, 40]. The numerical algorithms that can be obtained are robust and efficient, and efficiency is the main advantage over the penalty methods that require the inclusion of stiff forces to the problem and are impractical for problems with a high number of unilateral constraints. The main drawback of this approach is that the solutions have only first order accuracy.

Here are considered velocity-impulse LCP-based time-stepping methods. The introduction of inequalities in time-stepping schemes for Differential Variational Inclusions, leads to linear complementarity problems (LCP), which are systems of complementary inequalities to be satisfied simultaneously. These LCP problems must be solved at each time step in order to advance the integrator.

There exist different classes of LCP solvers. For a detailed overview of Complementarity Problem solvers see [2]. It is considered for the implementations in this chapter and in chapter 5 a quite straightforward solver based on simplex methods, also known as direct or pivoting methods, originating from the algorithms of Lemke and Dantzig.

Three-dimensional Coulomb friction problems result in nonlinear complementarity problems (NCP). It is possible, through the use of a polyhedral approximation to morph the friction cones as faceted friction pyramids, to cast the NCP into an LCP, and solve it in a way not dissimilar to the frictionless method presented here.. This approach to the frictional problem is the one chosen for extending the co-simulation approach to frictional cases in chapter 7 because of the simplicity of its implementation. This solution is not optimal because it introduces artificial anisotropy in the friction phenomenon, and augment the dimensions of the problem to solve, but it is meant to be applied to multibody problems with a limited number of unilateral constraints.

3.1.1 Frictionless impact law

A formulation of a frictionless impact law to be used in the following is explained here.

There are at least two historical approaches to impacts: Newton's kinematic impact law, which reverses the sign of the relative velocity at the impact and takes into account dissipation with a coefficient $0 < \varepsilon < 1$

$$v^+ = -\varepsilon v^-$$

and Poisson's impact law, which requires a decomposition of the impact process into a compression phase ($^-$) and a decompression phase ($^+$) in order to define the restitution coefficient ε by the ratio of the corresponding impulsive forces,

$$\Lambda^{(+)} = \varepsilon \Lambda^{(-)}$$

A complete review of the frictionless collision problem in rigid-body dynamics can be found in [14].

Let us now state the unilateral version of Newton's impact law for a single contact

.

Having defined $\boldsymbol{r}_D$ as the distance between the two proximal points between two bodies and $\boldsymbol{n}$ as the normal to one of the points coming in contact we can write the gap function defining the unilateral constraint as:

$$g(\boldsymbol{q}, t) = \boldsymbol{n}^T \boldsymbol{r}_D \geqslant 0$$

And its derivative $\dot{g}$, the normal relative velocity, as:

$$\dot{g} = \boldsymbol{n}^T (\boldsymbol{v}_{C_1} - \boldsymbol{v}_{C_2})$$

where $\boldsymbol{v}_{C_i}$are the absolute velocities of the rigid-body contour points involved in the contact.

The post- and pre-impact normal relative velocities, bounded variation functions (functions admitting a numerable set of discontinuities and having both a left and right limit for every time instant t), with possible discontinuities reflecting the impact, can be expressed as:

$$\dot{g}^{\pm} = \boldsymbol{H}^T(\boldsymbol{q}, t) \cdot \boldsymbol{u}^{\pm} + \hat{w}$$

The problem will be now stated in a form suitable to describe systems with multiple contacts.

We assume a total of m simple unilateral constraints $g_i(\boldsymbol{q}, t) > 0$ defining, for

any fixed time t, the feasible displacements C , and denote by I_a the active set at a probable impact event$(\boldsymbol{q}_0, t_0)$.

$$C := \{\boldsymbol{q} | g_i(\boldsymbol{q}_0, t_0) \geqslant 0, i = 1, ..., m\} \qquad I_a := \{i | g_i(\boldsymbol{q}_0, t_0) = 0\}$$

Newton's impact equations for a multi-contact configuration then read :

$$\boldsymbol{M}(\boldsymbol{u}^+ - \boldsymbol{u}^-) = 0 \quad if\, g > 0 \tag{3.1}$$

$$\boldsymbol{M}(\boldsymbol{u}^+ - \boldsymbol{u}^-) = \textstyle\sum_{i \in I_a} \boldsymbol{H_i \Lambda_i}, \quad (i \in I_a), \quad if\, g \leq 0 \tag{3.2}$$

$$\dot{g_i}^+ + \varepsilon_i \dot{g_i}^- \geqslant 0, \;\; \boldsymbol{\Lambda}_i \geqslant 0, \;\; (\dot{g}_i^+ + \varepsilon_i \dot{g}_i^-) \cdot \boldsymbol{\Lambda}_i = 0 \tag{3.3}$$

equation (3.1) concerns the case of open contact.

With a closed contact the equation (3.2) is derived from the Newton Euler or Lagrange equations, formulated as an equality of measures and integrated over a singleton $\{t_0\}$, in which a jump in velocity may happen. Together with equation (3.2), equation (3.3) is a complementarity condition expressing the following physical behavior. The impulsive force, if there is any, should act as a compressive magnitude, $\boldsymbol{\Lambda} \geq 0$. In the case of a non-vanishing impulse ($\boldsymbol{\Lambda} > 0$) we apply Newton's impact law as usual, i.e. $\dot{g}^+ = -\varepsilon \dot{g}$, which is expressed by the third condition in equation (3.3). The magnitude ε denotes Newton's coefficient of restitution with the usual values $0 \leq \varepsilon \leq 1$. The case $\varepsilon = 0$ corresponds to a completely inelastic impact with vanishing post-impact relative velocity ($\dot{g}^+ = 0$), whereas $\varepsilon = 1$ represents a completely elastic impact at which the relative velocity $\dot{g}^+$ is inverted $\dot{g}^+ = -\dot{g}^-$.

Suppose now that, for any reason, the contact does not participate in the impact, i.e. that the value of the impulsive force is zero, although the contact is closed. This happens normally for multi-contact situations as explained in the next paragraph. For this case we allow post-impact relative velocities higher than prescribed by Newton's impact law in the case of a non-vanishing impulse, $\dot{g}^+ = -\varepsilon \dot{g}^-$, in order to express that the contact is superfluous and could be removed without changing the contact-impact process. The graph of Newton's impact law in inequality form is depicted in figure 3.1 and is a unilateral primitive moved horizontally and expressed by the complementarity conditions $\Lambda > 0$, $\dot{g}^+ + \varepsilon \dot{g}^- > 0$, $\Lambda \cdot (\dot{g}^+ + \varepsilon \dot{g}^-) = 0$.

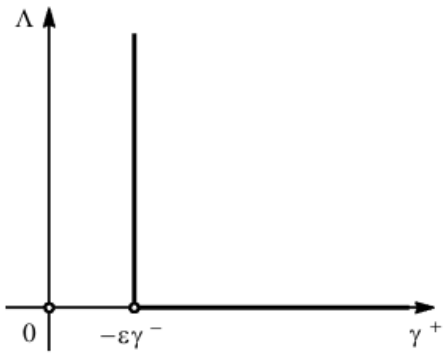

Figure 3.1: Newton's impact law *(figure from [14])*

In multi-contact problems there may be configurations at which no impulses are transferred at the contacts, although they are or have just been closed. There are two different classes of multi-contact impact problems which usually occur in combination and which are here illustrated by an example each.

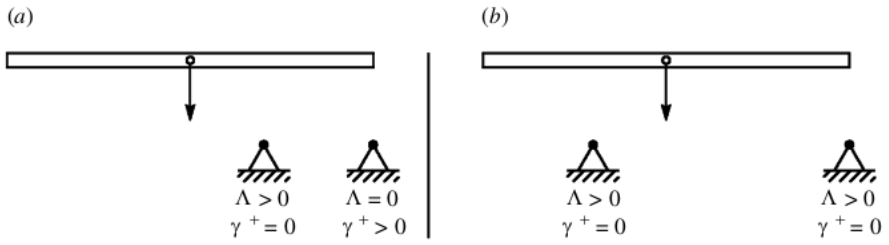

Figure 3.2: Impact of a rod against two obstacles *(figure from [14])*

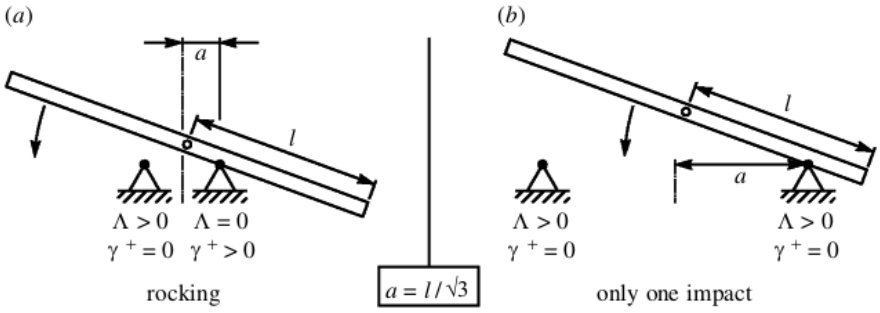

Figure 3.3: Rocking rod example *(figure from [14])*

The first class is characterized by the event that several contacts close at the same time, such as the rigid rod which impacts with two obstacles as depicted in figure 3.2. Note that it depends on the displacements of the obstacles relative to the rod whether impulses are transferred or not. When the obstacles are arranged on different sides of the rod's center of mass, one has $\Lambda > 0$ for both contacts and thus, for a completely inelastic impact ($\varepsilon = 0$) vanishing post-impact velocities

$\gamma^+ = 0$. This situation is depicted in figure 3.2b. In figure 3.2a both obstacles lie on the right-hand side of the rod. Here, the right obstacle does not participate in the impact and could be removed without changing the impact process. No impulse is transferred, and the associated relative velocity is greater than zero although $\varepsilon = 0$ has been chosen. This is due to the impulse acting from the left obstacle on the rod, which makes the rod also turn. Thus, the rod remains in contact with the left obstacle after the impact, but rotates counterclockwise and separates from the right obstacle.

The second class concerns impact problems at which impulsive forces at closed contacts or even separation processes are induced by other collisions. Both events may be seen from the example of a rocking rod ($\varepsilon = 0$) in figure 10. For small values of the distance between the obstacles ($a < l/\sqrt{3}$) the rod is rocking by an alternate turning around the two contact points (figure 3.3a). A collision with one of the obstacles causes an instantaneous detachment at the other contact with no impulse being transferred there. Note that completely inelastic impacts ($\varepsilon = 0$) at both contacts are assumed, leading to a loss of kinetic energy after each impact and finally, when the infinite impact sequence has been passed, to a state where the rod rests on both obstacles. In figure 3.3b the distance between the two obstacles is chosen large enough ($a > l/\sqrt{3}$) to admit a compressive impulse $\mathbf{\Lambda} > 0$ at both contacts, produced by the single collision of the rod against the left obstacle. Due to completely inelastic behavior ($\varepsilon = 0$) the rod stops turning immediately after this very first impact and is never moving again. The critical value $a >= l/\sqrt{3}$ at which rocking changes to a single impact corresponds to the situation where the generalized force directions H associated with the two contact points becomes orthogonal with respect to the inner product on the cotangent space at the displacements of impact.

3.1.2 Discretization of the equations of motion

In the following the equations of motion, usually written as differential equations, will be formulated in terms of equality of measures. Theory of measures provides a theoretically sound generalization to describe "impulses+finite forces" solutions and to formulate a theory of convergence for this solutions. The dynamics of systems of rigid bodies with unilateral constraints (contacts) and friction originates impulsive forces. The moment an impact happens, the velocity of a body changes instantaneously, and that requires impulsive forces, contrary to what happens to deformable bodies, and the acceleration cannot be defined as the usual second derivative of q. Time stepping methods are based on using the integrals of the forces over each integration step instead of the instant value of the functions that describe the forces. That way there isn't a clear distinction between finite forces and impulses, and the

latter can therefore be treated the same way. Velocities and impulses become the primary variables. Within this framework, *timestepping* methods consist in a time-discretization of the dynamics which can be advanced from step k to step $k+1$ by solving specific one-step nonsmooth problems (complementarity problems). A brief survey of *timestepping* methods can be found in [41], while a complete tractation is in [2].

We consider here a model including contacts without friction, for sake of simplicity, and whose equations of motion are derived from Lagrange formulation.

Let $\boldsymbol{q} = (q_1, ..., q_N) \in R^N$ be the generalized coordinates vector of a collection of n_b rigid bodies, with $N = 6n_b$. For simplicity, we assume that the eventually bilateral constraints imposed to the system have already been taken into account by reducing the size of $\boldsymbol{q}$.

Here the use of bold typography to indicate vectors or matrices is dropped in order to lighten the notation. The equation of motion for the general case is:

$$\begin{cases} M(q(t))d\nu + N(q(t), \nu^+(t))dt + F_{int}(t, q(t), \nu^+(t))dt = F_{ext}(t)dt + dr \\ \nu^+(t) = \dot{q}^+(t) \\ q(0) = q_0, \;\; \dot{q}(0^-) = \dot{q}_0 \end{cases}$$

These equations contain a Lebesgue-measurable part for the continuous components and an atomic part based on a Dirac point measure for the impact parts.

The measure for the velocities $d\nu$ can be split in a Lebesgue-measurable part $u \cdot dt$, which is continuous, and the atomic parts which occur at the discontinuity points, with the left and right limits u^+ and u^- and the Dirac point measure δ. Similarly, the measure for the impulses is defined as dr.

The case of linear time invariant dynamics is treated here, but the framework is extendable to nonlinear dynamics by means of linearization and Newton iteration solution.

With a lighter notation we can write:

$$\begin{cases} Md\nu + (Kq(t) + C\nu^+(t))dt = F_{ext}(t)dt + dr \\ \nu^+(t) = \dot{q}^+(t) \\ q(0) = q_0, \;\; \dot{q}(0^-) = \dot{q}_0 \end{cases}$$

We thus proceed to the time discretization of the dynamics. Applying the integral on the timestep $(t_k, t_{k+1}]$ of length $h > 0$, it yields:

$$\begin{cases} \int_{(t_k,t_{k+1}]} M d\nu + \int_{(t_k,t_{k+1}]} (Kq(t) + C\nu^+(t))dt = \int_{(t_k,t_{k+1}]} F_{ext}(t)dt + \int_{(t_k,t_{k+1}]} dr \\ q(t_{k+1}) = q(t_k) + \int_{(t_k,t_{k+1}]} \nu^+(t)dt \end{cases}$$

The first term is discretized by applying the definition of the differential measure $d\nu$:

$$\int_{[t_k,t_{k+1}]} M\, d\nu \approx M\left(\dot{q}\left(t_{k+1}\right) - \dot{q}\left(t_k\right)\right)$$

The approximation $M(q) \simeq M(q_{k+\gamma})$ with $\gamma \in [0,1]$ is used, where it is defined $q_{k+\gamma} = (1-\gamma)q_k + \gamma q_{k+1}$.

A θ-method, a first order scheme, is applied to the remaining terms. Stability considerations imply choosing $0.5 \leqslant \theta \leqslant 1$.

$$\int_{[t_k,t_{k+1}]} (C\dot{q} + Kq\,)dt \approx h\left[\theta\left(C\dot{q}_{k+1} + Kq_{k+1}\right) + (1-\theta)\left(C\dot{q}_k + Kq_k\right)\right]$$

$$\int_{[t_k,t_{k+1}]} F_{ext}\left(t\right)\, dt \approx h\left[\theta F_{ext}\left(t_{k+1}\right) + (1-\theta)\, F_{ext}\left(t_k\right)\right]$$

The generalized positions, which are absolutely continuous function, whereas velocity is a function of bounded variations, are approximated with the same $\theta - method$:

$$q_{k+1} = q_k + h\left[\theta\dot{q}_{k+1} + (1-\theta)\,\dot{q}_k\right]$$

Let's define $p_{k+1}$the approximated integral of the impulsive forces on the timestep: $\int_{(t_k,t_{k+1}]} dr$

Finally this expression is obtained:

$$\hat{M}\left(\dot{q}_{k+1} - \dot{q}_k\right) = -hC\dot{q}_k - hKq_k - h^2\theta K\dot{q}_k + h\left[\theta F_{ext}\left(t_{k+1}\right) + (1-\theta)\, F_{ext}\left(t_k\right)\right] + p_{k+1}$$

where $\hat{M} = [M + h\theta C + h^2\theta^2 K]$

Regrouping the equation to highlight the unknowns leads to the formulation:

$$\dot{q}_{k+1} = \dot{q}_{free} + \hat{M}^{-1} p_{k+1}$$

where $\dot{q}_{free}$ is the velocity of the unconstrained system.

Now it a discretization of the impact law of equation (3.3) is to be introduced.

In order to obtain that it is helpful to consider a transformation from generalized coordinates to local coordinates.

Generally speaking, for each contact α there exists a relation/mapping $H(q)$ between the relative velocity in correspondence of the contact, U, and the generalized variable representing velocity v.

Thus assuming the components of the relative velocity $U = \begin{pmatrix} U_T \\ U_N \end{pmatrix} \in \mathbb{R}^3$ and the components of the local reaction $R = \begin{pmatrix} R_T \\ R_N \end{pmatrix} \in \mathbb{R}^3$, we can write:

$$U^\alpha = H^{\alpha T}(q) \cdot \nu$$

$$p^\alpha = H^{\alpha T}(q) \cdot P^\alpha$$

The gap function, which gives the distance between the points that come to contact in the unilateral constraint α, is defined as $g^\alpha(q)$.

The discretized Newton law of impact expressed in local coordinates becomes:

$$\begin{cases} if\ g^\alpha(q_{k+1}) \leqslant 0 & then\ \ 0 \leqslant P^\alpha_{N,k+1} \perp U^\alpha_{N,k+1} + e^\alpha U^\alpha_{N,k} \geqslant 0 \\ if\ g^\alpha(q_{k+1}) > 0 & then\ \ P^\alpha_{N,k+1} = 0 \end{cases}$$

Based on the stated discretization and on the local coordinates previously introduced we can formulate the discretized problem as:

$$U_{N,k+1} = \hat{W}_{NN} P_{N,k+1} + U_{N,free}$$

Where $\hat{W}_{NN} = H_N^T \hat{M}^{-1} H_N$ is the so-called Delassus operator.

We expressed the relative velocity in function of the reaction due to the contact, so the frictionless problem can be cast in the terms of a Linear Complementarity Problem (LCP).

A usual definition of this problem can be formulated as follows:

Linear Complementarity Problem (LCP). Given $M \in R^{n \times n}$ and$q \in R^n$, find a vector $z \in R^n$ such that

$$0 \leq z \perp Mz + q \geq 0$$

The inequalities have to be understood componentwise and the relation $x \perp y$ means $x^T y = 0$.

In this case the variable z of the problem is $P_{N,k+1}$, M is $\hat{W}_{NN}$ and q is $U_{N,free}$. This is the One Step Non-Smooth Problem to be solved at each step of integration.

3.1.3 The NSCD algorithm

We present here a simple algorithm for the solution of Non Smooth Contact Dynamics proposed in [2]. It derives from the classic timestepping scheme from Moreau and Jean [21], and it will be used in the module developed in chapter 4 and in chapter 7, in the latter with a different formulation of the One Step Nonsmooth Problem to accomodate for a LCP based formulation of the frictional problem. A large variety of solvers exists for the LCP problem to be solved at each timestep. A complete range of solvers is available in state-of-the-art software library SiconosNumerics, cited in section 3.2.1 and used in the implementation in chapter 4. A comprehensive survey of solving strategies for complementarity problems is in [2].

Algorithm 3.1 Nonsmooth Contact Dynamics algorithm, *(from [2])*

Require: M,K,C,F_{ext} defining the linear dynamics
Require: H^α, g^α for each $\alpha \in I = \{1, ..., \nu\}$, the kinematics relations
Require: e, μ parameters of restitution and friction
Require: t_0, T
Require: q_0, ν_0
Require: h, θ, γ

$k \leftarrow 0$
$U_0 \leftarrow H^T \nu_0$
$\hat{M} \leftarrow [M + h\theta C + h^2\theta^2 K]$
$\hat{W}^{\alpha\beta} \leftarrow H^{\alpha T} \hat{M}^{-1} H^\beta$, $(\alpha, \beta) \in \{1, ..., \nu\}^2$
while $t_k < T$ do
  $\nu_{free} \leftarrow \nu_k + \hat{M}^{-1}[-hC\nu_k - hKq_k - h^2\theta K\nu_k + h[\theta(F_{extk+1}) + (1-\theta)(F_{ext})_k]]$
  //Update of the index set of forecast active constraints
  $\tilde{q}_{k+1} \leftarrow q_k + h\gamma\nu_k$
  $I_a(\tilde{q}_{k+1}) \leftarrow \{\alpha \in I \mid g^\alpha(\tilde{q}_{k+1}) \leqslant 0\}$
  for $\alpha \in I_a$ do
    $U_{free} \leftarrow H^T \nu_{free}$
    Assemble (if necessary) $\hat{W}$
  end for
  if $I_a \neq 0$ then
    $[U_{k+1}, P_{k+1}] \leftarrow solution\, of\, OSNSP$
  end if
  //State update
  $p_{k+1} \leftarrow \sum_{\alpha \in I_a} H^\alpha P^\alpha_{k+1}$
  $\nu_{k+1} \leftarrow \nu_{free} + \hat{M}^{-1} p_{k+1}$
  $q_{k+1} \leftarrow q_k + h[\theta\nu_{k+1} + (1-\theta)\nu_k]$
  $t_k \leftarrow t_{k+1}$
  $k \leftarrow k + 1$
end while

3.2 Some exploration steps

Three simple tests have been conducted and described here in order to gain familiarity with the approach in question.

First two benchmark problems have been simulated using the tools of an open source software, Siconos (http://siconos.gforge.inria.fr), dedicated to implement high end libraries to model and solve a large class of nonsmooth problems. Subsequently an implementation of the algorithm described in 3.1 has been made in Octave (http://www.octave.org), a Matlab-like scripting language, and a comparison has

been made to validate both the algorithm and the Siconos models. Both the models and the results are presented in section 3.2.2, while a short presentation of the Siconos software is given in section 3.2.1.

Finally since the modeling tools of Siconos at the time of this study didn't allow the creation of bilaterally constrained models, a technique to reduce a differential algebraic model to a simple ODE has been applied before the discretization of a nonsmooth problem with a time-stepping algorithm. The method proved successful for simple tests.

3.2.1 The Siconos Library

The Siconos Platform (http:\\siconos.gforge.inria.fr) is a scientific computing software dedicated to the modeling, simulation, control, and analysis of nonsmooth dynamical systems (NSDS), mainly developed in the Bipop team-project at INRIA in Grenoble, France, and distributed under GPL GNU license. Siconos aims at providing a general and common tool for nonsmooth problems in various scientific fields like applied mathematics, mechanics, robotics, electrical circuits, and so on. However, the platform is not supposed to re-implement the existing dedicated tools already used for the modeling of specific systems, but to possibly integrate them.

Siconos is composed of three main parts: Numerics, Kernel and Front-End. The SiconosKernel library is the core of the software, providing high-level description of the studied systems and numerical solving strategies. It is fully written in C++, using extensively the STL utilities. The SiconosNumerics library holds all low-level algorithms, to compute basic well-identified problems (ordinary differential equations, LCP, QP, NCP, etc...). The last component, Siconos Front-End, provides interfaces with some specific command-languages such as Python or Scilab. This to supply more pleasant and easy-access tools for users, during pre/post-treatment. Front-End is only an optional pack, while the Kernel cannot work without Numerics.

3.2.2 Implementation in Octave and comparison of results

In order to gain understanding of the NSCD algorithm for further application some simple tests have been implemented in Octave. The results have been compared with the same models implemented through the Siconos Kernel and Siconos Numerics library.

Two simple problems are presented here.

The first simulation involves a the problem of a ball falling on a tilted plane. The problem is illustrated in figure 3.4 and the geometrical values and the parameters used in the simulation are presented in table 3.1.

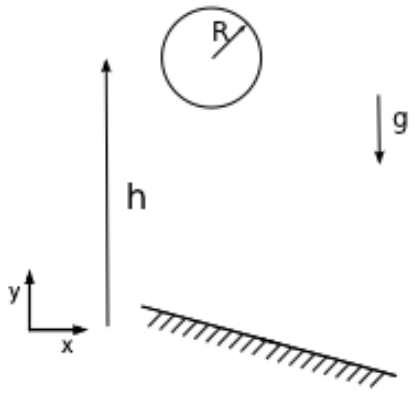

Figure 3.4: Ball on a tilted plane: geometry of the problem

Table 3.1: Ball on a tilted plane: parameters

radius R [m]	0.1
tilt angle [rad]	0.05
height h [m]	1.0
mass m [kg]	1.0
gravity acc. g [m/s]	-9.81
timestep [s]	$1.e-3$
Newton coef. of restitution	0.8

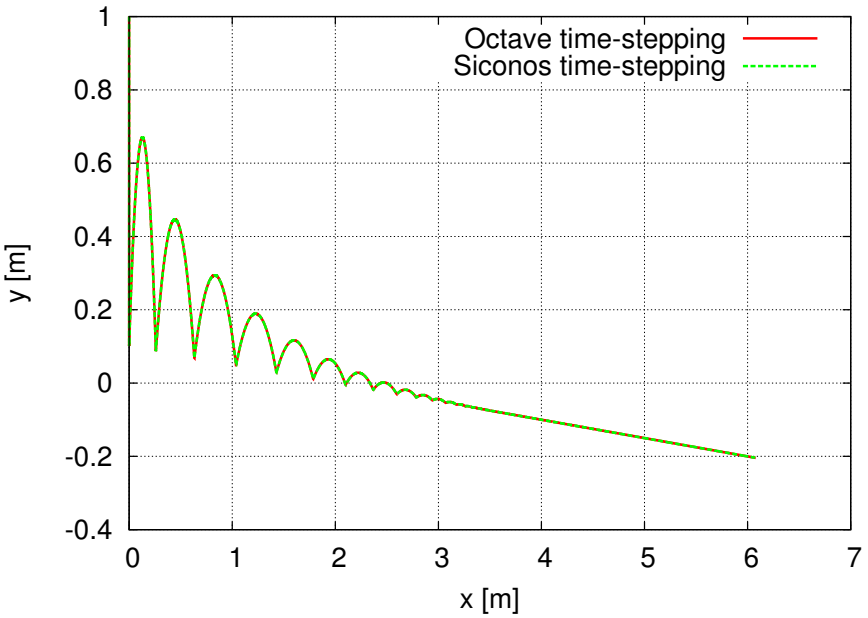

Figure 3.5: Ball on a tilted plane: position. Results are coincident

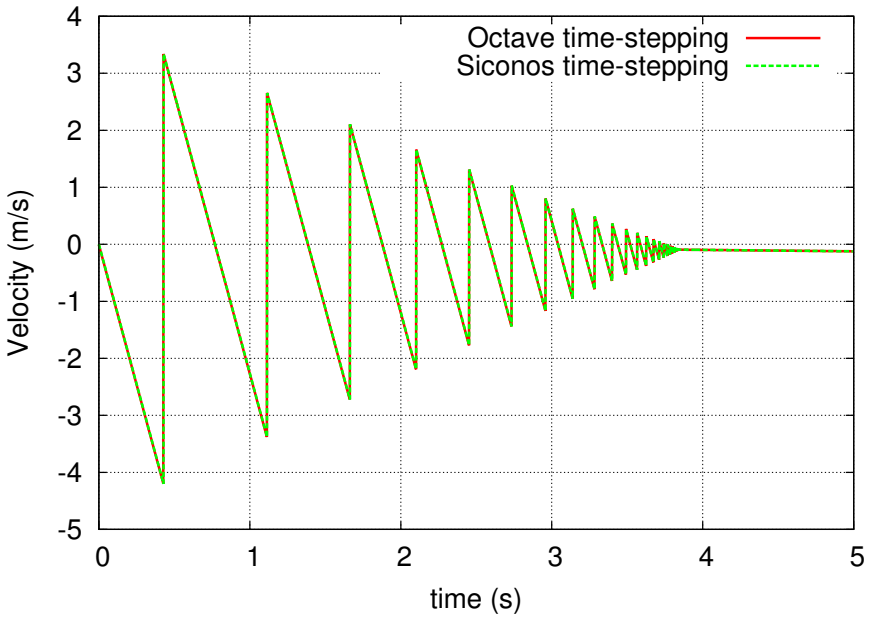

Figure 3.6: Ball on a tilted plane: vertical velocity. Results are coincident

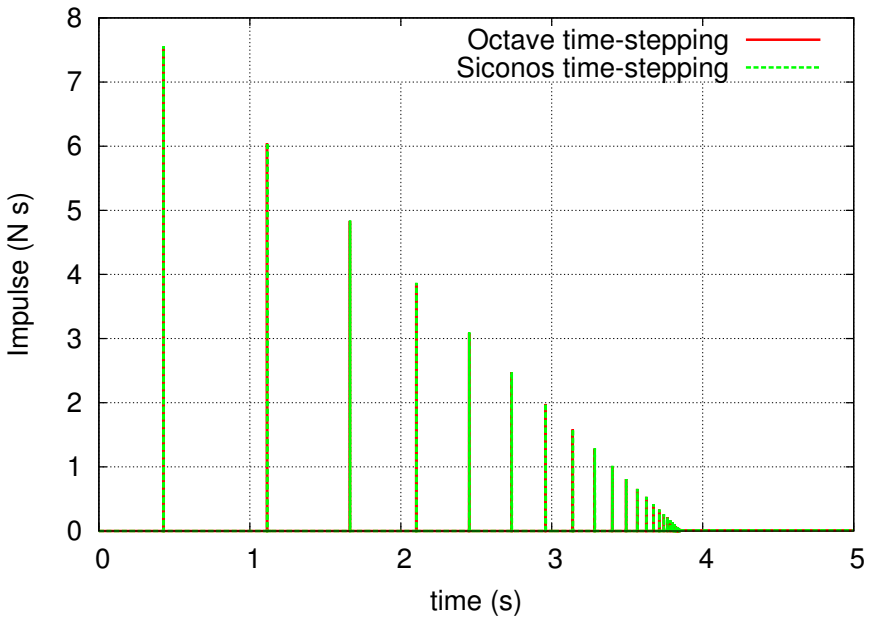

Figure 3.7: Ball on a tilted plane: impulse. Results are coincident

Another problem was simulated in order to validate the algorithm with respect to the constraints assembly and is illustrated in figure 3.8. The ball now falls with the geometrical center in line with the point where the two slopes are touching. At the moment of contact two geometrical unilateral constraints are to be satisfied. The parameters of the simulation are the same as in table 3.1.

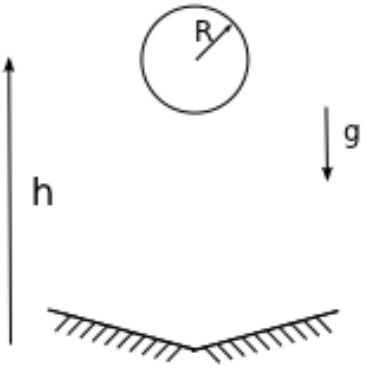

Figure 3.8: Double impact problem: geometry of the problem

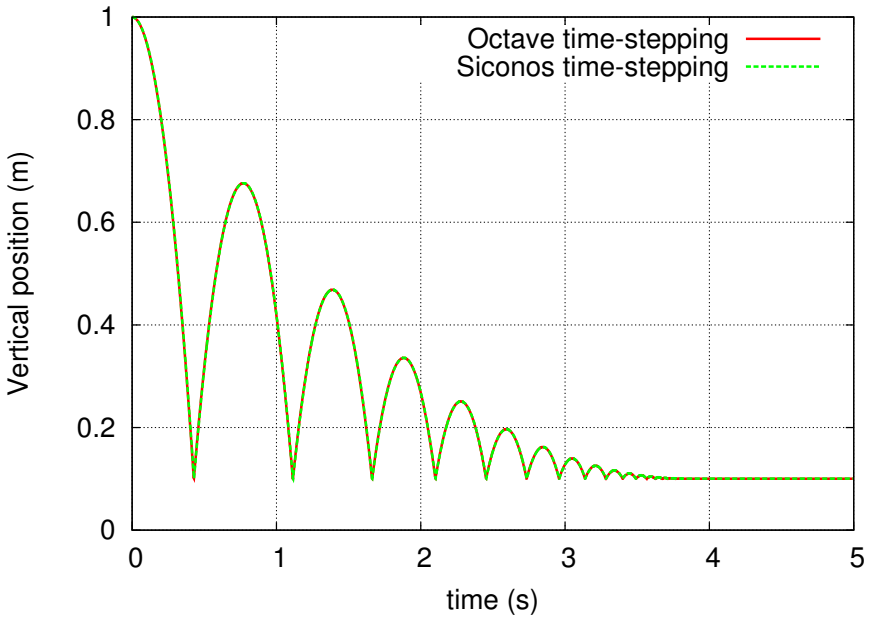

Figure 3.9: Double impact problem: vertical position. The results are coincident

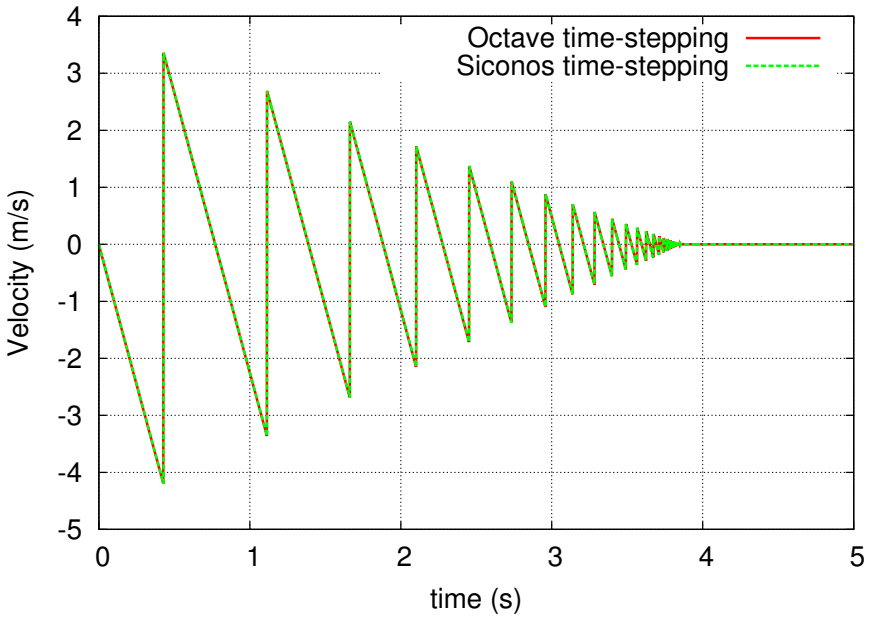

Figure 3.10: Double impact problem: vertical velocity. The results are coincident

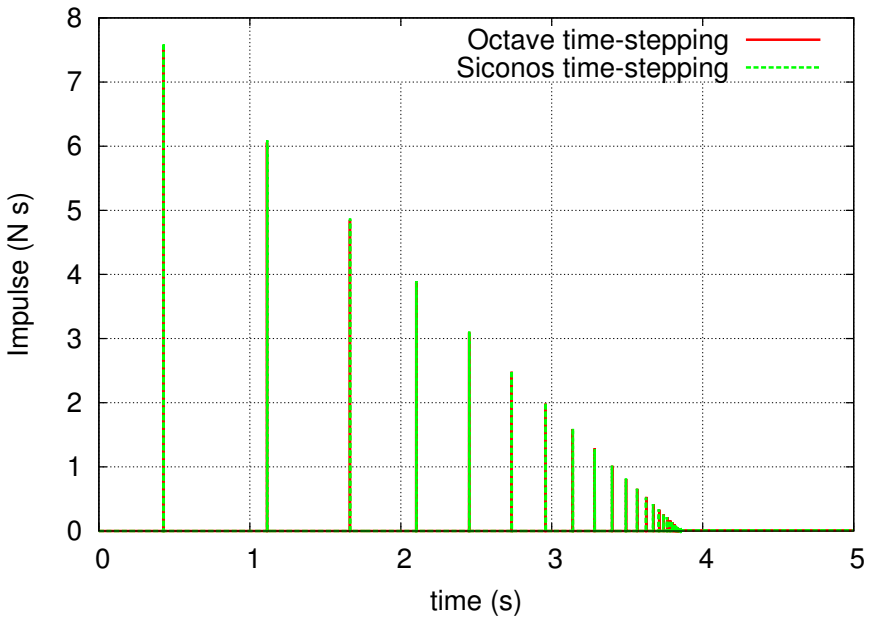

Figure 3.11: Double impact problem: impulse. The results are coincident

3.2.3 Application to a DAE problem through Direct Elimination of Lagrange Multipliers

The Siconos Kernel libraries do not allow the implementation of bilaterally constrained models at the time of writing. An example has been developed to test the use of a technique for reducing a DAE system to ODE in conjunction with the Siconos software in order to solve a problem with both bilateral and unilateral

constraints.

The method of Direct Elimination of Lagrange Multipliers [46, 11] has been used together with Baumgarte stabilization [3]. A Lagrangian system has been obtained, which has been implemented together with the unilateral constraint with the Siconos Kernel library.

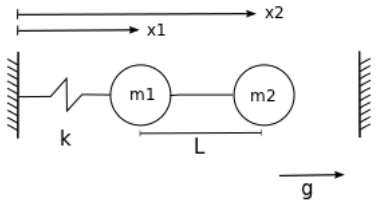

Figure 3.12: DAE problem illustration.

The problem considered is illustrated in figure 3.12 and can be expressed with the following equations:

$$\begin{cases} m_1 \cdot \ddot{x}_1 + r(\dot{x}_1 - \dot{x}_0) + k(x_1 - x_0) - \lambda & = +m_1 g \\ m_2 \cdot \ddot{x}_2 + \lambda & = +m_2 g + p_{ns} \\ x_2 - x_1 & = L \end{cases}$$

We therefore have a problem in the form:

$$\begin{cases} M\ddot{q} + C\dot{q} + Kq + A^T\lambda & = F \\ Aq + b & = 0 \end{cases}$$

described by the following matrixes:

$$M = \begin{bmatrix} m_1 & 0 \\ 0 & m_2 \end{bmatrix} \qquad C = \begin{bmatrix} r_1 & 0 \\ 0 & 0 \end{bmatrix} \qquad K = \begin{bmatrix} k_1 & 0 \\ 0 & 0 \end{bmatrix}$$

$$A = \begin{bmatrix} -1 & 1 \end{bmatrix} \qquad F = \begin{bmatrix} m_1 g + k_1 x_0 + r_1 \dot{x}_0 \\ m_2 g + p_{ns} \end{bmatrix}$$

with $q = \begin{Bmatrix} x_1 \\ x_2 \end{Bmatrix}$

In order to reduce the number of equations to the number of independent degrees of freedom we apply the method of Direct Elimination of Lagrange multipliers, consisting in the following steps:

1. the constraints equation is derived two times

2. $\ddot{q}$ is substituted in the dynamics equations to obtain an expression for λ

3. λ is substituted in the dynamics equations.

To make sure that not only the second derivative of the constraints but also the constraint equation is enforced, the differential equation obtained from the constraints is replaced by the Baumgarte equation:

$$\ddot{\phi} + 2 \cdot \alpha\dot{\phi} + \beta^2\phi = 0$$

where the derivatives are:

$$\phi(q) = 0 = Aq + b$$

$$\dot{\phi}(q) = 0 = \dot{A}q + A\dot{q} + \dot{b} = A\dot{q}$$

$$\ddot{\phi}(q) = 0 = \ddot{A}q + 2\dot{A}\dot{q} + A\ddot{q} + \ddot{b} = A\ddot{q}$$

So the problem becomes:

$$\begin{cases} M\ddot{q} + A^T\lambda & = Q(q, \dot{q}, t) \\ A\ddot{q} & = b'' \end{cases}$$

where

$$Q(q, \dot{q}, t) = F - C\dot{q} - Kq$$

$$b'' = -2\alpha A\dot{q} - \beta^2(Aq + b)$$

Direct Lagrange Elimination is then applied:

$$\ddot{q} = M^{-1}Q - M^{-1}A^T\lambda$$

$$AM^{-1}Q - AM^{-1}A^T\lambda = b''$$

$$\lambda = (AM^{-1}A^T)^{-1} \cdot (AM^{-1}Q - b'')$$

and substituting this expression for λ in the dynamics equation:

$$M\ddot{q} = (I - A^T(AM^{-1}A^T)^{-1} \cdot AM^{-1})Q + A^T(AM^{-1}A^T)^{-1} \cdot b''$$

For brevity we rename:

$$P = (I - A^T(AM^{-1}A^T)^{-1} \cdot AM^{-1})$$

and after replacing the definitions of Q and $b''$and regrouping it is possible to express the dynamics in the form of a Lagrangian system:

$$M\ddot{q} + C\dot{q} + Kq = \widetilde{F}$$

where

$$K = P \cdot K + A^T(AM^{-1}A^T)^{-1} \cdot \beta^2 A$$

$$C = P \cdot C + A^T(AM^{-1}A^T)^{-1} \cdot 2\alpha A$$

$$\widetilde{F} = P \cdot F - A^T(AM^{-1}A^T)^{-1} \cdot \beta^2 b$$

The principle of the Baumgarte method is based on the damping of acceleration of constraints violation by feeding back the position and velocity of constraint violation as in a closed loop system.

In general if α and β are chosen positive constants, the stability of the general solution is guaranteed, and when α is equal to β critical damping is achieved.

Baumgarte [3] showed that $\alpha = \beta = 5$ is a suitable choice for multibody systems made of rigid bodies and here is used that same choice.

A model using the software Siconos has been implemented, to simulate the non-smooth dynamical system. First it has been defined an object of class LagrangianTIDS, to define the purely differential dynamical system.

$$M\ddot{q} + C\dot{q} + Kq = \widetilde{F}$$

The dynamical system has then to be associated with a unilateral contact law:

$$0 \leq y \perp p \geq 0$$

and a Newton impact law:

$$if\ y(t) = 0\ \ then\ \ \dot{y}(t^+) = -e \cdot \dot{y}(t^+)$$

The set of parameters listed in table 3.2 has been used in the simulation:

Table 3.2: Reduced DAE model with Siconos: simulation parameters

mass 1 $m1$[kg]	0.5
mass 2 $m2$ [kg]	0.5
spring stiffness k [N/m]	10.
sphere radius R [m]	0.1
spheres distance L [m]	0.2
timestep h [s]	$1e-3$
Newton coef. of restitution	0.8

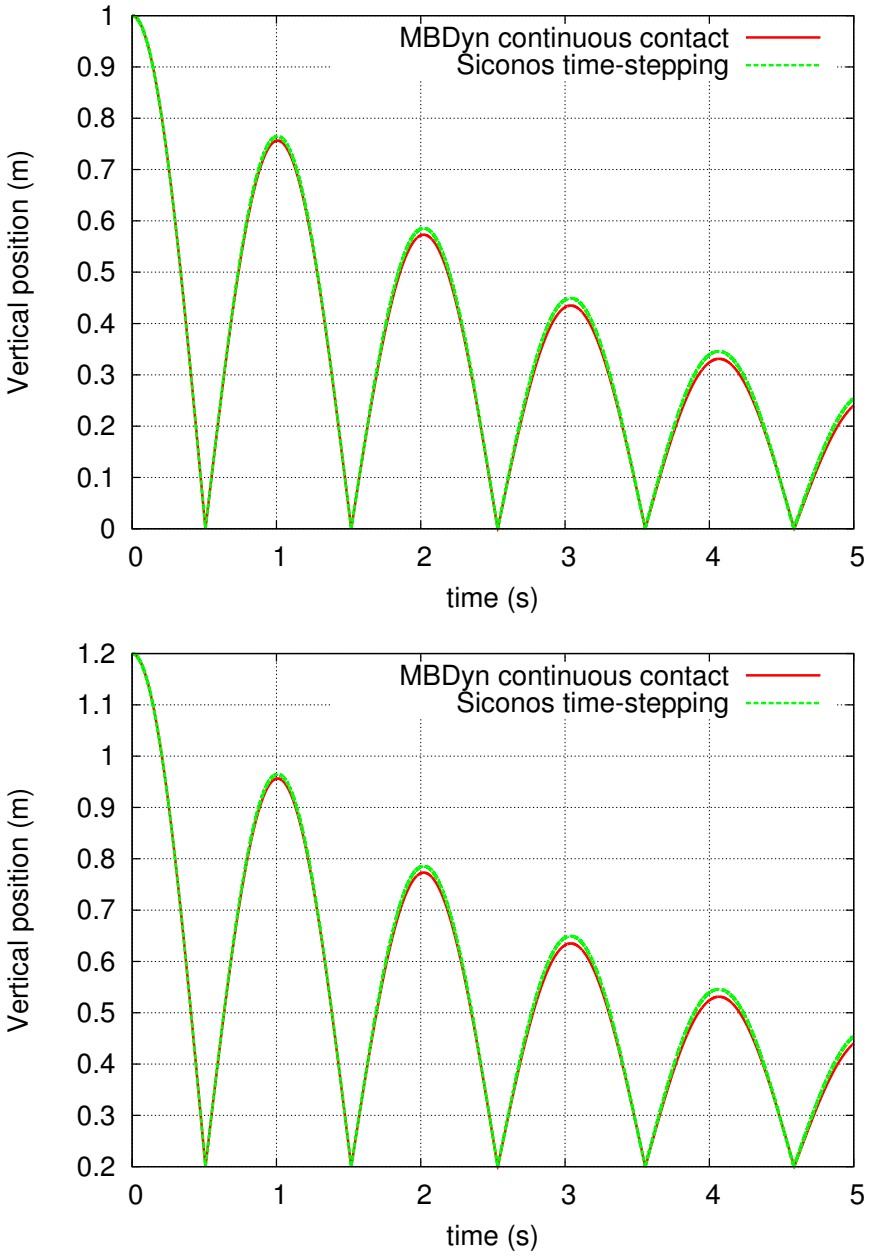

Figure 3.13: Position of the two masses vs time

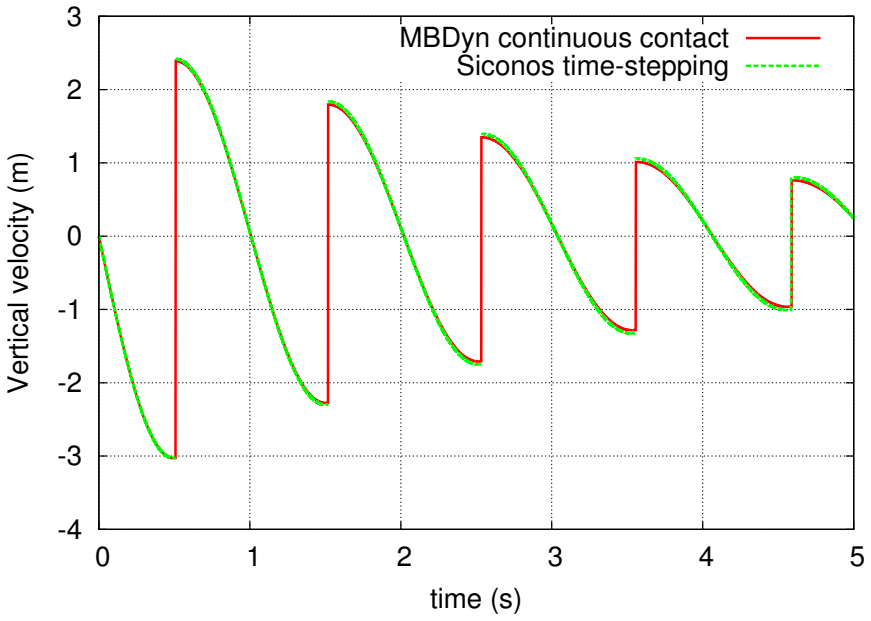

Figure 3.14: Velocity of the lower mass vs time

The method proposed has been compared with a model integrated with a continuous contact solution, using the previously described Flores constitutive law of equation (2.5) to simulate the contact. Due to the stiffness of the law the timestep used with the continuous contact solution has to be $h = 10^{-5}$, while the more efficient *time-stepping* on a constraint projected model is $h = 10^{-3}$. The solutions are almost coincident. The method proposed here shows a feasible way to address the solution of bilaterally constrained models with the classes available at this moment in the Siconos Kernel software (version 3.4.0), but it lacks the versatility needed to implement varied multibody models.

Chapter 4

A Co-simulation Approach

4.1 Introduction and motivation

A drawback of nonsmooth event capturing methods, also briefly called time-stepping methods, is their intrinsic low order of accuracy. When events are encountered, the local error of consistency is at best $\mathcal{O}(h)$. Over smooth periods, the order $\mathcal{O}(h^2)$ is expected to be as for the numerical integration of index-2 DAEs with the backward Euler method [2, 1, 43].

There are applications where it is of interest to simulate with higher–order accuracy mechanical systems with a limited number of rigid bodies, for which unilateral contact plays an important role for the behavior of a part of the system.

Those applications would benefit from the ability of time-stepping methods to robustly handle finite accumulation of events and accurately resolve frictional contact, and from the ability to solve the problem of contact without resorting to stiff contact forces that involve a bigger computational burden. It would also be useful though to retain the properties of higher order methods during the smooth phases of motion.

Attempts have been made to improve the global order of accuracy of time–stepping with nonsmooth events in recent research. The different approaches can be classified in two categories: mixed time-stepping schemes and augmented time-stepping schemes.

Mixed time-stepping schemes propose a combination of classic high-order DAE integration schemes for smooth intervals with time-stepping schemes for nonsmooth phases. In [1] a scheme combining an Implicit Runge Kutta method with a Moreau scheme is proposed. Higher order accuracy is sought by a localization of the nonsmooth event into a so-called critical time–step, which is integrated by Moreau's time-stepping. A method of order p with a time step h is chosen to integrate the smooth dynamics, and the integration over the critical time–step is performed with

a method of order q. The length of the critical time–step denoted by $\tilde{h}$ is chosen such that $\widetilde{h}_{q+1} = \mathcal{O}(h_{p+1})$. In [9] another implementation of a "hybrid" integration approach, switching between smooth and nonsmooth phases, has been proposed and implemented in the multibody software MBSim (http://mbsim.berlios.de).

Augmented time-stepping schemes are extensions of classic time-stepping schemes of Moreau-Jean type. Extrapolation techniques or time-step size adaptation are used to augment the integration order [43, 44, 19].

In this work a co-simulation approach is explored. The fundamental idea is to have a coupled integration with a part of the model integrated with classic DAE schemes and at the same time a part integrated with time-stepping schemes. This approach targets problems in which it is possible to separate a subsystem subject to dynamics with nonsmooth events, such as those determined by unilateral constraints, while the other part of the problem is a subsystem with a dynamics that we can consider only loosely coupled to the dynamics of the first subsystem, which therefore we can consider "smooth".

This solution is explored with the aim of adding a tool to deal with frictional contacts to the software MBDyn, overcoming the limitations of a penalty method, without altering the way it formulates the equations to solve and its core software architecture. This solution would retain the accuracy and robustness of MBDyn, as well as the versatility in modeling different kinds of problems, and aims to take advantage of the nonsmooth dynamical framework for a class of problems in which contact and friction are relevant in the dynamics of a part of the system. It is expected that co-simulation with existing state-of-art nonsmooth time-stepping solvers allows a satisfactory solution that avoids "re-inventing the wheel" in MBDyn, alas reformulating the whole problem in the nonsmooth framework. Indeed important efforts like the Saladyn project (http://saladyn.gforge.inria.fr/) already aim in this second direction, with the goal of developing a platform for the simulation of mechanical systems with interactive multi-modelling directly in the nonsmooth dynamical systems framework. It is supported by the French National Agency for Research and is the collaborative work of a consortium that includes INRIA. The platform is based on the integration of existing opensource software, Salomé-méca, LMGC90, and Siconos.

4.2 Co-simulation concept

Let's suppose that the dynamics of a generic problem can be decomposed into two interdependent subsystems, a smooth subsystem (4.2) and a nonsmooth one (4.3):

$$f\left(q,\dot{q},t\right)=0 \tag{4.1}$$

$$f_s\left(q_s,\dot{q}_s,q_{ns},\dot{q}_{ns},t\right)=0 \tag{4.2}$$

$$f_{ns}\left(q_s,\dot{q}_s,q_{ns},\dot{q}_{ns},t\right)=0 \tag{4.3}$$

Applying a classic multistep implicit integration solution involves a prediction phase:

$$q_{s,k}=\sum_{i=s,n}a_{1,i}q_{1,k-i}+h\sum_{i=0,n}b_{1,i}\dot{q}_{s,k-i}$$

$$q_{ns,k}=\sum_{i=1,n}a_{2,i}q_{ns,k-i}+h\sum_{i=0,n}b_{2,i}\dot{q}_{ns,k-i}$$

And a correction phase:

$$f_s+f_{s/q_s}\delta q_{s,k}+f_{s/\dot{q}_s}\delta\dot{q}_{s,k}+f_{s/q_{ns}}\delta q_{ns,k}+f_{s/\dot{q}_{ns}}\delta\dot{q}_{ns,k}=0$$

$$f_{ns}+f_{ns/q_s}\delta q_{s,k}+f_{ns/\dot{q}_s}\delta\dot{q}_{s,k}+f_{ns/q_{ns}}\delta q_{ns,k}+f_{ns/\dot{q}_{ns}}\delta\dot{q}_{ns,k}=0$$

Since the two systems are interdependent a consistent approach to the correction phase, with a Newton Raphson iteration, would be:

$$\begin{bmatrix} hbf_{s/q_s}+f_{s/\dot{q}_s} & hbf_{s/q_{ns}}+f_{s/\dot{q}_{ns}} \\ hbf_{ns/q_s}+f_{ns/\dot{q}_s} & hbf_{ns/q_{ns}}+f_{ns/\dot{q}_{ns}} \end{bmatrix}\begin{Bmatrix} \delta\dot{q}_{s,k} \\ \delta\dot{q}_{ns,k} \end{Bmatrix}=\begin{Bmatrix} -f_s \\ -f_{ns} \end{Bmatrix}$$

This approach can be termed as monolithic.

An approximated treatment of the problem would be:

$$\begin{aligned} \left(hbf_{s/q_s}+f_{s/\dot{q}_s}\right)\delta\dot{q}_{s,k} &= -f_s\left(q_s,\dot{q}_s,q_{ns},\dot{q}_{ns},t\right) \\ \dot{q}_{s,k} &+= \delta\dot{q}_{s,k} \\ q_{s,k} &+= b_{s,0}\delta\dot{q}_{s,k} \end{aligned}$$

$$\begin{aligned} \left(hbf_{ns/q_{ns}}+f_{ns/\dot{q}_{ns}}\right)\delta\dot{q}_{ns,k} &= -f_{ns}\left(q_s,\dot{q}_s,q_{ns},\dot{q}_{ns},t\right) \\ \dot{q}_{ns,k} &+= \delta\dot{q}_{ns,k} \\ q_{ns,k} &+= b_{ns,0}\delta\dot{q}_{ns,k} \end{aligned}$$

This approach is called here semi-implicit, and on that is based the solution proposed here. The difference from a coupled solution of DAE systems is that here the nonsmooth subsystem is advanced with a time-stepping scheme. This means that, at each iteration, a complementarity problem must be solved in order to update the generalized variables pertaining to the nonsmooth subsystem and advance the prob-

lem. The complementarity problem results from the discretization of the nonsmooth subsystem, comprising the unilateral constraints. The timestepping integration implemented follows the NSCD algorithm delineated in chapter 3.

4.3 Implementation

In order to test this approach a modular element of the software MBDyn has been developed. It implements a subsystem that is integrated with a time-stepping scheme, and interfaced with the rest of the model. In order to have a versatile module to enable the modeling of different problems the nonsmooth system has been reduced to a single node, on which the unilateral constraints acts, therefore modeling a part of the system subject to contact. The fundamental implementation exposed here consists of a static displacement node interacting with one non-smooth constraint, impact on one or more flat planes.

This nonsmooth node is coincident with a node of the MBDyn integrated model, to which it imposes the position and velocity obtained through Moreau-Jean timestepping integration, and to which it passes a reaction force. A total of nine constraint equations are contributed to the multibody model.

The first three equations added to the DAE integration are originated from the constraint imposing the coincidence of the position between the multibody static displacement node and the non-smooth node:

$$\boldsymbol{q}_{mb} - \boldsymbol{q}_{ns} = 0$$

The velocities also must be coinciding:

$$\boldsymbol{v}_{mb} - \boldsymbol{v}_{ns} = 0$$

This implies that the multibody static displacement node receives reaction forces represented by Lagrange multipliers:

$$\delta\mathbf{q}_{mb}^T\mathbf{f} = \delta\mathbf{q}_{mb}^T\boldsymbol{\lambda}$$

MBDyn integrates the smooth part of the problem, including the static displacement node, and passes the initial $\boldsymbol{q}$ and $\boldsymbol{v}$ together with the reaction forces $\boldsymbol{\lambda}$ to the non-smooth module.

The non-smooth module integrates with a time-stepping scheme a nonsmooth subsystem consisting of a single node, owner of mass, with the reaction forces $\boldsymbol{\lambda}$ and gravity as external forces and returns the motion $\boldsymbol{q}_{ns}$ and $\boldsymbol{v}_{ns}$ that must be prescribed to the multibody node, together with an updated reaction force that accounts for

the possible impact. This latter force results to be not stiff because does not have to account for a jump in the velocity.

On the MBDyn side, more specifically, the constraint equations contributed by the module are described in the following.

The linearization of the compatibility constraint, with a relaxation variable $\boldsymbol{\mu}$ to avoid over-constraining, is:

$$\boldsymbol{I}\Delta\boldsymbol{q}_{mb} + \boldsymbol{I}\Delta\boldsymbol{\mu} = \frac{(\boldsymbol{q}_{ns} - \boldsymbol{q}_{mb})}{\mathrm{c}} - \boldsymbol{\mu}$$

where c is a constant derived from the integration method.

The constraint on velocity is:

$$\boldsymbol{I}\Delta\boldsymbol{v}_{mb} = \boldsymbol{v}_{ns} - \boldsymbol{v}_{mb}$$

The module contributes to the equilibrium equations of the static displacement node by adding the terms:

$$\boldsymbol{I}\Delta\boldsymbol{\lambda} = -\boldsymbol{\lambda}$$

This approach is formulated to work best the more the two subsystems are loosely coupled. For that reason the static displacement node on the MBDyn side should be connected to a smooth sub-model by a compliant element (a beam, a spring or so). Kinematic constraints should be avoided.

In this initial simple implementation the module only handles frictionless contact-impacts with flat planes, possibly more than one. The nonsmooth node can be set with a mass and a radius. The planes are defined by a point and an orientation both in relation with the position and orientation of another node of the model, and a Newtonian restitution coefficient can be set for each plane.

The nonsmooth problem is solved by an NSCD algorithm analogous to the one presented in 3.1. The Siconos Numerics library described in section 3.2.1 provides state of the art solvers for the Linear Complementarity Problem obtained. All the solvers and solver parameters are accessible through the module input interface with MBDyn, with the default settings using the Lexico Lemke algorithm with pivoting.

4.4 First tests of the approach

The approach proposed is first illustrated with a simple example of a linear oscillator, a model comprising of two masses connected with a linear spring, of which one is subject to impact with a plane. Furthermore, in order to validate the module developed the two simple examples considered in chapter 2 are implemented, verify-

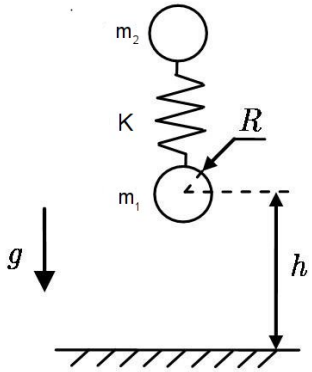

Figure 4.1: Oscillator example

Table 4.1: Oscillators example: simulation parameters

restitution coefficient	e	0.8	[non dim.]
mass 1	m	1.	[Kg]
mass 2	m	1.	[Kg]
radius 2	R	0.2	[m]
spring stiffness	K	1.e3	[Nm]
gravity	g	10.	$[m/s^2]$
initial height	H	1.001	[m]
Multistep spectral radius	ρ	0.82	[non dim.]
Moreau Jean theta	θ	0.5	[non dim.]

ing the NSCD algorithm and the correct assembly of a complementarity problem in presence of more than one unilateral constraint. In subsequent chapters a comparison will be made with an alternative approach adapting higher order integration schemes to the nonsmooth integration and subsequently the method will be tested with more complex applications.

The method developed is applied to a basic model in order to illustrate the concept. It is represented in figure figure 4.1 and the parameters of the simulation are listed in table table 4.1. In this model the subsystem whose dynamics is mainly affected by the nonsmooth constraint, in this case the non-interpenetration constraint with respect to a horizontal plane, consists of node 1. The motion of node 1 is determined by the nonsmooth integration implemented in the module. The "smooth" subsystem, handled entirely by MBDyn integration routines, is comprising of the sole mass 2. The two part of the model are connected by means of a spring and the system is subject to gravity. The results of the co-simulation approach are shown against those from the classic Moreau-Jean time-stepping implemented in state-of-the-art library SiconosKernel.

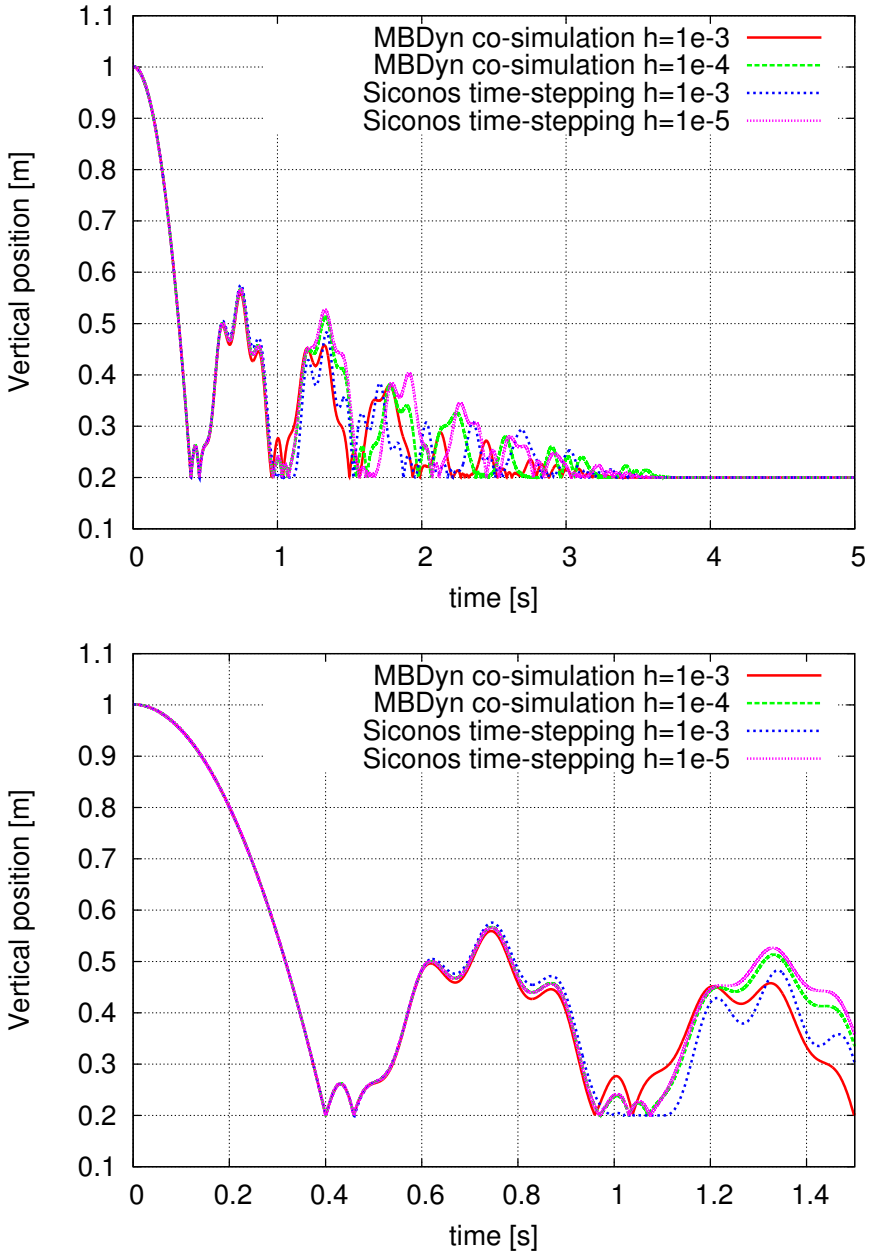

Figure 4.2: Oscillator simulation: vertical position of node 1, with different time-steps

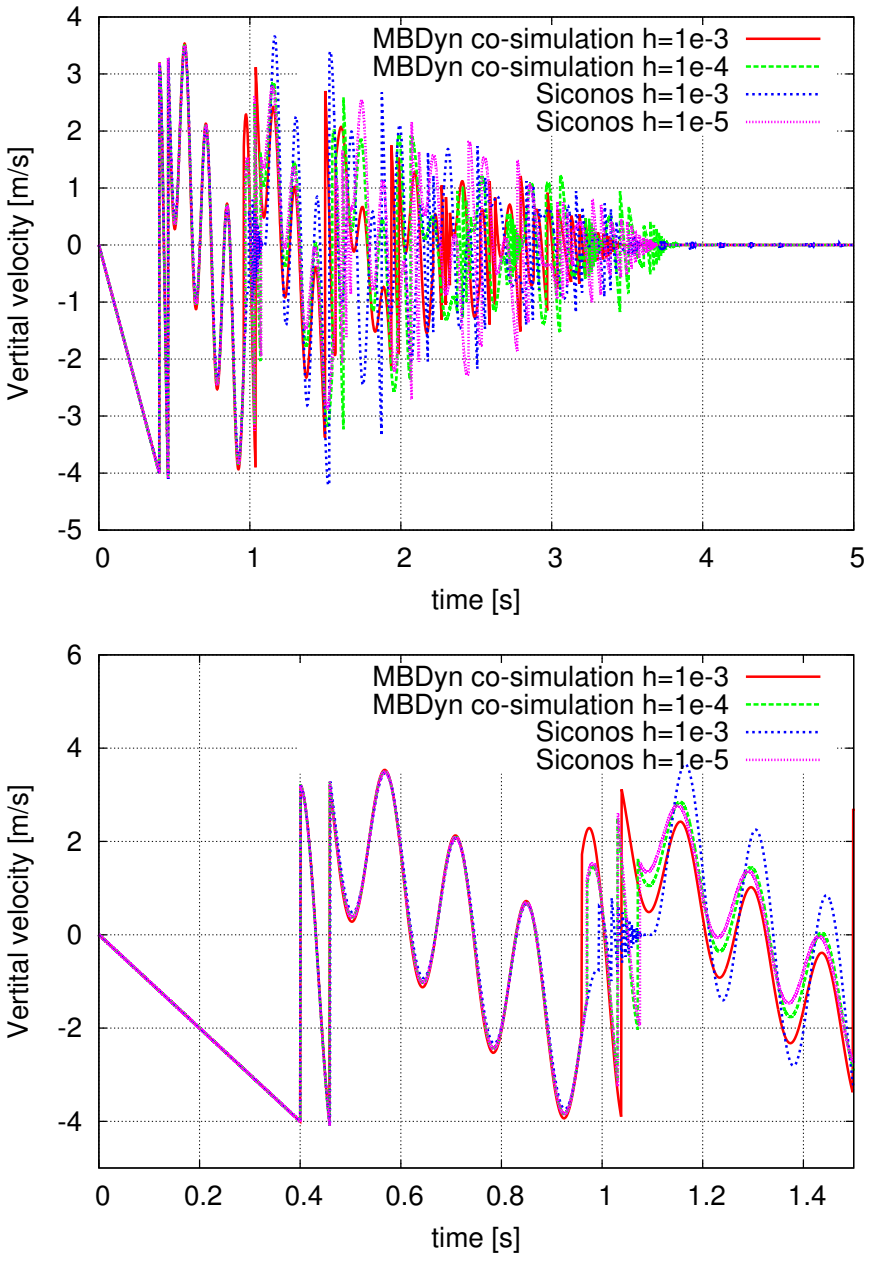

Figure 4.3: Oscillator simulation: vertical velocity of node, with different time-steps

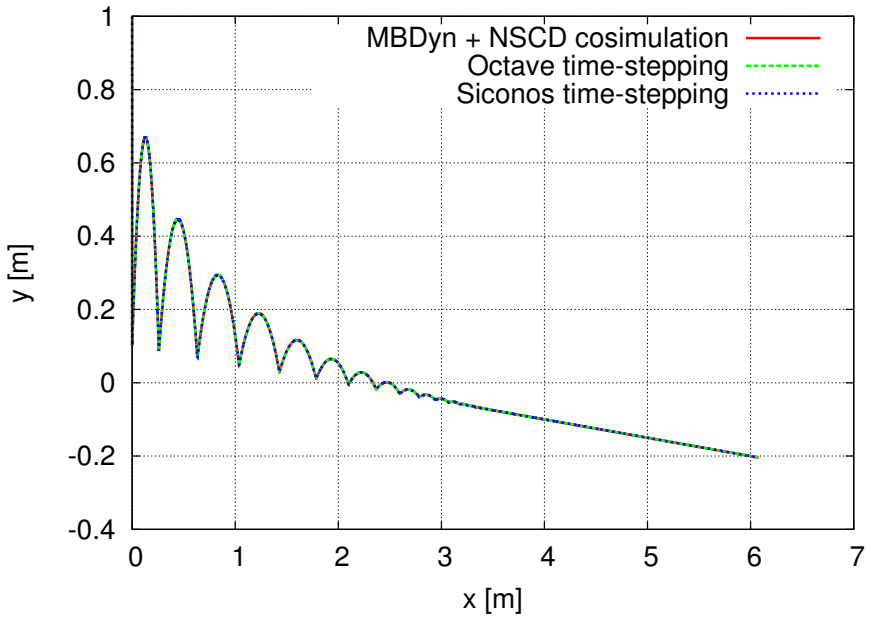

Figure 4.4: Co-simulation approach: tilted plane. Position of the ball. The solutions are coincident.

The results in figure 4.2 and figure 4.3 show the position and velocity of the bottom mass, with a detail of the first 1.5 seconds of the simulation. For all the simulations with the MBDyn module and the simulation with Siconos with h=10^{-3} double impacts occur due to the compression of the spring. The co-simulation approach with MBDyn integration shows, in this simple example, more accurate results for smaller time-steps.

The module has also initially been tested with the two simple examples in chapter 3 in order to verify the correctness of the implementation of the NSCD algorithm, thus in this models the "smooth" part does not come into play. First is considered the problem of the ball falling on an inclined plane. The problem is illustrated in figure 3.4 and the parameters used for the simulation are those set in table 3.1. The timestep used in the MBDyn simulation is $h = 10^{-3}$.

The plot shows a perfect superposition between the results of the simulations done with Siconos and the NSCD algorithm implemented in Octave of chapter 3, both implementing a Moreau Jean time-stepping approach.

The second test presented, used to validate the module in a situation where it is necessary a composition of multiple unilateral constraints, is the same described in figure 3.8. Results are coincident with those found with a classic time-stepping strategy.

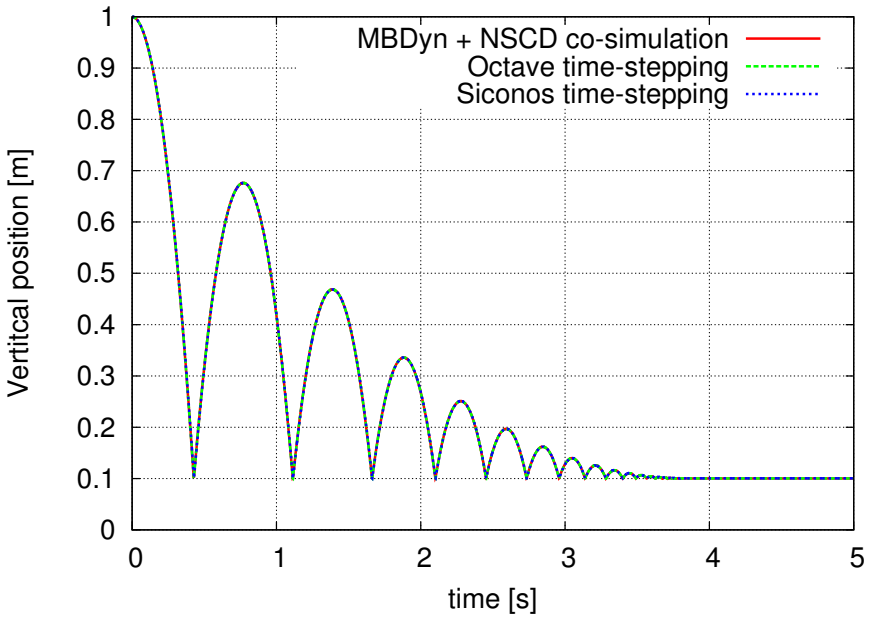

Figure 4.5: Co-simulation approach: double impact. Vertical position vs time. The solutions are coincident.

Chapter 5

Nonsmooth Multistep Integration

The aim of this chapter is to apply and adapt a multistep integration formula particularly suited for the analysis of multibody systems, implemented in the software MBDyn, to the solution of problems involving nonsmooth unilateral constraints.

Although the global order of accuracy for time-stepping schemes is brought to one by nonsmooth events [2, 16], the development of higher order time-stepping methods is an active subject of research, to improve local accuracy during the smooth phases of the motion [44, 1].

The method proposed in [7] is followed. In [7] Chen et al. have shown a way to take advantage of the accuracy and stability properties of the Hilbert-Hughes-Taylor integration scheme [18] together with the consistent treatment of impulses and jumps in velocity of the Moreau-Jean time-stepping method [34][2]. Here the same method is applied to a 2nd order, A/L stable, two-step integration formula [32]. With some further adjustment in the implementation of the prediction phase a method is obtained that in the smooth phases benefits from the properties of the multistep method, whereas in the nonsmooth events it benefits of the consistency of the time-stepping approach.

The results of simple tests are shown to empirically illustrate the properties of the method, and a comparison is made between the Moreau-Jean approach, the nonsmooth multistep approach presented here and the co-simulation of the MBDyn integration and the Moreu-Jean time-stepping proposed in the previous chapters. This comparison allows us to empirically validate this last approach.

5.1 Two-step implicit A-L stable integration

A 2nd order, A/L stable, two-step integration formula is introduced here. It represents a tested and viable choice for the numerical integration of multibody dynamics and DAE problems, with tunable algorithmic dissipation. The details of its development and the properties are discussed in [32], [30]. This 2nd order two-step algorithm

has been applied to the multibody analysis of complex multidisciplinary systems, e.g. helicopter rotors including aerodynamics, hydraulic controls and active control by means of smart materials. It is implemented in the software MBDyn.

The method requires the computation of a single Jacobian matrix at the end of the timestep and no Jacobian matrix multiplications, thus it is a viable and optimized choice for the implementation of DAE problems.

A two-step method can be expressed as:

$$x_{k+1} = a_0 x_k + a_{-1} x_{k-1} + b_1 \dot{x}_{k+1} + b_0 x_k + b_{-1} \dot{x}_{k-1}$$

where, calling Δt_c the current time step and Δt_p the previous one we can express the coefficients as function of the following α, β, δ. We can write β and δ as a function of the asymptotic spectral radius, in order to tune the desired algorithmic dissipation. A good trade-off between accuracy and algorithmic dissipation is found by choosing an asymptotic spectral radius of 0.6 .

$$\alpha = \frac{\Delta t_p}{\Delta t_c}$$

$$\beta = \alpha \frac{(2+\alpha)(1-\rho_\infty)^2 + 2(1+\alpha)(2\rho_\infty - 1)}{2(1+\alpha) - (1-\rho_\infty)^2}$$

$$\delta = \frac{\alpha^2 (1-\rho_\infty)^2}{2(2(1+\alpha) - (1-\rho_\infty)^2)}$$

$$a_0 = 1 - \beta$$

$$a_{-1} = \beta$$

$$b_1 = \Delta t_c (\frac{\delta}{\alpha} + \frac{\alpha}{2})$$

$$b_0 = \Delta t_c (\frac{\beta}{2} + \frac{\alpha}{2} - (1-\alpha)\frac{\delta}{\alpha})$$

$$b_{-1} = \Delta t_c (\frac{\beta}{2} + \delta)$$

The method can be extended to second order equations as follows:

$$\mathbf{v}_{n+1} = b_1 \mathbf{a}_{n+1} + a_0 \mathbf{v}_n + a_{-1} \mathbf{v}_{n-1} + b_0 \mathbf{a}_n + b_{-1} \mathbf{a}_{n-1}$$

$$\mathbf{q}_{n+1} = b_1^2\mathbf{a}_{n+1}+a_0\mathbf{q}_n+a_{-1}\mathbf{q}_{n-1}+(b_1a_0+b_0)\mathbf{v}_n+(b_1a_{-1}+b_{-1})\mathbf{v}_{n-1}+b_1b_0\mathbf{a}_n+b_1b_{-1}\mathbf{a}_{n-1}$$

which is a convenient form to treat equations of motion of mechanical systems.

The multistep method presented is therefore able to treat problems governed by differential equations of both first and second order naturally, without additional manipulation, whereas the HHT scheme needs further derivation of first order problems [5, 6].

In figures 5.1 5.2 5.3 are shown some characteristics of different A-stable, L-stable and A-L stable integration schemes as a function of the integration step h and the period associated to the problem T. Figure 5.1 shows the absolute value of the spectral radius, the multistep scheme with tunable algorithmic dissipation with the selected optimal choice for asymptotic spectral radius shows a sensibly less pronounced decaying of the spectral radius for $h/T < 1$ with respect to the other methods. Figure 5.2 shows the amplitude error, as 1 minus the ratio between the absolute value of the spectral radius and the exact value, which is 1 for a not damped problem. The error for the multistep scheme with tunable algorithmic dissipation remains limited for big values of h/T . The error for the HHT method, with $\alpha = -0.264$ in order to have asymptotic spectral radius equal to the multistep one, is sensibly bigger. Figure 5.3 shows the phase error, as 1 minus the ratio between the absolute value of the spectral radius and the exact value, which is ωh for a not damped problem. Here the error for the multistep solution is near the one for Crank-Nicolson method, and slightly inferior to the one pertaining to the HHT method.

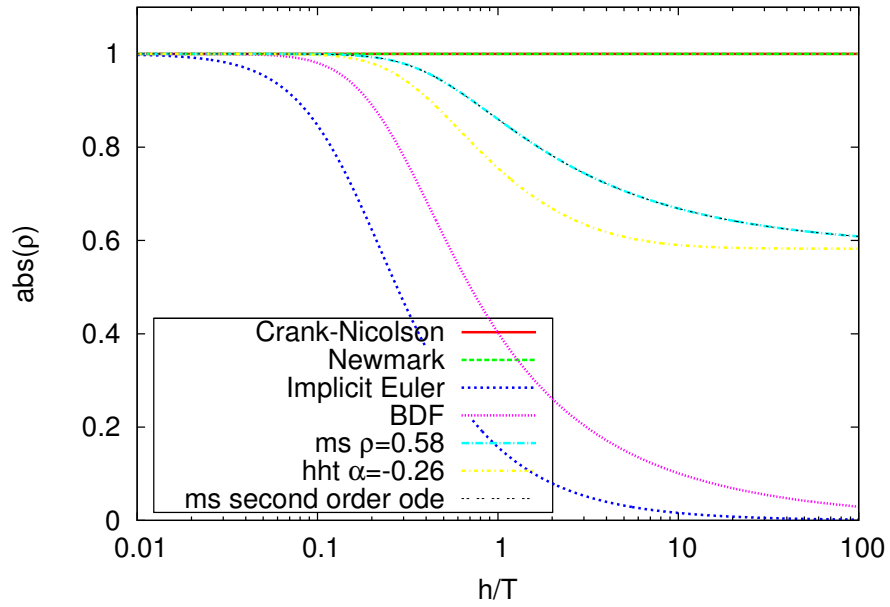

Figure 5.1: Absolute value of the , $\|\rho\|$, of different A-stable, L-stable and A-L-stable methods

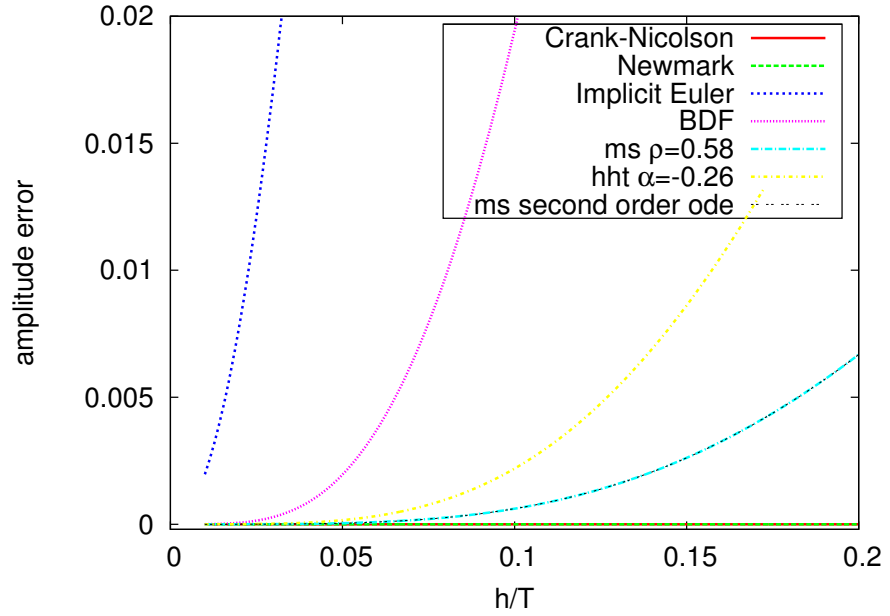

Figure 5.2: Amplitude error, $1 - \|\rho\| \,/\, \left\|e^{j\omega h}\right\|$, of different A-stable, L-stable and A-L-stable methods (note: $\left\|e^{j\omega h}\right\| \equiv 1$).

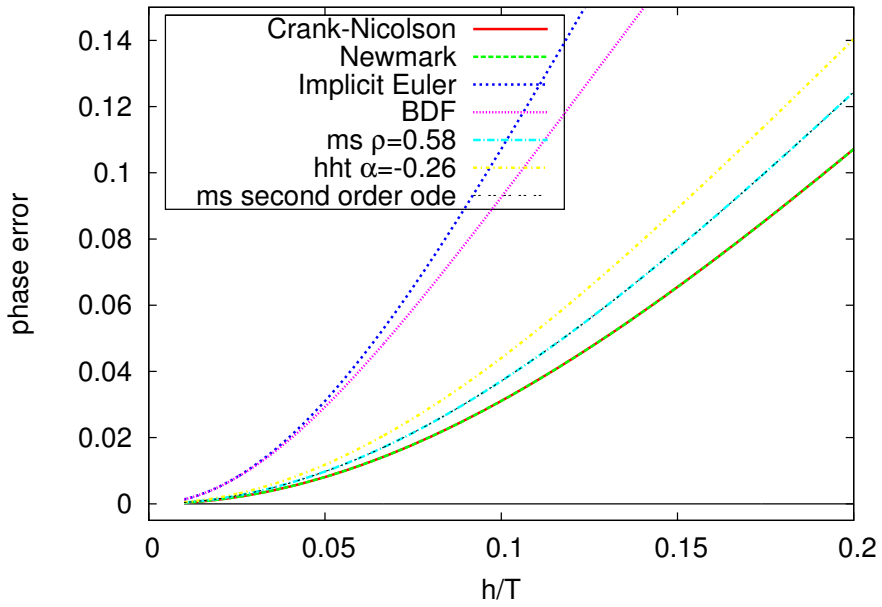

Figure 5.3: Phase error, $1- < \|\rho\| \,/\, \|\omega h\|$, of different A-stable, L-stable and A-L-stable methods

5.2 Equations of motion

This section briefly formulates the non-smooth problem, following the notation proposed in [7]. The innovative contribution is essentially related to the use of the two step scheme discussed in the previous section.

Following the same notation in [7] it is possible to write the equations of a flexible multibody system including bilateral and unilateral constraints in this form:

$$\mathbf{M}(\mathbf{q})d\mathbf{v} + \mathbf{\Phi}_{\mathbf{q}}^{\mathbf{T}} d\mathbf{i}^b = \mathbf{h}dt + \mathbf{g}_q^T d\mathbf{i}^u \tag{5.1}$$

$$\mathbf{\Phi}(\mathbf{q}) = \mathbf{0}$$

$$\text{if } \overline{\mathbf{g}}(\mathbf{q}) \leq 0 \text{ then } 0 \leq \mathbf{g}_q \mathbf{v}(t^+) + e\mathbf{g}_q \mathbf{v}(t^-) \perp d\mathbf{i}^u \geq 0 \tag{5.2}$$

where:

- $\mathbf{q}$ is the vector of generalized coordinates
- $\mathbf{h} = \mathbf{f}^{ext} - \mathbf{f}^{int}(\mathbf{q}) - \mathbf{f}^{damp}(\mathbf{q}, \mathbf{v})$ collects the external, internal and damping forces
- $\mathbf{M}$ is the mass matrix

- $\mathbf{\Phi}$ is the vector of bilateral holonomic constraints and $\mathbf{\Phi}_q$ is the matrix of constraint gradients.
- $\mathbf{g}$ is the vector of unilateral holonomic constraints and $\mathbf{g}_q$ is the matrix of constraint gradients, and $\boldsymbol{\lambda}^u$ is the vector of associated Lagrange multipliers.
- $d\mathbf{v}$ is the differential measure associated with the velocity $\mathbf{v}$ and assumed to be of bounded variation
- dt is the standard Lebesgue measure
- $d\mathbf{i}^u$ and $d\mathbf{i}^b$ are the impulse measure of the contact reaction and the bilateral force, respectively.

Equation 5.2 is the complementarity condition of the unilateral constraint at velocity level together with the Newton impact law, whereas e is the coefficient of restitution.

Since the motion might be nonsmooth it is necessary to take into account jumps in the velocity and corresponding impacts with the following decomposition of measures:

$$\begin{aligned} d\mathbf{v} &= \dot{\mathbf{v}}dt + \textstyle\sum_i (\mathbf{v}(t_i^+) - \mathbf{v}(t_i^-))\delta_{t_i} \\ d\mathbf{i}^u &= \boldsymbol{\lambda}^u dt + \textstyle\sum_i \mathbf{p}_i^u \delta_{t_i} \\ d\mathbf{i}^b &= \boldsymbol{\lambda}^b dt + \textstyle\sum_i \mathbf{p}_i^b \delta_{t_i} \end{aligned}$$

where $\boldsymbol{\lambda}^b$ is the vector of Lagrange multipliers associated with bilateral constraints; $(\mathbf{v}(t_i^+) - \mathbf{v}(t_i^-))$ is the jump in velocity at the instant t_i, δ_{t_i} is the Dirac atom supported at t_i; $\mathbf{p}_i^u$ and $\mathbf{p}_i^b$ are the force impulses corresponding to unilateral and bilateral constraints.

We can then separate the equation of motion

$$\mathbf{M}\dot{\mathbf{v}}dt + \mathbf{\Phi}_\mathbf{q}^\mathbf{T}\boldsymbol{\lambda}^\mathbf{b}dt = \mathbf{h}dt + \mathbf{g}_q^T\boldsymbol{\lambda}^u dt$$

and the impact equation at time t_i

$$\mathbf{M}(\mathbf{v}(t_i^+) - \mathbf{v}(t_i^-)) + \mathbf{\Phi}_q^T\mathbf{p}_i^b = \mathbf{g}_q^T\mathbf{p}_i^u$$

5.3 Time integration method

In order to present the time-stepping method, in the following implementation we refer to systems without bilateral constraints, in order to deal with simple Linear Complementary Problems instead of Mixed Linear Complementary Problems.

We enucleate the contact part from the equation of motion, such that:

$$\mathbf{M}d\mathbf{v} = \mathbf{M}\mathbf{a}dt + \mathbf{M}d\mathbf{v}^{con}$$

with

$$\begin{cases} \mathbf{M}\mathbf{a}dt & = \mathbf{h}dt \\ \mathbf{M}d\mathbf{v}^{con} & = g_{\mathbf{q}}^{T}d\mathbf{i}^{u} \end{cases}$$

where $\mathbf{a}$ is the acceleration and $d\mathbf{v}^{con}$ is the contribution to the velocity increment due to the contact impulse.

After defining the set of active constraints $\mathbf{g}^A$ as the set of all the unilateral constraints satisfying $\overline{\mathbf{g}} \leq 0$ and $\mathbf{\Lambda}^A$ as the corresponding Lagrange multipliers, the discretized equations of motion become:

$$\mathbf{M}\mathbf{a}_{n+1} = \mathbf{h}_{n+1} \tag{5.3a}$$

$$\mathbf{M}\Delta\mathbf{v}_{n+1}^{con} = (\mathbf{g}_{q,n+1}^{A})^{T}\mathbf{\Lambda}_{n+1}^{A} \tag{5.3b}$$

$$0 = \Psi(\mathbf{\Lambda}_{n+1}^{A},\ \mathbf{g}_{q,n+1}^{A}\mathbf{v}_{n+1} + e\mathbf{g}_{q,n}^{A}\mathbf{v}_{n}) \tag{5.3c}$$

$$0 = \mathbf{\Phi}_{q}\mathbf{v}_{n+1} \tag{5.3d}$$

where $\Psi(a,b) = 0 - max(0, a - \rho b),\ \rho > 0$ expresses the complementarity condition.

Here equation (5.3a) describe the smooth dynamics, eq. equation (5.3b) describe the impulsive contribution to the velocity, equation (5.3c) is the complementarity condition, equation (5.3d) describe bilateral constraints.

If an impact is detected at time $t_i \in [t_n, t_{n+1}]$, the impact reaction only occurs in the atomic measure at the instant t_i. The influence of the impact is thus considered only at the current timestep without affecting any other timesteps.

The contribution of the nonsmooth force to the velocity and position is then derived as:

$$\Delta\mathbf{v}_{n+1}^{con} = \int_{[t_n, t_{n+1})} d\mathbf{v}^{con}$$

$$\Delta\mathbf{q}_{n+1}^{con} = \int_{[t_n, t_{n+1})} \int_{[t_n, t_{n+1})} d\mathbf{v}^{con}dt = 0.5h\Delta\mathbf{v}_{n+1}^{con}$$

where $\Delta\mathbf{v}_{n+1}^{con}$ also satisfies the discrete equation of motion . Combining with the expression for generalized position and velocity by the classic multistep method :

$$\mathbf{v}_{n+1} = b_1\mathbf{a}_{n+1} + a_0\mathbf{v}_n + a_{-1}\mathbf{v}_{n-1} + b_0\mathbf{a}_n + b_{-1}\mathbf{a}_{n-1} + \Delta\mathbf{v}_{n+1}^{con} \tag{5.4}$$

$$\mathbf{q}_{n+1} = b_1^2\mathbf{a}_{n+1}+a_0\mathbf{q}_n+a_{-1}\mathbf{q}_{n-1}+(b_1a_0+b_0)\mathbf{v}_n+(b_1a_{-1}+b_{-1})\mathbf{v}_{n-1}+b_1b_0\mathbf{a}_n+b_1b_{-1}\mathbf{a}_{n-1}+0.5h\Delta\mathbf{v}_{n+1}^{con} \tag{5.5}$$

5.3.1 Prediction

In order to solve the implicit problem a first tentative value for $\mathbf{a}_{n+1}$ must be predicted with an explicit method of accuracy better or equal to the multistep method.

A Hermite interpolation is used here:

$$\mathbf{a}_{n+1} = m_0\mathbf{v}_k + m_{-1}\mathbf{v}_{k-1} + n_0\mathbf{a}_k + n_{-1}\mathbf{a}_{k-1}$$

where

$$m_o = -m_{-1} = \frac{-6\alpha(1+\alpha)}{\Delta t_c}$$

$$n_0 = 1 + 4\alpha + 3\alpha^2$$

$$n_{-1} = \alpha(2+3\alpha)$$

It is then possible to formulate a Linear Complementarity Problem (LCP), in order to find the contribution of the impulsive forces to the velocity, with the following steps.

From equation (5.3b):

$$\Delta\mathbf{v}_{n+1}^{con} = \boldsymbol{M}^{-1}(\boldsymbol{g}_{q,n+1}^{A})^T\boldsymbol{\Lambda}_{n+1}^{A}$$

then substituting in the expression for the velocity:

$$\mathbf{v}_{n+1} = b_1\mathbf{a}_{n+1} + a_0\mathbf{v}_n + a_{-1}\mathbf{v}_{n-1} + b_0\mathbf{a}_n + b_{-1}\mathbf{a}_{n-1} + \boldsymbol{M}^{-1}(\boldsymbol{g}_{q,n+1}^{A})^T\boldsymbol{\Lambda}_{n+1}^{A}$$

Replacing $\mathbf{v}_{n+1}$ in equation (5.3c) it is possible to write an LCP with unknown $\boldsymbol{\Lambda}_{n+1}^{A}$:

$$0 \leqslant \boldsymbol{\Lambda}_{n+1}^{A} \perp \boldsymbol{D}\boldsymbol{\Lambda}_{n+1}^{A} + b \geqslant 0$$

with

$\boldsymbol{D} = -\boldsymbol{g}_{q,n+1}^{A}\boldsymbol{M}^{-1}(\boldsymbol{g}_{q,n+1}^{A})^T$,

$b = \boldsymbol{g}_{q,n+1}^{A}(b_1\mathbf{a}_{n+1} + a_0\mathbf{v}_n + a_{-1}\mathbf{v}_{n-1} + b_0\mathbf{a}_n + b_{-1}\mathbf{a}_{n-1}) + e\boldsymbol{g}_{q,n}^{A}\mathbf{v}_n$

Having predicted the value for $\mathbf{\Lambda}^A_{n+1}$ we can find $\Delta\mathbf{v}^{con}_{n+1}$, and subsequently $\mathbf{v}_{n+1}$ and $\mathbf{q}_{n+1}$ using equation (5.4) and equation (5.5).

The prediction after nonsmooth events depends on the values of velocity in the two preceding steps, and after an impact this can evolve with a nonsmooth jump.

Therefore in the timesteps after those events the two-step formula is ill-suited to accurately predict the solution without ignoring the nonsmooth nature of the evolution of the generalized velocity. A re-initialization is then necessary after those events with a 2nd order Crank Nicolson prediction. This is also needed to start the algorithm, since it is not self-starting due to its multistep nature.

5.3.2 Correction

The linearized equation for Newton iteration becomes:

$$\begin{bmatrix} \boldsymbol{M} + b_1\boldsymbol{C}_t + b_1^2\boldsymbol{K}_t & \boldsymbol{C}_t + 0.5h\boldsymbol{K}_t & 0 \\ b_1^2\boldsymbol{K}_t^{con} & \boldsymbol{M} + 0.5h\boldsymbol{K}_t^{con} & -(\boldsymbol{g}_q^A)^T \\ b_1\boldsymbol{\Psi}_v + b_1^2\boldsymbol{\Psi}_q & \boldsymbol{\Psi}_v + 0.5h\boldsymbol{\Psi}_q & \boldsymbol{\Psi}_{\Lambda^A} \end{bmatrix} \begin{bmatrix} \Delta\boldsymbol{a} \\ \Delta(\Delta\boldsymbol{v}^{con}) \\ \Delta\boldsymbol{\Lambda}^A \end{bmatrix} = \begin{bmatrix} -\mathrm{res}^{\boldsymbol{q}} \\ -\mathrm{res}^{\boldsymbol{con}} \\ -\boldsymbol{res}^{\boldsymbol{\Psi}} \end{bmatrix}$$

where the tangent stiffness and damping matrices are defined as: $\mathbf{K}_t = \partial(M\mathbf{a} - \mathbf{h})/\partial\mathbf{q}$ and $C_t = -\partial\mathbf{h}/\partial\mathbf{v}$.

We define also $\boldsymbol{K}_t^{con} = \partial(\boldsymbol{M}\Delta\boldsymbol{v}^{con} - (\boldsymbol{g}_q^A)^T\boldsymbol{\Lambda}^A)/\partial\boldsymbol{q}$.

The terms $\boldsymbol{\Psi}_v$, $\boldsymbol{\Psi}_q$, and $\boldsymbol{\Psi}_{\Lambda^A}$ are the partial derivatives of the function Ψ with respect to $\boldsymbol{v}_{n+1}$, $\boldsymbol{q}_{n+1}$ and $\boldsymbol{\Lambda}^A_{n+1}$, respectively and are the generalized Jacobians at the point of discontinuity.

A consistent update of the solution is then:

$$\begin{aligned} \boldsymbol{a}_{n+1} &\mathrel{+}= \Delta\boldsymbol{a} \\ \Delta\boldsymbol{v}^{con} &\mathrel{+}= \Delta(\Delta\boldsymbol{v}^{con}) \\ \boldsymbol{\Lambda}^A &\mathrel{+}= \Delta\boldsymbol{\Lambda}^A \\ \boldsymbol{v}_{n+1} &\mathrel{+}= b_0\Delta\boldsymbol{a} + \Delta(\Delta\boldsymbol{v}^{con}) \\ \boldsymbol{q}_{n+1} &\mathrel{+}= b_0^2\Delta\boldsymbol{a} + 0.5h\cdot\Delta(\Delta\boldsymbol{v}^{con}) \end{aligned}$$

5.4 Numerical Results

5.4.1 Bouncing Ball

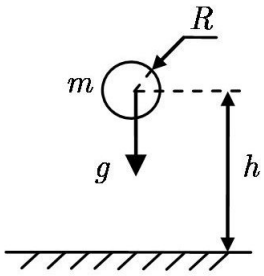

Figure 5.4: Model simulated

The first example is a classic ball bouncing on a horizontal plane, a well known benchmark example in the field of nonsmooth mechanics. Both the ball and the plane are rigid. The ball, subjected to gravity, bounces on the rigid plane with a restitution coefficient $e = 0.8$. Thus, it introduces a unilateral constraint on the vertical position of the ball. The ball is standstill in the beginning. Other physical parameters of this example are as follows: mass m = 1kg, radius $R = 0.2m$, gravity acceleration $g = 10m/s^2$, initial height $h = 1.001m$. The numerical parameters are set as: time step $h = 1e - 3$ for all the methods; for the nonsmooth multistep method, ρ is chosen as 0.6, for the Moreau–Jean time stepping method, θ= 0.5.

All parameters of the simulations are listed in table 5.1.

All the methods show consistent impact characteristics and the results are coincident.

Table 5.1: Test parameters

restitution coefficient	e	0.8	non dim.
timestep	h	$1.e-3$	s
mass	m	1.	Kg
radius	R	0.2	m
gravity	g	10.	m/s^2
initial height	H	1.001	m
Multistep spectral radius	ρ	0.82	non dim.
Moreau Jean theta	θ	0.5	non dim.
MBDyn's Moreau Jean module theta	θ	0.5	non dim.
HHT alpha (corresponding to $\rho_\infty = 0.82$)	α	0.1	non dim.

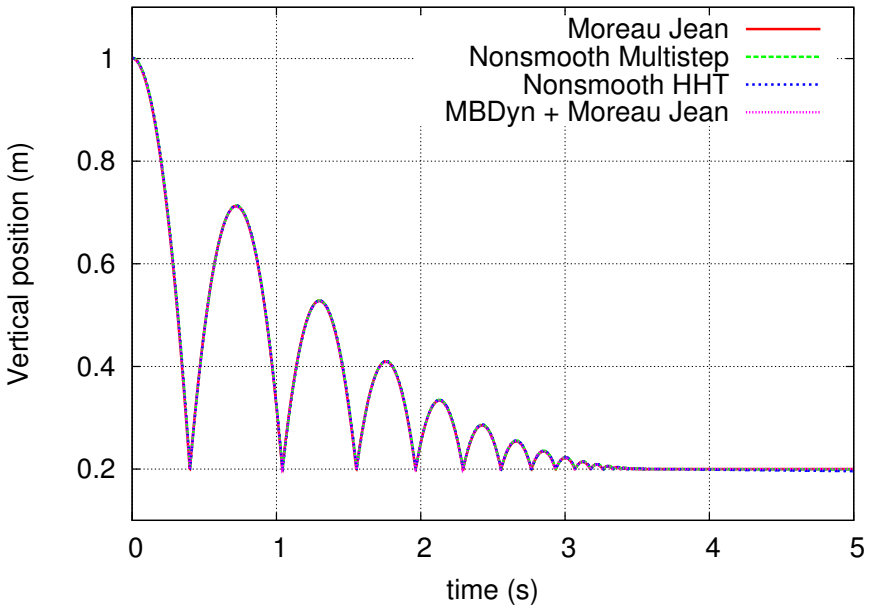

Figure 5.5: Bouncing ball vertical position vs time: Moreau Jean method, Nonsmooth HHT, Nonsmooth Multistep, MBDyn+Moreau Jean.
The results of the four integration methods are coincident.

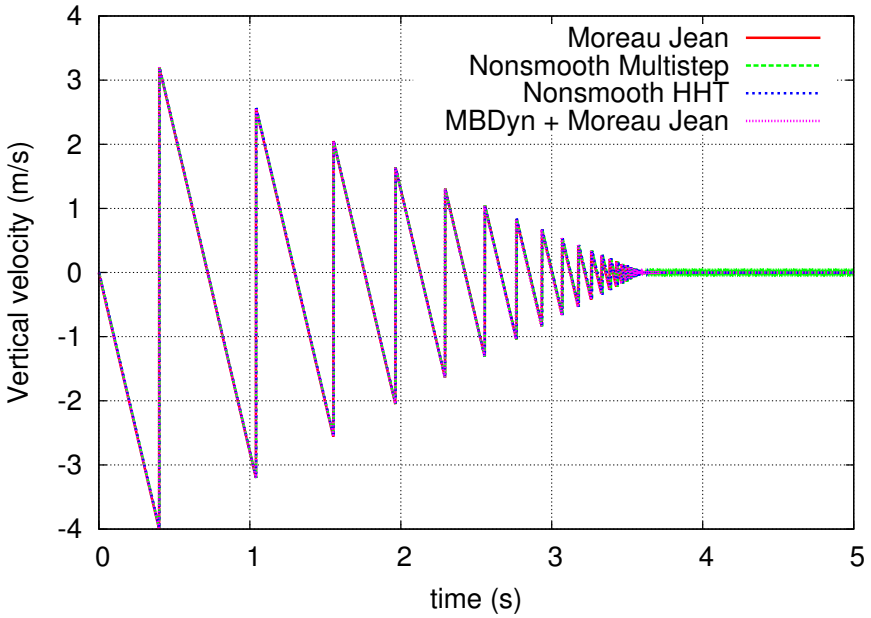

Figure 5.6: Bouncing ball vertical velocity vs time: Moreau Jean method, Nonsmooth HHT, Nonsmooth Multistep, MBDyn+Moreau Jean.
The results of the four integration methods are coincident.

5.4.2 Linear oscillator

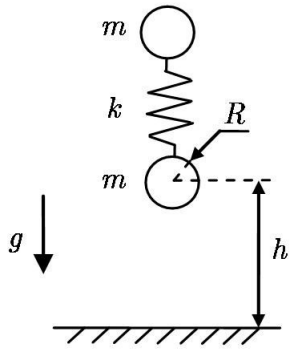

Figure 5.7: Model simulated

In this example the motion of a vertical linear oscillator is studied. The model of the oscillator is shown in Fig. 5.7, where two masses are connected by a spring. The oscillator is subjected to gravity $g = 10m/s^2$, and has two DOF in the vertical direction. After the lower ball gets in contact with the smooth plane, it bounces with a restitution coefficient of 0.8. In the meanwhile, it is also subjected to a force by the compressed spring. Thus, a second impact or multiple impacts can happen. In the free-flight mode, the system is oscillating with its natural frequency. The mass is of 1kg for each ball, and the stiffness of the spring is 10^4 N/m. The initial velocity is zero and the initial height of the masses is of $1.001m$.

Numerical parameters are the same as in table 5.1.

Due to the compression force by the spring, a second impact happens right after the first one. Fig 5.11 shows the total energy, numerical dissipation appears larger for the Moreau Jean method with $\theta = 1$ (implicit Euler discretization).

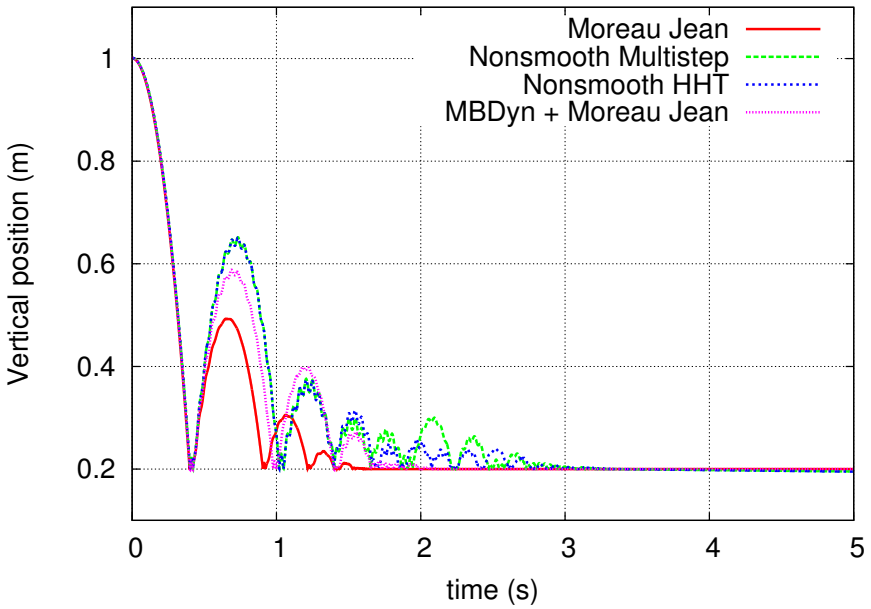

Figure 5.8: Linear oscillator. Vertical position vs time: Moreau Jean method, Nonsmooth HHT, Nonsmooth Multistep, MBDyn+Moreau Jean.

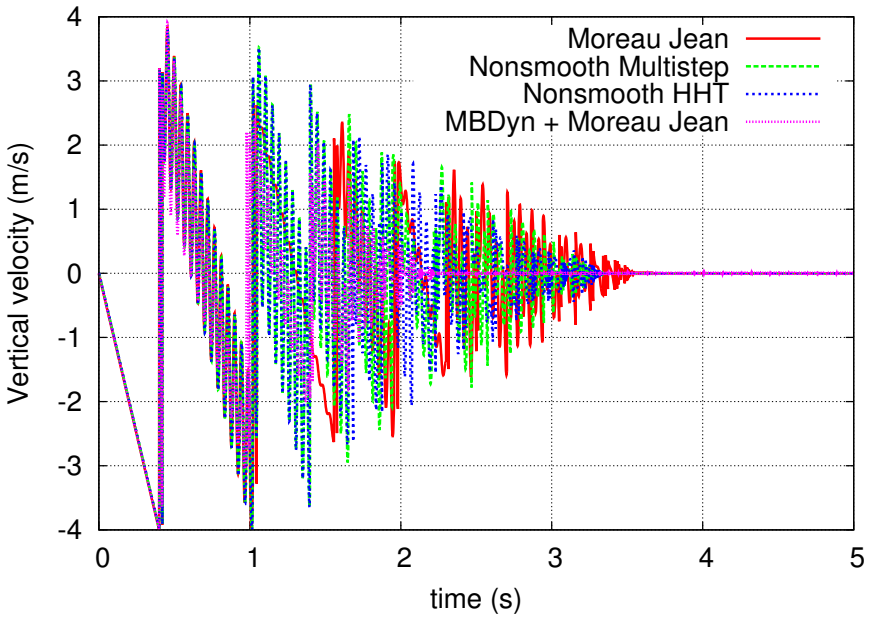

Figure 5.9: Linear oscillator. Vertical velocity vs time: Moreau Jean method, Nonsmooth HHT, Nonsmooth Multistep, MBDyn+Moreau Jean.

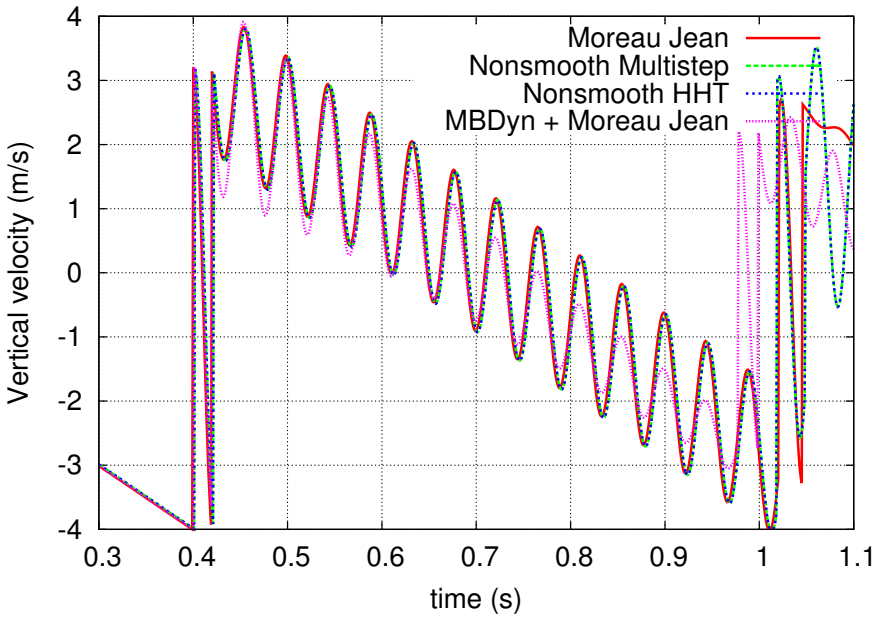

Figure 5.10: Linear oscillator. Vertical velocity vs time (Zoom): Moreau Jean method, Nonsmooth HHT, Nonsmooth Multistep, MBDyn+Moreau Jean.

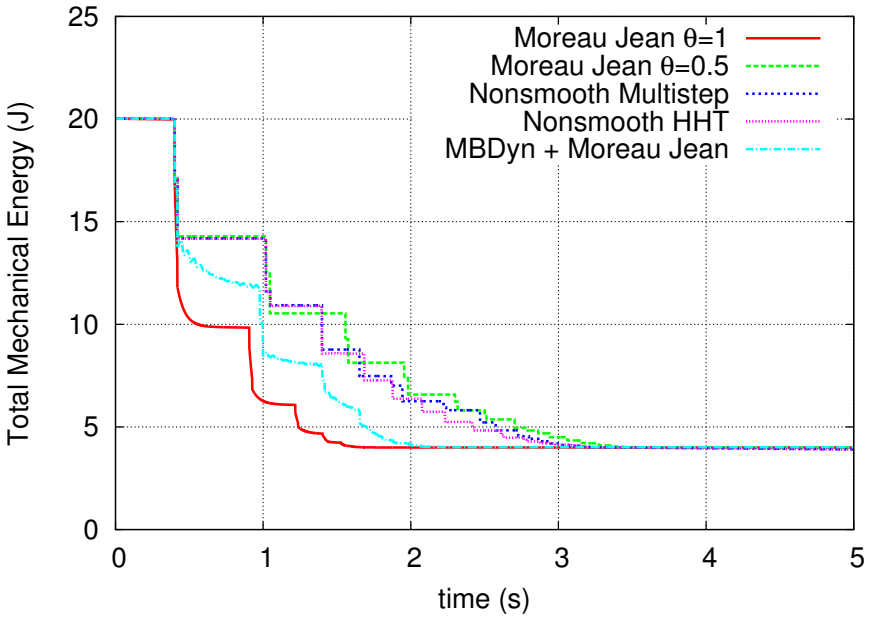

Figure 5.11: Linear oscillator. Total mechanical energy vs time.

5.4.3 Chain of oscillators

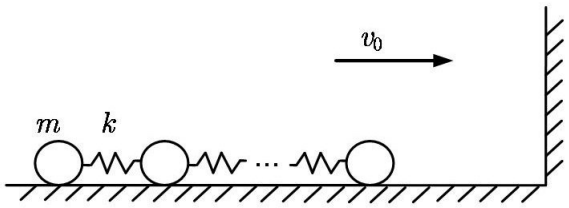

Figure 5.12: Chain model

The example is considered in order to study the numerical results when a persistent closed contact occurs. This model comprises 100 masses and 99 springs, which connect the masses one by one. The chain of oscillators model is placed on a smooth plane without friction, see Fig 5.12. It moves toward a wall on the left, and the first mass is subject to a unilateral constraint due to the wall, with a Newton restitution impact law. The initial velocity of the chain is set as $v_0 = -1m/s$, (the positive direction is to the left). The rest of the physical and numerical parameters are the same of the above two examples.

The closed contact constraint is stable for the four methods considered, there is no drifting of the constraint formulated at velocity level.

The algorithmic dissipation is comparably small for all the methods with the exception of the Moreau-Jean time-stepping with $\theta = 1$, which is equivalent to a discretization with implicit Euler.

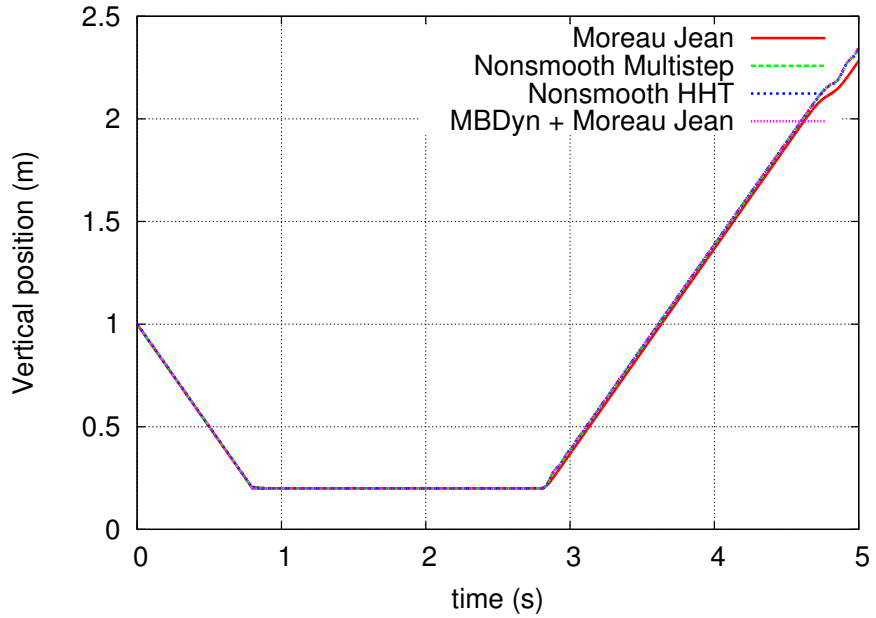

Figure 5.13: Chain example. Vertical position of the unilaterally constrained mass vs time: Moreau Jean method, Nonsmooth HHT, Nonsmooth Multistep, MBDyn+Moreau Jean.

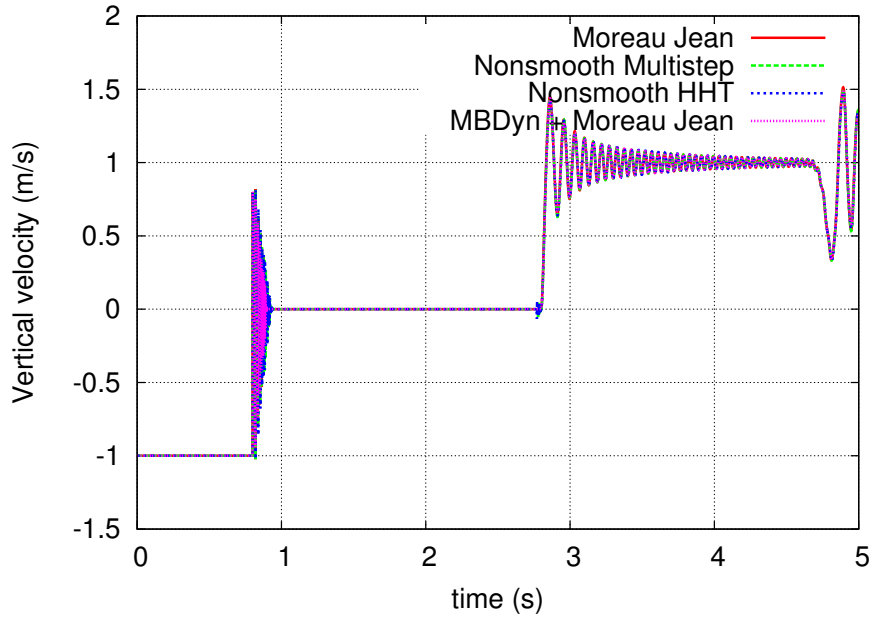

Figure 5.14: Chain example. Vertical velocity of the unilaterally constrained mass vs time: Moreau Jean method, Nonsmooth HHT, Nonsmooth Multistep, MBDyn+Moreau Jean.

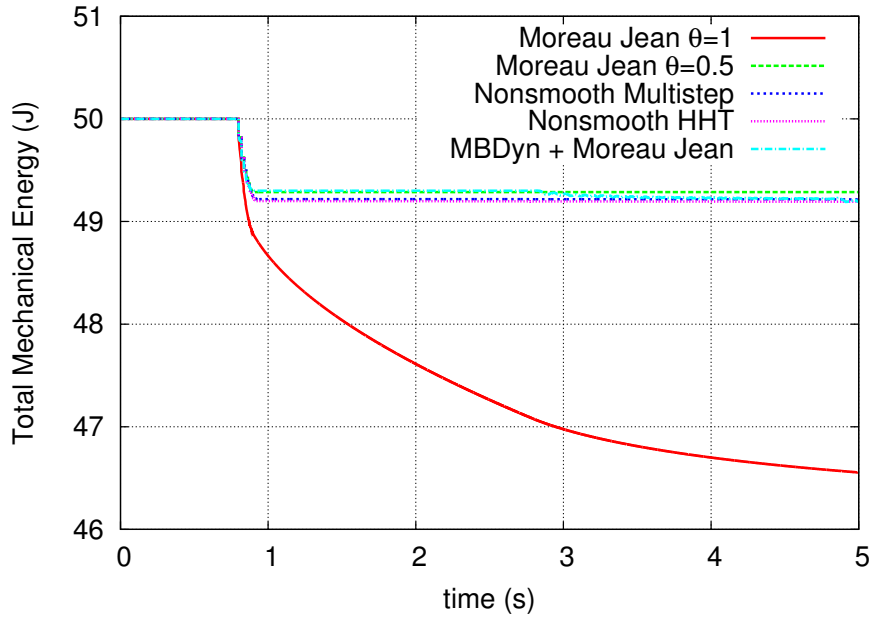

Figure 5.15: Chain example. Total mechanical energy vs time

5.5 Conclusions

The 2nd order, A/L stable, two-step integration formula considered in this chapter presents advantages in the analysis of complex multibody and multidisciplinary systems, as it is suited to deal with first and second order dynamics alike and with DAE formulations providing a good trade-off between accuracy and computation time.

This chapter presents its adaptation to problems that include the nonsmooth characteristics of unilateral constraints, following the method proposed in [7] for Newmark-type integration schemes.

Since it is a two step formula special care has been taken in the implementation of the prediction phase of the method in the steps following a velocity jump, where a single-step second order accurate re-initialization of the analysis is required.

The solution of some numerical examples empirically shows that the method is valid and stable.

The comparison of the results with those from the cited nonsmooth adaptation of the Newmark-type HHT algorithm [7] further validate the MBDyn-MoreauJean co-simulation approach proposed in the previous chapters. This last strategy shows a comparatively larger numerical dissipation, though smaller than the Moreau-Jean method with $\theta = 1$.

Chapter 6

An Application: Helicopter Rotor Sailing

6.1 A test on a realistic application

In the following the approach presented in previous chapters is tested on a more realistic application of aerospace interest. The problem considered is the modeling of the droop-stop and flap-stop contacts on helicopter blades. In the phases of rotor engagement and disengagement, at low rotor speed in high wind conditions, an aeroelastic phenomenon called blade sailing can ensue, with potentially dangerous blade motion and excessive flapwise tip deflections [37]. In case of an articulated rotor support points in correspondance of the blade cuff are needed to overcome the effect of the blade weight at low rotation speeds, and this devices are called droop stops. Additional restraint is required to prevent upward vertical movement of the blade, in case of wind speed gust at low rotor speed. That is provided by the antiflap assembly.

An aeroservoelastic model of the SA-330 Puma helicopter rotor, implemented in MBDyn, has been used as a base for the simulations. The nonlinear multibody aeroelastic model of the SA-330 Puma helicopter implemented in MBDyn was already available from previous work by [36]. The SA-330 Puma has been characterized mainly using the appendix of the NASA Technical Manual [4] as data source.

The model consists in the main rotor modeled using the multibody approach: kinematically exact constraints, enforced by means of Lagrange multipliers, describe the relative motion between rigid bodies, while structural dynamics is dealt with by a Finite Element approach using nonlinear, geometrically exact beam elements, and by lumped masses. Each blade of the main rotor is therefore modeled using 5 three-node nonlinear beam elements, resulting in 11 structural nodes per blade. A Blade Element/Momentum Theory aerodynamic model has been included through

the use of off the shelf MBDyn elements. The model is described by a total of 672 equilibrium (differential) equations and 805 smooth (algebraic) constraints.

In this model, derived from cited previous work, two ways of describing the contact at droop-stops and anti-flap stops have been implemented, allowing a comparison of the results. The first model uses the continuous contact implementation described in chapter 2, and the second one uses the nonsmooth module introduced in chapter 4.

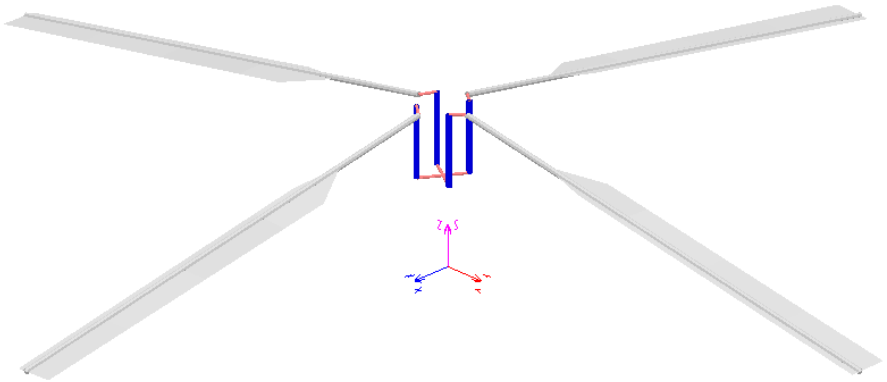

Figure 6.1: Helicopter rotor model

6.1.1 Contact assembly modeling

The continuous contact way of modeling the droop and anti-flap stops introduces a regularization of the nonsmooth properties of the contact. Here for simplicity it is modeled as two deformable hinges coincident the blade flap hinge, each provided of a steep stiffness law in correspondance of the angles at which the droop and antiflap mechanisms are set to intervene. It uses the constitutive laws considered in 2, and added to the modeling capabilities of MBDyn.

In a second model the droop and anti-flap contacts have been modeled through the use of the nonsmooth-node module introduced in 4. Here the mechanism is described as a contact point rigidly attached under the first node after the flap hinge, at an offset. This node representing the contact point has his movement limited by a vertical plane set in a position such that it limits, through the rigid joint, the angles that the blade root can assume with respect to the horizontal plane. The node subject to the unilateral constraint represents the nonsmooth subsystem integrated by the nonsmooth-node module, and the plane is defined as an unilateral constraint that rotates with the rotor hub. The contact node is linked to the blade cuff through a rigid joint constraining its offsetted position and orientation in relation to the first node after the flap hinge, at the root of the blade. This is done through the use of the total joint element of the library of MBDyn, and geometry of this contact model

is illustrated in figure 6.2. Figure 6.2 shows the unilateral constraint modeled as a plane, and in red the point of contact. The plane is linked to the first node after the lag hinge, in order to be always aligned with the blade direction, even in case of ample lag in the motion of the blade with respect to the hub.

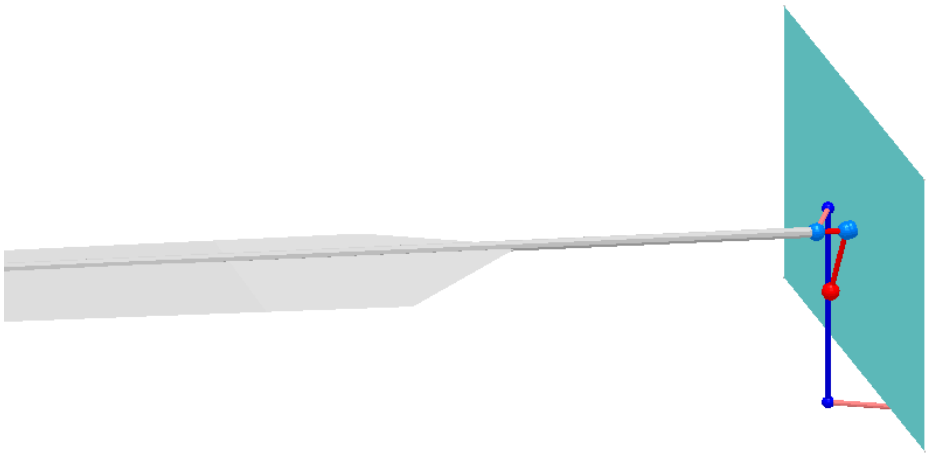

Figure 6.2: Modeling of the droop-stop contact with the nonsmooth module

To compensate from overconstraining a relaxation of this rigid joint has been necessary, and has been implemented through the use of a Tikhonov regularization element, already available in the library of the MBDyn software. The Tikhonov regularization consists in modifying a constraint so that it can be violated by an amount that depends on the multipliers. Given a dynamics described by a set of differental equations together with constraint algebraic equations:

$$\begin{cases} \boldsymbol{F}\left(x, \dot{x}, \ddot{x}, t\right) + \boldsymbol{\Phi}_{/x}^{T} \boldsymbol{\lambda} = 0 \\ \boldsymbol{\Phi}\left(x\right) = 0 \end{cases}$$

the Tikhonov regularization introduces a term of relaxation on the constraints as:

$$\begin{cases} \boldsymbol{F}\left(x, \dot{x}, \ddot{x}, t\right) + \boldsymbol{\Phi}_{/x}^{T} \boldsymbol{\lambda} = 0 \\ \boldsymbol{\Phi}\left(x\right) - \mathrm{c}\boldsymbol{\lambda} = 0 \end{cases}$$

where c is a small constant that can be set in the input: the larger the coefficient, the larger the constraint violation for a given value of the reaction $\boldsymbol{\lambda}$.

This is an application that shows the versatility of the co-simulation module implementation, which allow to add points of frictionless and frictional contact to a model, in which the nonsmoothness due to the unilaterality is dealt with event-capturing timestepping techniques. But this application is also a particularly challenging situation for the concept, since through the rigid joint the two subsystems co-simulated are very strictly coupled.

6.2 Simulation: rotor engagement and disengagement

In order to test this two modelizations of a contact problem two operational conditions of interest have been simulated.

First the rotor engagement and disengagement phases have been considered.

The hub rotation speed through the lenght of the simulation is illustrated in figure 6.3, and follows two cosine laws for the rotor start and disengagement phases of the kind written in equation 6.1.

$$f(t) = \omega \cdot \left(1\text{-}\cos\left(\frac{\pi}{20} \cdot t\right)\right) \tag{6.1}$$

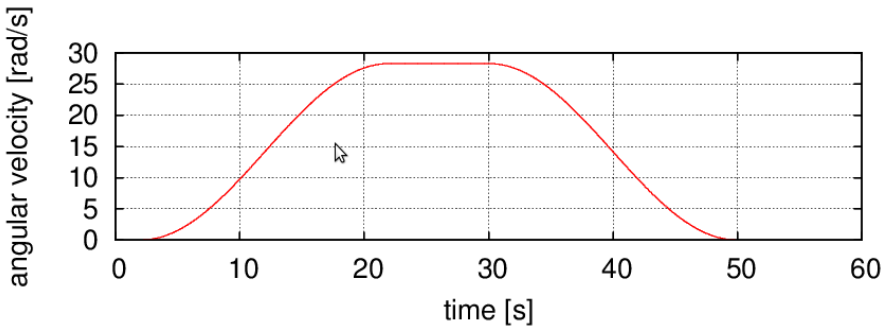

Figure 6.3: Rotor speed vs time

The motion of each blade through the simulation can be discerned with figure figure 6.4, representing the flap angle between the blade and the horizontal plane, and the lag angle of the articulated rotor. The blades are initially still, their weight supported by the flap stops at an angle of $-10°$. Each blade gradually elevates from the contact, then stays at a regime for 10 seconds and afterwards winds down with the same cosine law but opposite sign. The simulation is not realistic and much shorter than actual start-stop procedures but it is set to highlight the developed module capabilities of modeling the non inter-penetration unilateral constraint of the flap-stop contact.

The simulation has been carried out with the collective, aft, and lateral commands set to zero, and it includes gravity. The properties of the airstream refer to standard air , still.

Simulation parameters are gathered in table 6.1.

Table 6.1: SA 330 Puma. Simulation parameters

Nonsmooth Node Model	
Restitution coefficient	0.8
Timestep	$1.e-4$
Tolerance	$1.e-4$
Tikhonov constant	$5.e-9$
Continuous Contact Model	
Constitutive law	Flores et al.
Restitution coefficient	0.8
Timestep	$1.e-4$
Tolerance	$1.e-4$
Contact stiffness	$1.e9$

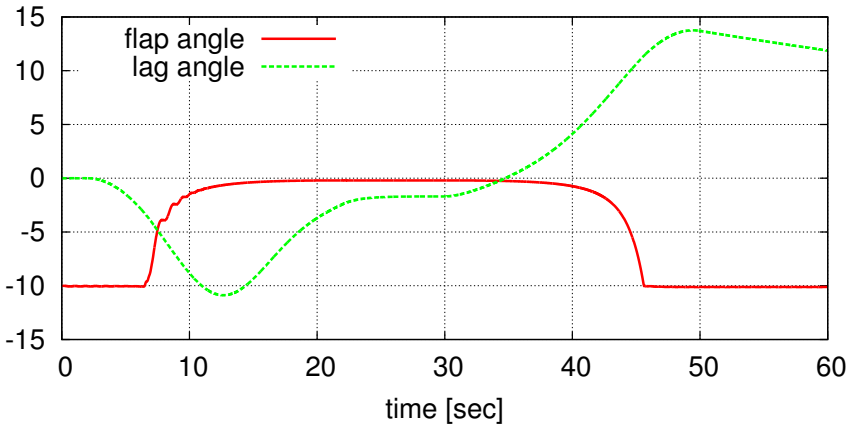

Figure 6.4: Flap and lag hinge angle of the articulated rotor

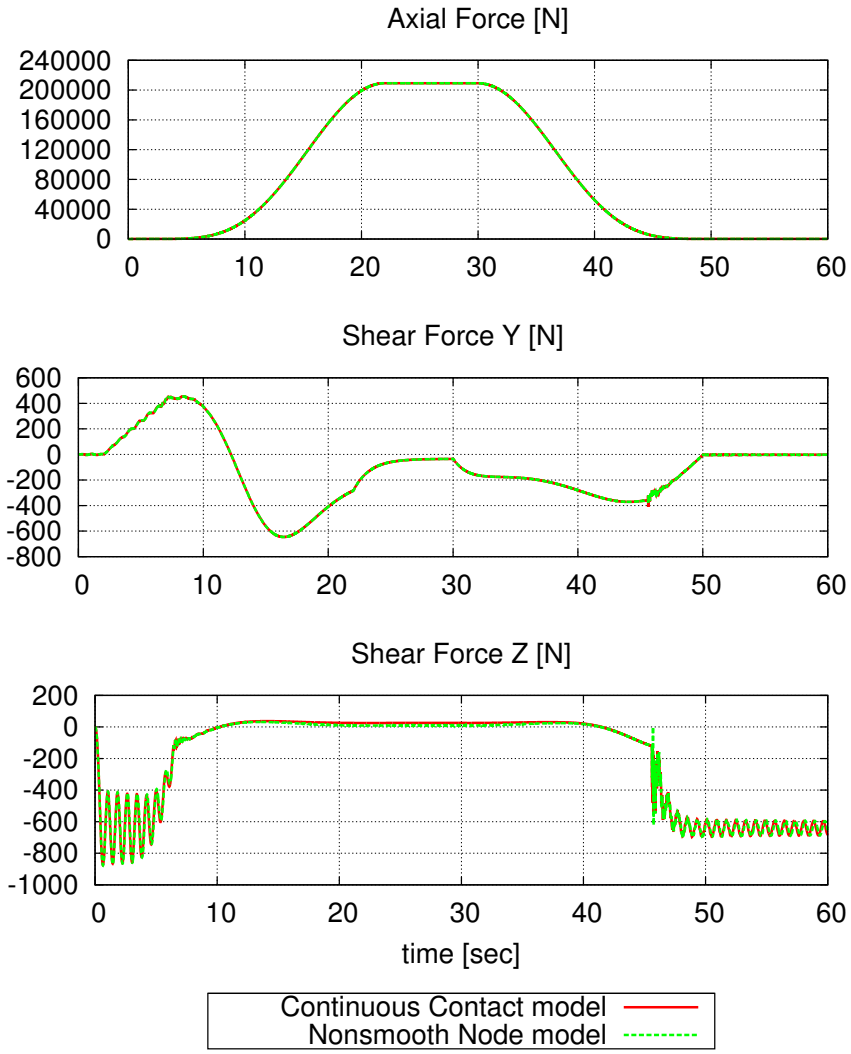

Figure 6.5: Vertical force components in the root section of the first blade.

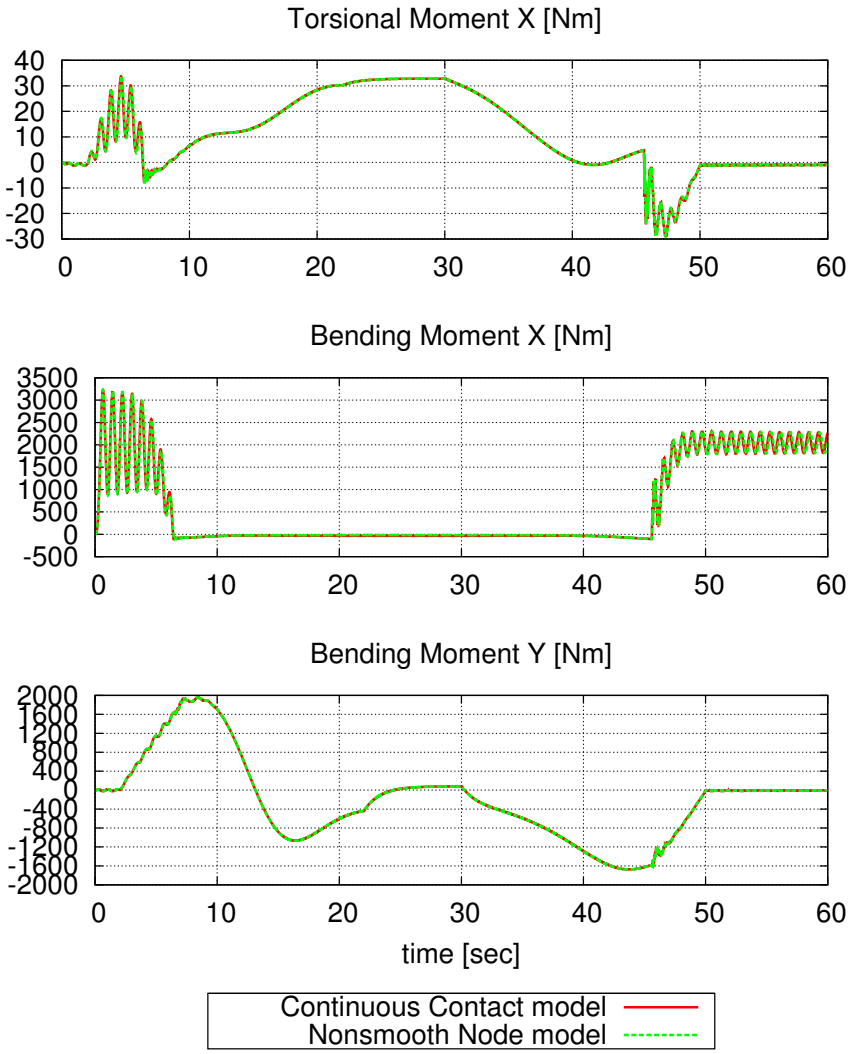

Figure 6.6: Bending moments in the root section of the first blade.

In figure figure 6.6 and figure 6.5 are shown the three components of the force and the moment in the beam section at the root of the first blade. The results of the continuous contact approach and the modelization through the nonsmooth node are well correlated, and they show in the initial phases and end phases a more relevant shear force along the vertical due to the contact with the droop stop. The force and moment are oscillating due to the flexibility of the blade.

The table 6.2 shows that in this application the method developed doesn't show an advantage in computing times, because of the higher number of iterations necessary at each step to arrive at convergence for the co-simulation of the smooth and non-smooth dynamics integrations. This application put the cosimulation concept at test in its limits, since there's a rigid connection between the two subsystems cosimulated, hence the bigger number of iterations to converge. But even in this limit application the method is shown to arrive at a solution, and it can be a tool for dealing with frictional contacts more effectively than with a regularized solution,

and in applications where the contact point, or the "nonsmooth subsystem" is less rigidly coupled with the rest of the system.

Table 6.2: Computation load comparison

	Continuous contact	Nonsmooth Node
CPU time	2867 seconds of CPU time	10331.460 seconds of CPU time
Total number of steps	600000	600000
Total iterations	1153635	6614384
Total Jacobians	599373	1905732
Total Error	6.83966	17.5347

6.3 Simulation: rotor sailing

To further test the robustness of the model, a different simulation condition has been considered. The rotor, initially still with the four blades weighting on the droop stop contacts, is invested by an intense wind gust, whose profile is represented in figure 6.7. The direction of the gust front and its profile are on the horizontal plane, directed transversally with respect to the first blade elongation.

The gust model consists in a unifom front :

$$\mathbf{v}(\mathbf{x}, t) = \mathbf{n} \cdot g \cdot (\mathbf{f} \cdot \mathbf{x} + V_{ref} t)$$

where

- $\mathbf{v}$ is the velocity perturbation;
- $\mathbf{x}$ is the position of the point whose airstream velocity is being computed;
- t is the current time;
- $\mathbf{n}$ is the unit vector perturbation_direction that defines the direction of the velocity perturbation;
- $g()$ is the function front_profile that defines the gust profile; In our case a cosine law illustrated in 6.7.

$$g(t) = 15 \cdot \left(1\text{-}\cos\left(\frac{\pi}{100} \cdot t\right)\right) \tag{6.2}$$

- $\mathbf{f}$ is the unit vector front_direction that defines the direction of propagation of the front;
- V_{ref} is the velocity front_velocity of propagation of the front in direction f .

The blades have a collector angle of 10°. The first blade is therefore raised by the aerodynamic force, until the flap stop comes into contact. after the gust passes the blade fall on the droop-stop contact, with some bouncing due to the flexibility of the blade. This behaviour is illustrated in figure figure 6.8, which shows the flap hinge angles limited by the droop-stop and anti-flap contacts, at -10° and +10°. On the other side of the rotor the third blade experience a downward force, while blades 2 and 4 are not sensibly interested by the gust.

In figures figure 6.9 and figure 6.10 are shown the three components of the force and the moment in the beam section at the root of the first blade. The results of the continuous contact approach and the modelization through the nonsmooth node are well correlated.

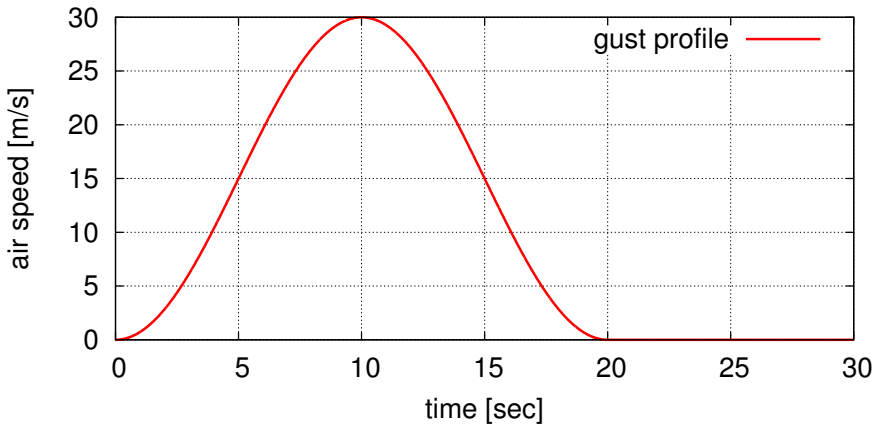

Figure 6.7: Gust profile at the hub of the articulated rotor

Table 6.3: SA 330 Puma. Simulation parameters

Nonsmooth Node Model	
Restitution coefficient	0.8
Timestep	$1.e-4$
Tolerance	$1.e-2$
Tikhonov constant	$5.e-9$
Continuous Contact Model	
Constitutive law	Flores et al.
Restitution coefficient	0.8
Timestep	$1.e-4$
Tolerance	$1.e-2$
Contact stiffness	$1.e9$

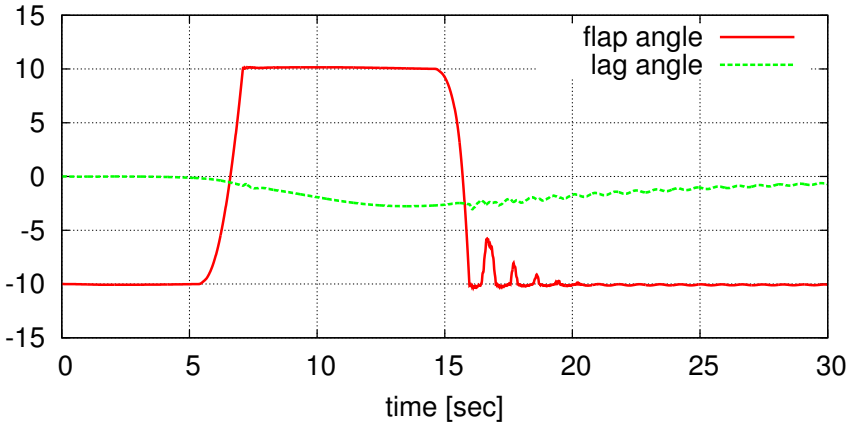

Figure 6.8: Flap and lag hinge angles, in degrees, of the first blade

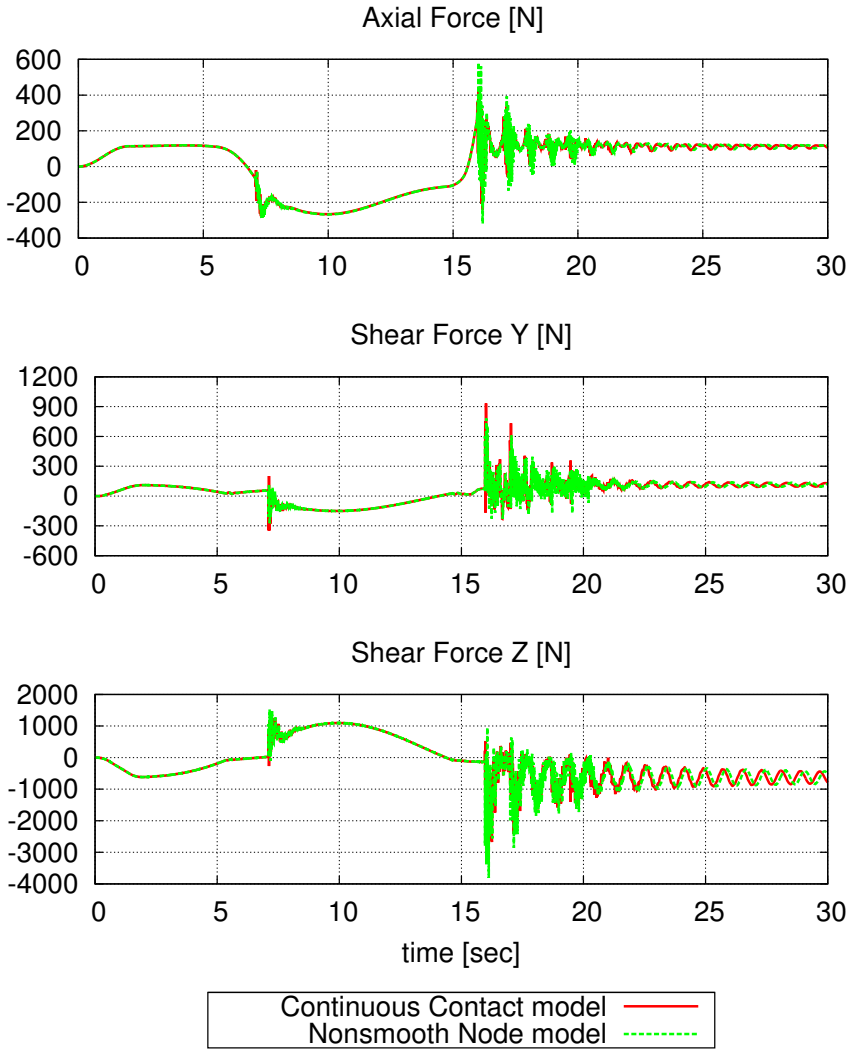

Figure 6.9: Vertical force components in the root section of the first blade.

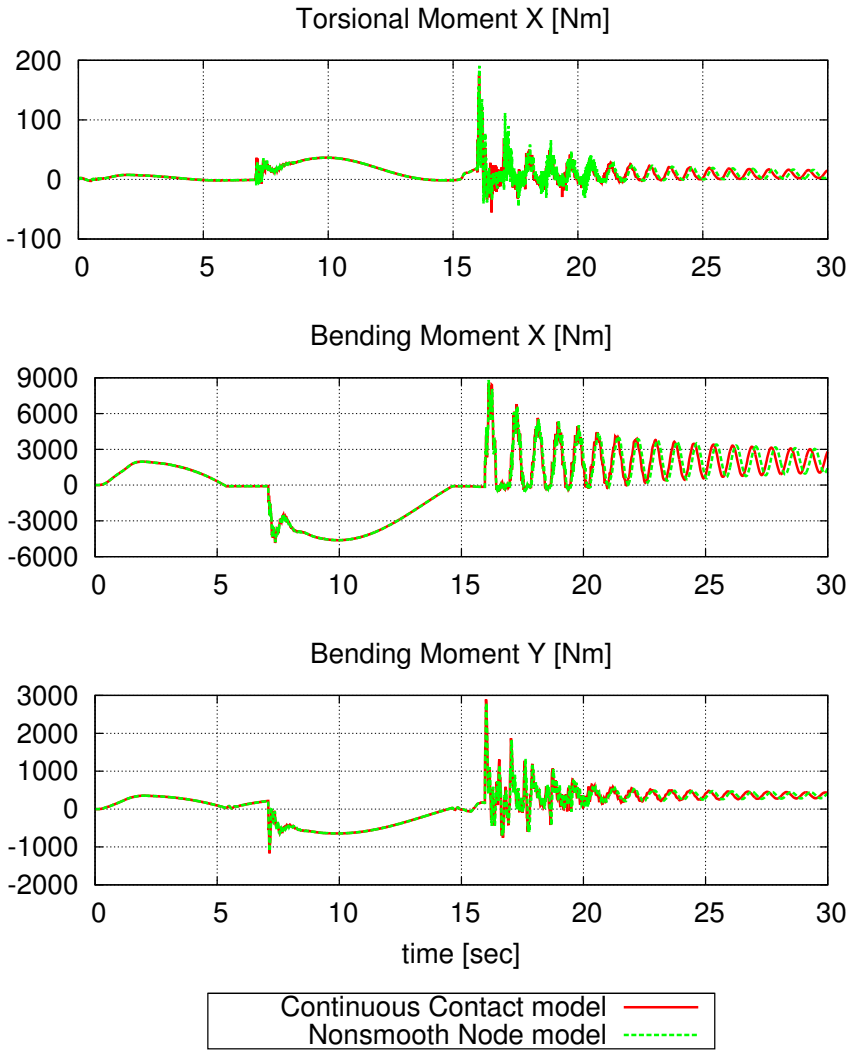

Figure 6.10: Bending moments in the root section of the first blade.

Table 6.4: Computation load comparison

	Continuous contact	Nonsmooth Node
CPU time	1275 seconds of CPU time	2009 seconds of CPU time
Total number of steps	300000	300000
Total iterations	263619	879676
Total Jacobians	260920	346068
Total Error	385.514	2262.5

Chapter 7

Frictional Contact Problem Co-simulation

An extension of the module introduced in chapter 4 is presented here, in which the nonsmooth subsystem integrated with the *time-stepping* strategy comprises frictional contacts.

In order to deal with the nonsmoothness of the frictional phenomena, as described by the Coulomb's law, a polyhedral approximation of the friction cone is used, so that it has been possible to cast the problem as an LCP. This is a well known approach that is not optimal for problems with a large number of contacts, since the number of facets of the approximation of the friction cone directly augment the size of the problem. Also it introduces anisotropy in the description of the problem. It is nonetheless a simple and suitable approach for problems of limited dimensions, and can take advantage of the vast availability of LCP solver implementations.

It is the aim of this chapter to test the approach described in chapter 4 with a simple LCP-based approach to frictional contacts. The approximation of the friction cone and the reduction of the problem to an LCP is briefly described in section 7.1. The implementation through a dynamically loaded module in MBDyn is then introduced. The results of some tests are compared with those from the Siconos Kernel algorithms, which comprises more sophisticated techniques for solving the Frictional Contact problem. The approach is then applied to a more complex example of a walking mechanism.

7.1 Three-dimensional Coulomb's friction

The most used model for friction is the one obtained by C.A. Coulomb by experimental investigation [8].

It states that the friction force acting on sliding bodies has magnitude propor-

tional to the normal contact force holding the two contacting bodies together. The constant of proportionality $\mu \geqslant 0$ is called coefficient of friction.

If there is sliding, the friction force is in the opposite direction to the relative direction of sliding.

If the bodies are not sliding, the friction force may have any value provided that its magnitude does not exceed μ times the normal contact force.

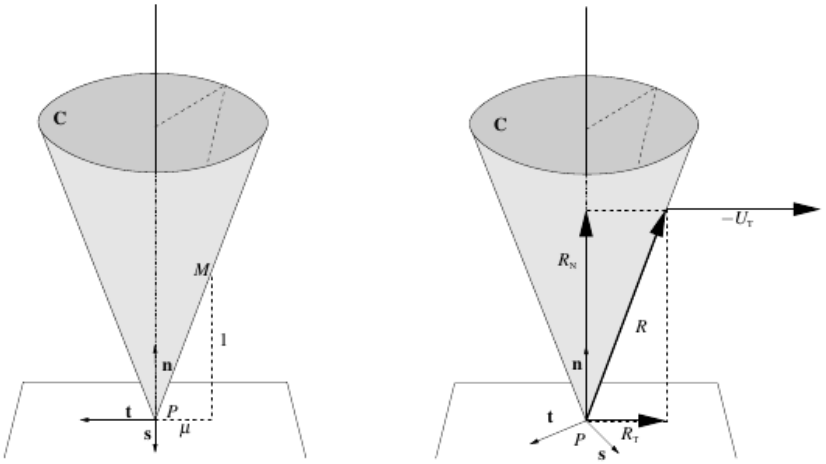

Figure 7.1: Three-dimensional Coulomb's friction cone *(figure from [2])*

Using some basic concepts from convex analysis we can restate the problem as follows. Coulomb's model links the reaction force $R \in \mathbb{R}^3$ to the tangential relative velocity $U_T \in \mathbb{R}^2$, through the friction cone $\mathbf{C}$. The cone $\mathbf{C}$ is a second-order convex cone with its apex at the contact point P, whose sections by planes parallel to the tangent plane are discs, and the angle between the normal $\mathbf{n}$ and any vector PM with M on the boundary of $\mathbf{C}$ is equal to $arctan\mu$. The Coulomb friction cone is depicted in figure 7.1.

Coulomb's friction says the following. If there's contact, alas the gap $g(q) = 0$, then

$$\begin{cases} if\, U_T(t) = 0 \,\text{then}\, R \in \mathbf{C} \\ if\, U_T \neq 0 \,\text{then}\, \|R_T(t)\| = \mu\,|R_N| \quad \text{and there exists a scalar } a \geqslant 0 \\ \qquad\qquad\qquad\qquad\qquad\qquad \text{such that } R_T(t) = -aU_T(t) \end{cases}$$

where we recall that in the above notation $R_T \in \mathbb{R}^2$, $R_N \in \mathbb{R}$. Thus Coulomb's model says that if the sliding velocity is not zero, then the reaction R lies on the boundary of $\mathbf{C}$, and its projection on the tangent plane has the same direction as but opposite sense to the sliding velocity. When the sliding velocity is zero, R is in $\mathbf{C}$, possibly on its boundary. The fact that $U_T = 0$ and R is on $\delta\mathbf{C}$ is therefore a

necessary condition to have a transition from sticking to sliding. A sliding case is depicted in figure 7.1. The Coulomb model is also often written as follows:

$$\|R_T(t)\| \leqslant \mu\,|R_N| \text{ and } \begin{cases} \|R_T(t)\| < \mu\,|R_N| & \Rightarrow U_T(t) = 0 \\ \|R_T(t)\| = \mu\,|R_N| & \Rightarrow \text{and there exists a scalar } b \geqslant 0 \\ & \text{such that } U_T(t) = -bR_T(t) \end{cases} \tag{7.1}$$

Let D_1 be a given closed convex subset of the common tangent plane between the two contacting bodies. Let $D = \mu D_1$. Let us introduce the following inclusion [34] using the indicator function $\psi_D(\cdot)$:

$$-U_T \in \delta\psi_D(R_T) \tag{7.2}$$

The meaning of equation (7.2) is as follows. If $R_T \in Int(D)$, then the normal cone to D is the singleton $\{0\}$, so the tangential relative velocity is null. If $R_T \in \delta D$, the boundary of D, then $-U_T$ is in the normal cone to D computed at R_T. Let D_1 be a disc with radius $|R_N|$, so that when R_T is on the boundary of D one has $\|R_T\| = \mu\,|R_N|$. Then the normal cone to D at R_T is nothing else but the ray passing through the center of the R disc (the apex of the cone C) and whose direction is that of R_T . If we denote $\mathbf{d} = \|R_T\|$, T the sliding direction, then $-U_T = b\mathbf{d}$ for some real $b \geqslant 0$. One sees that in this case equation (7.2) does represent the model in equation (7.1). When D_1 is not a disc the model may incorporate anisotropic effects (the friction coefficient may vary with the direction of sliding).

7.1.1 Implementation aspects

The notation and the approach used in this chapter follows the ones in [2]. The index set of all unilateral constraints in the system is:

$$I = \{1...\nu\} \subset \mathbb{N}$$

The index set I_a is the set of all forecast active constraints of the system:

$$I_a(\tilde{q}_{k+1}) = \{\alpha \in I \mid g^\alpha(\tilde{q}_{k+1}) \leqslant 0\} \subseteq I$$

where $\tilde{q}_{k+1}$ is the predicted status of the system. For instance Moreau takes $\tilde{q}_{k+1} = q_k + \gamma h v_k$ with $\gamma = \frac{1}{2}$ [35].

For each index $\alpha \in I_a(\tilde{q}_{k+1})$ it is specified here the notation for expressing the set of constraints in local coordinates.

$$
\begin{aligned}
U^a_{k+1} &= \left[U^\alpha_{k+1}\right]_{\alpha\in I_a(\tilde{q}_{k+1})} \\
U^a_{N,k+1} &= \left[U^\alpha_{N,k+1}\right]_{\alpha\in I_a(\tilde{q}_{k+1})} \\
U^a_{T,k+1} &= \left[U^\alpha_{T,k+1}\right]_{\alpha\in I_a(\tilde{q}_{k+1})} \\
P^a_{k+1} &= \left[P^\alpha_{k+1}\right]_{\alpha\in I_a(\tilde{q}_{k+1})} \\
P^a_{N,k+1} &= \left[P^\alpha_{k+1}\right]_{\alpha\in I_a(\tilde{q}_{k+1})} \\
P^a_{T,k+1} &= \left[P^\alpha_{k+1}\right]_{\alpha\in I_a(\tilde{q}_{k+1})} \\
H^a\left(\tilde{q}_{k+1}\right) &= \left[H^\alpha\left(\tilde{q}_{k+1}\right)_{k+1}\right]_{\alpha\in I_a(\tilde{q}_{k+1})} \\
H^a_N\left(\tilde{q}_{k+1}\right) &= \left[H^\alpha_N\left(\tilde{q}_{k+1}\right)_{k+1}\right]_{\alpha\in I_a(\tilde{q}_{k+1})} \\
H^a_T\left(\tilde{q}_{k+1}\right) &= \left[H^\alpha_T\left(\tilde{q}_{k+1}\right)_{k+1}\right]_{\alpha\in I_a(\tilde{q}_{k+1})} \\
p = \sum_\alpha p^\alpha \quad &= \sum_{\alpha\in I_a(\tilde{q}_{k+1})} H^\alpha\left(\tilde{q}_{k+1}\right) P^\alpha = H^a\left(\tilde{q}_{k+1}\right) P
\end{aligned}
$$

The components of the local velocities U and reactions P are expressed through the mappings H^α for every contact α with respect to the generalized variable q.

With this notation it is possible to construct a Delassus operator for the set of forecast active constraints:

$$
\begin{cases}
\hat{W}^a &= H^{a,T}\hat{M}^{-1}H^a \\
\hat{W}^a_{NN} &= H^{a,T}_N\hat{M}^{-1}H^a_N \\
\hat{W}^a_{TT} &= H^{a,T}_T\hat{M}^{-1}H^a_T \\
\hat{W}^a_{NT} &= H^{a,T}_N\hat{M}^{-1}H^a_T
\end{cases}
$$

7.1.2 Outer faceting the Coulomb's cone

In order to lighten the notation the subscript $_{k+1}$and the superscript $^\alpha$, indicating the indexes of the contacts, are dropped here.

Contrary to the two-dimensional frictional contact problem, the three-dimensional case cannot be directly cast into an LCP standard form. This is mainly due to the second-order cone C which cannot be written as a polyhedral cone. The nonlinear nature of the section of the friction cone, i.e., the disk $D(\mu R_N)$ defined by:

$$
D\left(\mu R_N\right) = \left\{R_T \mid \sigma\left(R_T\right) = \mu R_N - \|R_T\| \geqslant 0\right\}
$$

adds new difficulties from the formulation point of view. To overcome this difficulty, some approximations have been proposed which consist in faceting C. Following the presentation in [2], which refers to the original work in [24] and [25], the friction disk D can be approximated by an outer polygon:

$$
D_{outer}\left(\mu R_N\right) = \bigcap_{i=1}^{\omega} D_i\left(\mu R_N\right)
$$

$$D_i(\mu R_N) = \left\{ R_T \mid \sigma_i(R_T) = \mu R_N - c_i^T R_T \geqslant 0 \right\}$$

Where $\omega \in \mathbb{N}$ is the number of facets. The functions $\sigma_i(R_T)$ are the friction saturation with respect to the cone $D_i(\mu R_N)$ generated by an outward unit vector $c_i \in \mathbb{R}$. Using the framework of convex analysis we now assume that the contact law equation (7.2) is of the form

$$-U_T \in N_{\mathbf{D}_{outer}(\mu R_N)}(R_T)$$

The normal cone to $\mathbf{D}_{outer}(\mu R_N)$ is given by

$$N_{\mathbf{D}_{outer}(\mu R_N)}(R_T) = \sum_{i=1}^{\omega} N_{\mathbf{D}_i(\mu R_N)}(R_T)$$

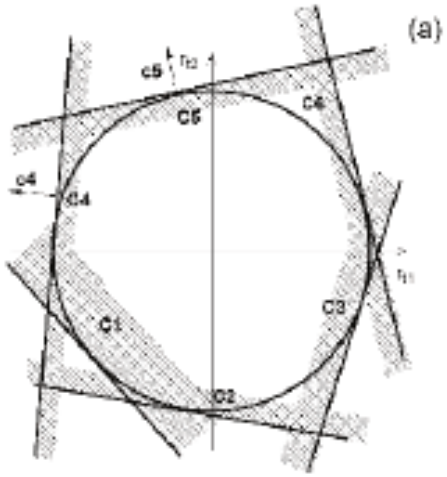

Figure 7.2: Approximation of the base of the Coulomb cone by an outer approximation

and the inclusion can be stated as:

$$-U_T = \sum_{i=1}^{\omega} k_i \delta\sigma_i(R_T), \quad 0 \leqslant \sigma_i(R_T) \perp k_i \geqslant 0$$

Since $\sigma_i(R_T)$ is linear with respect to R_T, we obtain the following MLCP:

$$-U_T = \sum_{i=1}^{\omega} k_i c_i, \quad 0 \leqslant \sigma_i(R_T) \perp k_i \geqslant 0$$

Assuming for the sake of simplicity that the vectors c_i are chosen equal for all contacts α, the time-discretized linear One Step Non Smooth Problem (OSNSP), $(\mathcal{P}_L)$, can be written as

$$(\mathcal{P}_L)\begin{cases} U_{k+1} = \hat{W} P_{k+1} + U_{free} \\ \begin{cases} -U_T^\alpha = \sum_{i=1}^{\omega} k_i^\alpha c_i & \forall \alpha \in I_a\left(\tilde{q}_{k+1}\right) \\ \sigma_i\left(P_{T,k+1}^\alpha\right) = \mu P_{N,k+1}^\alpha - c_i^T P_{T,k+1}^\alpha \\ 0 \leqslant U_{N,k+1}^\alpha + e^\alpha U_{N,k}^\alpha \perp P_{N,k+1}^\alpha \geqslant 0 \\ 0 \leqslant \sigma_i^\alpha\left(P_{T,k+1}^\alpha\right) \perp k_i^\alpha \geqslant 0 \end{cases} \end{cases} \tag{7.3}$$

The fact that the friction saturation functions $\sigma_i\left(P_{T,k+1}\right)$ are linear shows that the previous problem is an MLCP.

7.1.3 The LCP in a single-contact case

Generally, the MLCP equation (7.3) can be reduced into an LCP in standard form assuming that at least one pair of vectors c_i is linearly independent. The most simple way to transform an MLCP into an LCP is to compute a Schur complement of the MLCP matrix, which necessitates to invert a sub-matrix. To be able to invert a sub-matrix of the MLCP equation (7.3), we assume that a pair of c_i^α vectors is linearly independent for $i \in \mathcal{P}^\alpha \subset \{1...\omega^\alpha\}$, where it is recalled that ω^α is the number of facets of the approximation of the cone at the contact α . Following [12], we introduce the following notation,

$$\mathcal{R} = \{1...\omega\} \backslash \mathcal{P}^\alpha$$

$$I_{\mathcal{P}^\alpha} = [c_i^\alpha]_{\mathcal{P}^\alpha}$$

$$I_{\mathcal{R}^\alpha} = [c_i^\alpha]_{\mathcal{R}^\alpha}$$

Thanks to this notation, we may write

$$\sigma_i^\alpha\left(\lambda_T^\alpha\right) = \mu^\alpha R_N^\alpha - c_i^\alpha \lambda_T^\alpha, \ \forall i \in \{1...\omega\}$$

as

$$\sigma_{\mathcal{P}^\alpha}^\alpha\left(\lambda_T^\alpha\right) = \mu_{\mathcal{P}^\alpha} R_N^\alpha - I_{\mathcal{P}^\alpha}^T \lambda_T^\alpha$$

$$\sigma_{\mathcal{R}^\alpha}^\alpha\left(\lambda_T^\alpha\right) = \mu_{\mathcal{R}^\alpha} R_N^\alpha - I_{R^\alpha}^T \lambda_T^\alpha$$

where the vector $\mu_{\mathcal{P}^\alpha}$ and μ_{R^α} are defined by

$$\mu_{\mathcal{P}^\alpha} = \begin{bmatrix} \mu^\alpha \\ \mu^\alpha \end{bmatrix} \in \mathbb{R}^2$$

$$\mu_{\mathcal{R}^\alpha} = \begin{bmatrix} \mu^\alpha \\ \vdots \\ \mu^\alpha \end{bmatrix} \in \mathbb{R}^{\omega^\alpha - 2}$$

Since $I_{\mathcal{P}^\alpha}$ is assumed to be invertible, one obtains

$$\lambda_T^\alpha = I_{\mathcal{P}^\alpha}^{-T} \mu_{\mathcal{P}^\alpha} R_N^\alpha - I_{\mathcal{P}^\alpha}^{-T} \sigma_{\mathcal{P}^\alpha}^\alpha \tag{7.4}$$

and then by substitution,

$$\sigma_{\mathcal{R}^\alpha}^\alpha \left(\lambda_T^\alpha\right) = \mu_{\mathcal{R}^\alpha} R_N^\alpha - I_{\mathcal{R}^\alpha}^T I_{\mathcal{P}^\alpha}^{-T} \mu_{\mathcal{P}^\alpha} R_N^\alpha + I_{\mathcal{R}^\alpha}^T I_{\mathcal{P}^\alpha}^{-T} \sigma_{\mathcal{P}^\alpha}^\alpha$$

In the same manner, the equation

$$-U_T^\alpha = \sum_{i=1}^{\omega^\alpha} k_i^\alpha c_i^\alpha = I_{\mathcal{P}^\alpha} k_{\mathcal{P}^\alpha} + I_{\mathcal{R}^\alpha} k_{\mathcal{R}^\alpha}$$

can be written as

$$k_{\mathcal{P}^\alpha} = -I_{\mathcal{P}^\alpha}^{-1} U_T - I_{\mathcal{P}^\alpha}^{-1} I_{\mathcal{R}^\alpha} k_{\mathcal{R}^\alpha} \tag{7.5}$$

We drop the superscript α to lighten the notation. Substituting the value of $P_{T,k+1}$ given by the discrete analog to equation (7.4) into the first equation of equation (7.3) and substituting the velocity $U_{T,k+1}$ into the discrete analog to equation (7.5) one obtains the following LCP in standard form:

$$\begin{cases} \begin{bmatrix} U_{N,k+1} + eU_{N,k} \\ k_{\mathcal{P}} \\ \sigma_{\mathcal{R}} \end{bmatrix} = M \begin{bmatrix} P_{N,k+1} \\ \sigma_{\mathcal{P}} \\ k_{\mathcal{R}} \end{bmatrix} + q \\ 0 \leqslant \begin{bmatrix} U_{N,k+1} + eU_{N,k} \\ k_{\mathcal{P}} \\ \sigma_{\mathcal{R}} \end{bmatrix} \perp \begin{bmatrix} P_{N,k+1} \\ \sigma_{\mathcal{P}} \\ k_{\mathcal{R}} \end{bmatrix} \geqslant 0 \end{cases} \tag{7.6}$$

where

$$M = \begin{bmatrix} \hat{W}_{NN} + \hat{W}_{NT} I_{\mathscr{P}}^{-T} \mu_{\mathscr{P}} & -\hat{W}_{NT} I_{\mathscr{P}}^{-T} & 0 \\ -I_{\mathscr{P}}^{-1} \left[\hat{W}_{TN} + \hat{W}_{TT} I_{\mathscr{P}}^{-T} \mu_{\mathscr{P}}\right] & I_{\mathscr{P}}^{-1} \hat{W}_{TT} I_{\mathscr{P}}^{-T} & -I_{\mathscr{P}}^{-1} I_{\mathscr{R}} \\ \mu_{\mathscr{R}} - I_{\mathscr{R}}^T I_{\mathscr{P}}^{-T} \mu_{\mathscr{P}} & I_{\mathscr{R}}^T I_{\mathscr{P}}^{-T} & 0 \end{bmatrix}$$

$$q = \begin{bmatrix} U_{N,free} + eU_{N,free} \\ -I_P^{-1}U_{T,free} \\ 0 \end{bmatrix}$$

In the multi-contact case, the matrix notation must be enlarged to extend the formulation equation (7.6). Let us first introduce the index sets

$$\mathcal{P} = \{\mathcal{P}^\alpha \mid \alpha \in I_a(\tilde{q}_{k+1})\},\ \mathcal{R} = \{\mathcal{R}^\alpha \mid \alpha \in I_a(\tilde{q}_{k+1})\}$$

In order to perform this extension, we introduce the following notation:

$$\mu_{\mathcal{P}} = \begin{bmatrix} \mu_{\mathcal{P}^1} & & & \\ & \ddots & & (0) \\ & & \mu_{\mathcal{P}^\alpha} & \\ & (0) & & \ddots \\ & & & \mu_{\mathcal{P}^\nu} \end{bmatrix},\ \mu_{\mathcal{R}} = \begin{bmatrix} \mu_{\mathcal{R}^1} & & & \\ & \ddots & & (0) \\ & & \mu_{\mathcal{R}^\alpha} & \\ & (0) & & \ddots \\ & & & \mu_{\mathcal{R}^\nu} \end{bmatrix}$$

For $\mu_{\mathcal{P}^\alpha} \in \mathbb{R}^{2a\times a}$and $\mu_{\mathcal{R}^\alpha} \in \mathbb{R}^{(\sum_\alpha(\omega^\alpha-2)a)\times a}$ where $a \leqslant \nu$ is the cardinal of $I_a\left(\tilde{q}_{k+1}\right)$.

Finally, we define

$$I_{\mathcal{P}} = \begin{bmatrix} I_{\mathcal{P}^1} & & & \\ & \ddots & & (0) \\ & & I_{\mathcal{P}^\alpha} & \\ & (0) & & \ddots \\ & & & I_{\mathcal{P}^\nu} \end{bmatrix},\ \mu_{\mathcal{R}} = \begin{bmatrix} I_{\mathcal{R}^1} & & & \\ & \ddots & & (0) \\ & & I_{\mathcal{R}^\alpha} & \\ & (0) & & \ddots \\ & & & I_{\mathcal{R}^\nu} \end{bmatrix}$$

For $I_{\mathcal{P}^\alpha} \in \mathbb{R}^{2a\times 2a}$ and $I_{\mathcal{R}^\alpha} \in \mathbb{R}^{2a\times(\sum_\alpha(\omega^\alpha-2)a)}$.

With the notation extended the way described, the LCP given by equation (7.6) is valid for the multicontact case.

7.2 Co-simulation of the frictional contact problem in MBDyn

The ability to instantiate a frictional nonsmooth subproblem has been added to the dynamically loaded module introduced in 4. Using the same input interface of the previously described module a user defined element can be provided that links a node of the model with a subsystem subject to unilateral frictional constraints,

which is integrated with a *time-stepping* method. The same approach described in section 4.3 is used. The module integrates the dynamic of a node which can come in contact with one or more planes, with friction. It formulates the problem assembling an LCP as described in section 7.1, and it implements the NSCD algorithm 3.1 where the OSNSP is the one expressed in equation (7.3).

7.2.1 First validation with a simple model

In order to validate the formulation for frictional contact adopted in the module the example in section 3.2.2 has been reconsidered, and friction has been added to the definition of the problem.

The problem has been described in figure 3.4 and the parameters used are those in table 7.1. A friction coefficient $\mu = 0.02$ has been used.

The same model has been implemented also using the Siconos Kernel library, which, along with classes to describe Lagrangian Time Invariant Dynamical Systems, provides an updated choice of Frictional Contact Problem solvers. The model implemented in Siconos is solved with a Non-Smooth Gauss Seidel solver, based on a projection onto the Friction Cone, which is an iterative method that doesn't rely on a faceting discretization of the problem.

The good correlation between the results of the two models, shown in 7.3, helped validate the implementation.

Table 7.1: Ball on a tilted frictional plane: parameters

radius R [m]	0.1
tilt angle [rad]	0.05
height h [m]	1.0
mass m [kg]	1.0
gravity acc. g [m/s]	-9.81
timestep [s]	$1.e-3$
Newton coef. of restitution	0.8
Number of facets for the friction cone ω	16
Friction coefficient μ	0.02

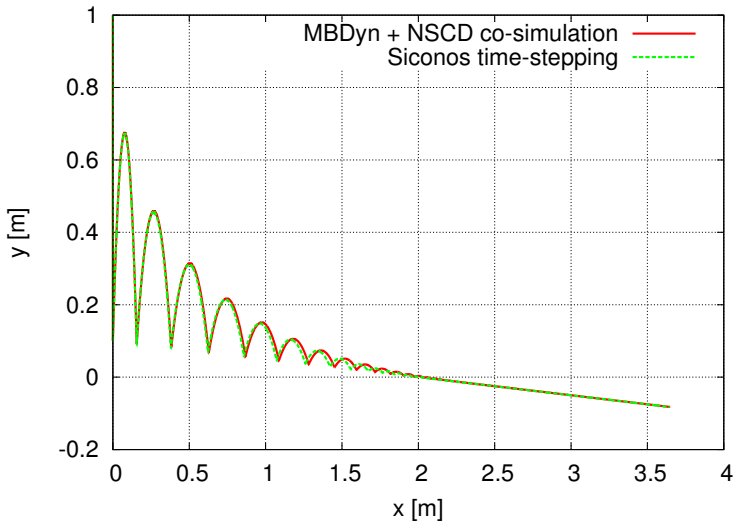

Figure 7.3: Ball falling on a tilted plane with friction. Results are coincident.

7.2.2 Theo Jansen's mechanism

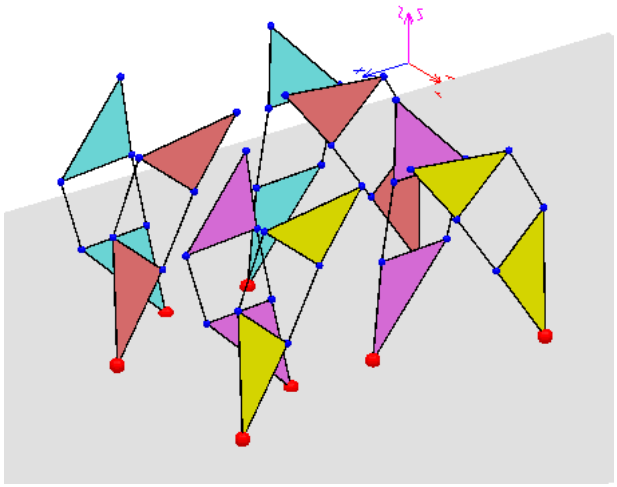

Figure 7.4: Jansen's walking model

The approach described has been applied to a more complex multibody application, consisting of a walking mechanism. It is based on a planar mechanism designed by the Dutch artist Theo Jansen, converting rotary motion into leg movements. The model has been considered for the only purpose of testing the suitability of the approach proposed in providing frictional contact elements to a multibody problem.

The linkage provides a constant axle height, uses only pivot joints and a rotating crank for input. The artist developed it with the goal of obtaining a visually elegant walking motion, so the linkage is not necessarily the most efficient way of implementing this movement. For example comparable linkages, like Joseph Klann's

linkage, may provide better step height and stride lenght in order optimize velocity and the ability to overcome obstacles.

The model consists of four planar sections of Jansen's linkage, disposed in parallel planes, in order to have a set of 8 legs able to walk on a 3D plane. At the tip of each leg a contact point has been modeled through the use of the module co-simulating a nonsmooth subproblem. The contact point at each leg has been defined and its relative position constrained, with a total joint, to the position of the bottom leg node. Tikhonov regularization has been applied to this joint, in order to avoid overconstraining. The approach to the contact point definition is analogous to the one explained in section 6.1.1.

In figure 7.5 is shown a cycle of the mechanism in order to illustrate its motion, whereas the 3D MBDyn model sketched with the software Easyanim, a free visualization tool initially developed by Olivier Verlinden (Olivier.Verlinden@fpms.ac.be), *Faculté Polytechnique de Mons*, is shown in figure 7.4. The different planes are highlighted with different colors and the contact points are the red dots.

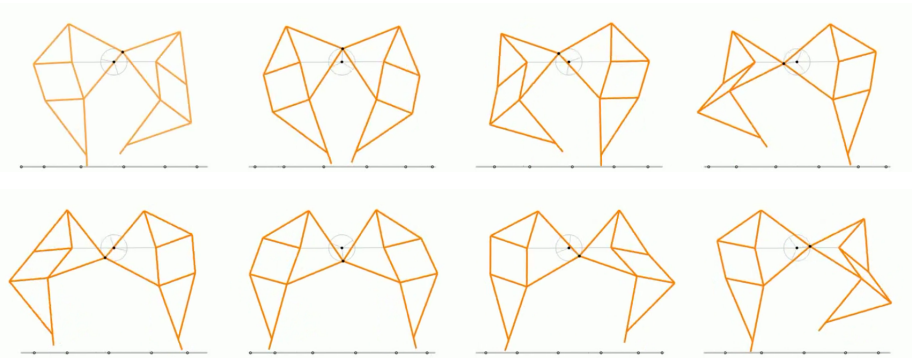

Figure 7.5: Jansen's linkage phases

The parameters used in the simulation are detailed in table 7.2. Figure 7.6 illustrate the vertical stride movement of the two legs of the first planar mechanism, from which it is possible to discern a duty cycle, calculated as a ratio of the time of ground contact with the total time of simulation, of 0.5%. The figure 7.7 shows the reaction forces in the contact point at the base of the first leg. As expected normal and tangent contact forces are present in the interval of time where the vertical position of the leg is coinciding with the ground, as seen in the red plot in figure figure 7.6. The tangential force along x axis is proportional to the normal force by a factor determined by the friction coefficient, and it is present a smaller tangential force along the y axis due to the anisotropy introduced by the 16 faced polyhedral discretization of the friction cone used. Better results would be possible by using better formulations of the frictional problem, as those surveyed in [2]. This LCP-based formulation has been chosen for simplicity of implementation in this explorative phase.

This application of the method proves it suitable to add frictional contact elements to a multibody problem, in which the nonsmooth part of the problem is isolated and co-simulated alongside the DAE integration of MBDyn.

Table 7.2: Jansen's simulation parameters

Timestep	$1.e-4$
Friction coefficient	1.2
Newton coefficient	0.8
Tikhonov constant	$5.e-8$
Crank speed [rad/s]	0.031416
LCP solver	Lexico Lemke

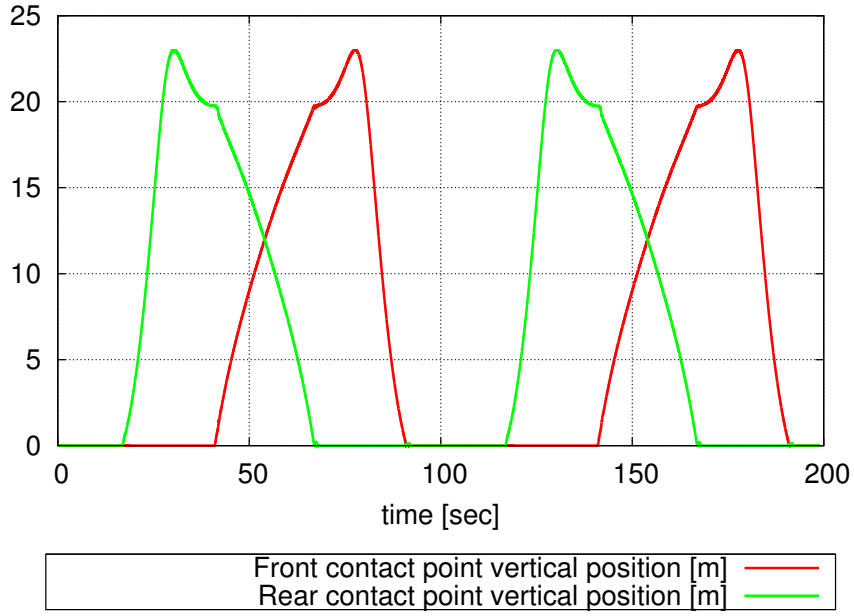

Figure 7.6: Stride vertical movement

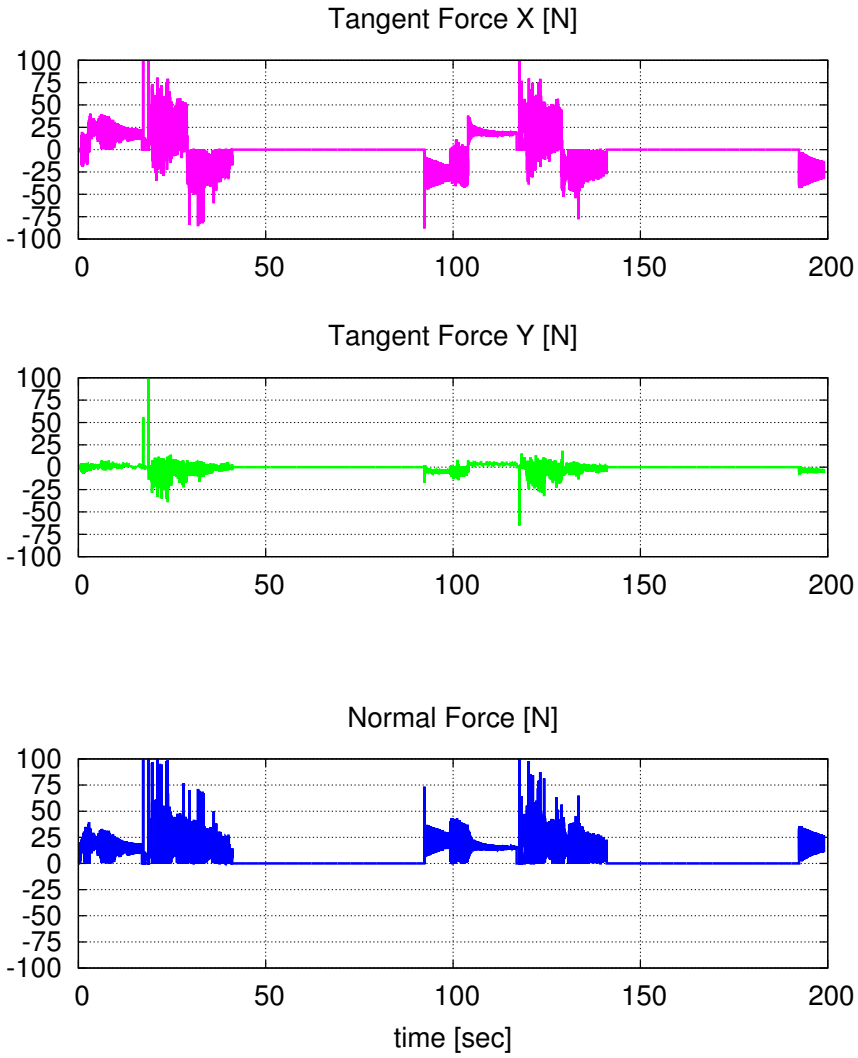

Figure 7.7: Reactions with ground in the first leg contact point

Chapter 8

Conclusions

The aim of this work was to explore a solution allowing to add a tool to model unilateral constraints to the multibody analysis software MBDyn. A requirement of the research has been the desire to retain the architecture of the MBDyn integration engine to take advantage of the properties of accuracy and versatility of the MBDyn integration scheme and because it would have required a broader programming effort.

First, following a path already adopted by commercial multibody softwares, a continuous contact solution has been explored, resulting in the implementation of stiff constitutive laws to use in conjunction with deformable elements in order to model a regularized version of the phenomena of contact and impact. This approach proved suitable but results in very stiff problems that require small steps of integration, and requires .

A radically different approach to the nonsmoothness introduced in the problem by non-interpenetration constraints and dry friction law is the nonsmooth contact dynamics. A nonsmooth framework allows precise definitions of solutions for nonsmooth problems together with uniqueness and existence results and the use of specific algorithms (time-stepping, LCP solvers with polynomial complexity) leads to an efficient simulation environment, allowing to treat large dimension problems or systems with impact accumulation. A co-simulation approach has been developed, to integrate alongside a part of the problem treated with the DAE integration of the MBDyn software and a nonsmooth subproblem that makes use of the nonsmooth contact dynamics algorithm. The cosimulation has been developed through a dynamically loaded module in MBDyn, implementing the integration of a nonsmooth subproblem interfaced to the main model. The module has been validated through comparison with results from state-of-the-art nonsmooth dynamics software Siconos.

An exploration of an approach to apply the multistep MBDyn integration to nonsmooth problems has been advanced, following a recent work regarding the adaptation of the HHT integration scheme to the nonsmooth timestepping algorithm with the aim of obtaining a higher order nonsmooth integration scheme. While compara-

ble results have been reached, the necessity to reinitialize the algorithm after each nonsmooth events renders this solution more complex on the implementation side. The results for simple benchmark examples have been compared with those from the co-simulation approach, with good correlation.

The cosimulation approach has been tested with more complex examples, in order to test its robustness and versatility. The modelization of the droop-stop and antiflap contacts of an articulated helicopter rotor has been considered and compared against a continuous contact solution, and a model of a walking mechanism has been used to test the modelization of the contact with friction. This applications consider models in which only the contact point is comprised in the nonsmooth subproblem, and that sub-model is rigidly attached to the rest of the MBDyn integrated model. The simulations show that the tool developed is capable of providing a solution even in problems in which the two sub-problems are not well separated, but instead strictly coupled. This requires though quite stiff forces exchanged between the two subproblems, requiring thus a relevant computational aggravation compared to a completely nonsmooth formulation. With the very simple formulation of dry friction implemented, LCP based through a facetization of the friction cone, it is possible to deal with stick-slip frictional contact state, thus overcoming a drawback of a continuous contact solution.

The co-simulation approach developed can be a valuable tool for a class of problems in which it is possible to isolate the nonsmooth dynamics to a part of the model. More tests need to be made with applications in which the two co-simulated parts are connected through the use of a compliant element. It is expected that, within this class of applications, significant efficiency gains can be obtained over the continuous contact solution, adding to the advantage of a more consistent treatment of the nonsmooth aspects of the problems, such as the resolution of the stick-slip phases of dry-friction law. Future developements may include a more thorough analysis of the class of applications of interest, enhancements in the interaction process between the two integration methods, especially during the smooth phases of motion, enhancements in the formulation of the frictional problem and a more versatile way of defining the unilateral constraints, with the possibility of definition of more generic surfaces as boundaries and the possibility of defining contact between two or more parts, or nodes, of the same model.

Bibliography

[1] V. Acary. Higher order event capturing time-stepping schemes for nonsmooth multibody systems with unilateral constraints and impacts. *Applied Numerical Mathematics*, 62(10):1259 – 1275, 2012. Selected Papers from NUMDIFF-12.

[2] V. Acary and B. Brogliato. *Numerical Methods for Nonsmooth Dynamical Systems*. Springer, 2008.

[3] J. Baumgarte. Stabilization of constraints and integrals of motion in dynamical systems. *Computer methods in Applied Mechanics and Engineering*, 1:1–16, 1972.

[4] W. G. Bousman, C. Young, F. Toulmay, N.E. Gilbert, R.C. Strawn, J.V. Miller, T.H. Maier, M. Costes, and P. Beaumier. A comparison of lifting-line and cfd methods with flight test data from a research puma helicopter. *NASA Technical Memorandum 110421*, 1996.

[5] O. Brüls and M. Arnold. The generalized-α scheme as a linear multistep integrator: toward a general mechatronic simulator. *Journal of computational and nonlinear dynamics*, 3(4), 2008.

[6] O. Brüls and J.C. Golinval. The generalized-α method in mechatronic applications. *ZAMM - Journal of Applied Mathematics and Mechanics / Zeitschrift fÃŒr Angewandte Mathematik und Mechanik*, 86(10):748–758, 2006.

[7] Q. Chen, V. Acary, G. Virlez, and O. Brüls. A newmark-type integrator for flexible systems considering nonsmooth unilateral constraints. *2nd Joint International Conference on Multibody System Dynamics*, 2012.

[8] C. A. Coulomb. *Théorie des machines simples, en ayant égard au frottement de leur parties, et la roideur des cordages.* 1781.

[9] B. Esefeld and H. Ulbrich. A hybrid integration scheme for nonsmooth mechanical systems. 2011.

[10] P. Flores, M. Machado, M. T. Silva, and J. M. Martins. On the continuous contact force models for soft materials in multibody dynamics. *Multibody System Dynamics*, 25(3):357–375, 2011.

[11] C. F. Gauss. Ueber ein neues algemeines grundgesetz der mechanik. *J. fuer die reineund angewandte Mathematik*, 4:232–235, 1829.

[12] Ch. Glocker. Formulation of spatial contact situations in rigid multibody systems. pages 199–214, 1999.

[13] Ch. Glocker. On frictionless impact models in rigid-body systems. *Phil. Trans. R. Soc. London 359*, 2001.

[14] Ch. Glocker and F. Pfeiffer. Multiple impacts with friction in rigid multibody systems. *ASME Journal of Nonlinear Dynamics*, 1995.

[15] W. Goldsmith. *Impact: The Theory and Physical Behaviour of Colliding Solids.* 1960. cited By (since 1996) 500.

[16] E. Hairer and G. Wanner. *Solving Ordinary Differential Equations II. Stiff and Differential- Algebraic Problems.* Springer, 1996.

[17] H. Hertz. On the contact of solids - on the contact of rigid elastic solids and on hardness. *Miscellaneous papers*, pages 146–183, 1896. cited By (since 1996) 8.

[18] H. Hilbert, T. Hughes, and R. Taylor. Improved numerical dissipation for time integration algorithms in structural dynamics. *Earthquake Engineering and Structural Dynamics*, 5:283–292, 1977.

[19] R. Huber and H. Ulbrich. Higher order integration of non-smooth dynamical systems using parallel computed extrapolation methods based on time-stepping schemes. *Proceedings of 1st Joint International Conference on Multibody System Dynamics, Lappeenranta*, 2010.

[20] K. H. Hunt and F. R. E. Crossley. Coefficient of restitution interpreted as damping in vibroimpact. *Journal of Applied Mechanics, Transactions ASME*, 42 Ser E(2):440–445, 1975. cited By (since 1996) 286.

[21] M. Jean. The nonsmooth contact dynamics method. *Computer Methods in Applied mechanics and Engineering*, 177:235 – 257, 1999.

[22] A. Klabring and J. S. Pang. Existance of solutions to discrete semicoercive frictional contact problems. *SIAM J. Optimization*, 1997.

[23] J. C. Klann. Jansen - klann linkage comparison.

[24] A. Klarbring. A mathematical programming approach to three-dimensional contact problems with friction. pages 175–200, 1986.

[25] A. Klarbring. Mathematical programming in contact problems. In C. A. Brebbia M. H. Aliabadi, editor, *Computational Methods in Contact Mechanics*, pages 233–263. M.H. Aliabadi, C.A. Brebbia, 1993.

[26] A. Klarbring and G. Björkman. A mathematical programming approach to contact problems with friction and varying contact surface. pages 1185–1198, 1988.

[27] H. M. Lankarani and P. E. Nikravesh. Contact force model with hysteresis damping for impact analysis of multibody systems. *Journal of mechanisms, transmissions, and automation in design*, 112(3):369–376, 1990. cited By (since 1996) 147.

[28] H. M. Lankarani and P. E. Nikravesh. Continuous contact force models for impact analysis in multibodysystems. *Nonlinear Dynamics*, 5(2):193–207, 1994. cited By (since 1996) 97.

[29] R. I. Leine and N. van de Wouw. *Stability and Convergence of Mechanical Systems with Unilateral Constraints*. Springer, 2008.

[30] G. L.Ghiringhelli, P. Masarati, P. Mantegazza, and M. W. Nixon. Multibody analysis of a tiltrotor configuration. *Nonlinear Dynamics*, 19:333–357, 1999.

[31] M. D. P. Monteiro Marques. Differential inclusions in nonsmooth mechanical problems: shocks and dry friction. *Progress in Nonlinear Differential Equations and Their Apllications*, 9, 1993.

[32] P. Masarati, M. Lanz, and P. Mantegazza. Multistep integration of ordinary, stiff and differential-algebraic problems for multibody dynamics applications. *XVI Congresso Nazionale AIDAA*, 2001.

[33] J. J. Moreau. *Non-smooth mechanics and applications*, chapter Unilateral contact and dry friction in finite freedom dynamics. Springer, 1988.

[34] J. J. Moreau. Unilateral contact and dry friction in finite freedom dynamics. *Nonsmooth mechanics and applications, CISM, Courses and lectures, Springer-Verlag*, 302:1–82, 1988.

[35] J. J. Moreau. Numerical aspects of the sweeping process. *Computer Methods in Applied mechanics and Engineering*, 177:329 – 349, 1999.

[36] V. Muscarello, P. Masarati, and G. Quaranta. Multibody analysis of rotorcraft-pilot coupling. In *presented at IMSD 2012, Stuttgart, Germany, May 29-June 1, 2012.*, 2012.

[37] S. Newman. The phenomenon of helicopter rotor blade sailing. *Proceedings of the Institution of Mechanical Engineers, Part G: Journal of Aerospace Engineering*, 213(6):347–363, 1999.

[38] F. Pfeiffer and Ch Glocker. Multibody dynamics with unilateral contacts. *Multibody Dynamics with Unilateral Contacts*, 1996. cited By (since 1996) 412.

[39] T. Schlinder and V. Acary. Timestepping schemes for nonsmooth dynamics based on discontinuous galerkin methods: Definition and outlook. 2012.

[40] D. E. Stewart. Convergence of a timestepping scheme for rigid-body dynamics and resolution of painlevè's problem. *Archives of Rational Mechanics and Analysis*, 145:215–260, 1998.

[41] D. E. Stewart. Time-stepping methods and the mathematics of rigid body dynamics. In *COMPLEX SYSTEMS, CHAPTER 6*. Cambridge University Press, U.K, 2000.

[42] W. J. Stronge. *Impact Mechanics*. 2000. cited By (since 1996) 262.

[43] C. Studer. Numerics of unilateral contact and friction - modeling and numerical time integration in non-smooth dynamics. *Lecture Notes in Applied and Computational Mechanics*, 47, 2009.

[44] C. Studer, R. I. Leine, and Ch. Glocker. Step size adjustment and extrapolation for time stepping schemes in non-smooth dynamics. *International Journal for Numerical Methods in Engineering*, 76:1747–1781, 2008.

[45] S. P. Timoshenko and J. N. Goodier. *Theory of Elasticity*. 1970. cited By (since 1996) 6645.

[46] F. E. Udwadia and R. E. Kalaba. *Analytical Dynamics*. New York: Cambridge University Press, 1996.